Epigenomic and Transcriptomic Changes in the Onset of Disease

Lynette Brigitte Naler

Dissertation submitted to the faculty of the Virginia Polytechnic Institute and State University in partial fulfillment of the requirements for the degree of

Doctor of Philosophy

In

Chemical Engineering

Chang Lu, Chair

Richey M. Davis

Aaron S. Goldstein

Rong Tong

April 22, 2021

Blacksburg, VA

Keywords: Epigenomics, Transcriptomics, Chromatin Immunoprecipitation, RNA Sequencing, Breast Cancer, BRCA1, Inflammation, Lipopolysaccharide, Maternal Immune Activation, Cross-Fostering

Epigenomic and Transcriptomic Changes in the Onset of Disease

Lynette Brigitte Naler

Abstract

Current sequencing technologies allows researchers unprecedented insight into our biology, and how these biological mechanisms can become distorted and lead to disease. These aberrant mechanisms can be brought about by many causes, but some occur as a result of genetic mutations or external factors through the epigenome. Here, we used our microfluidic technology to profile the epigenome and transcriptome to study such aberrant mechanisms in three different diseases and illnesses: breast cancer, chronic inflammation, and mental illness. We profiled the epigenome of breast tissue from healthy women with the *BRCA1* mutation to understand how the mutation may facilitate eventual breast cancer. Epigenomic changes in breast cells suggest that cells in the basal compartment may differentiate into a different cell type, and perhaps become the source of breast cancer. Next, we compared the epigenome and genome of murine immune cells under low-grade inflammation and acute inflammation conditions. We found that low-grade inflammation preferentially utilizes different signaling pathways than in acute inflammation, and this may lead to a non-resolving state. Finally, we analyzed the effect of the maternal immune activation on unborn offspring, and how these changes could cause later mental illness. The insights we made into these diseases may lead to future therapies.

Epigenomic and Transcriptomic Changes in the Onset of Disease

Lynette Brigitte Naler

General Audience Abstract

Despite advances in medical and scientific research, there is still a dearth of information on how diseases affect the expression of our genes, such as breast cancer, chronic inflammation, and influenza. Mutation in the BRCA1 gene is probably the most well-known mutation that can lead to breast cancer. We know the overarching reason that mutation in BRCA1 can lead to cancer, as BRCA1 is responsible for repairing damage in the DNA, so mutations can compound and create cancerous cells. However, we do not know the exact mechanisms by which this actually happens. Another widespread problem is chronic inflammation, which can promote or lead to diseases such as diabetes, cancer, Alzheimer's, Rheumatoid arthritis, and heart disease. In addition, there are many causes of chronic inflammation that many people have experienced at some point in time, including stress, insomnia, being sedentary, poor eating habits, and obesity. Despite this, we still do not fully understand why chronic inflammation differs from normal inflammation, which is a healthy process, or why it does not resolve. There are also other connections that are surprising, and many are not aware of. If a pregnant woman gets the flu during her second trimester, her baby has much higher odds of developing schizophrenia later in its lifetime. Given the prevalence of the flu, there is a very real chance that an expecting mother will be infected during her pregnancy.

Acknowledgments

It was only with the encouragement and support of my mentors, my family, and my friends that I was able to pursue my research and complete my dissertation. Each of these people have played different, sometimes overlapping, roles in helping me grow and flourish during my time at Virginia Tech. If it were not for them, it is unclear where I would be today, and I wish to thank them for all that they have done for me.

First, I must thank my advisor, Dr. Chang Lu. He accepted me into his group under unexpected circumstances without a second thought, and it truly was the best thing that could have happened to me. He has been a kind, caring, and supportive mentor that would speak with me frankly and with respect. We have had many discussions over many topics, which have helped me become a more effective researcher and a well-rounded person. His mentorship and authentic concern for each of his students made me want to be someone he could be proud of, and his faith in me helped me build faith in myself. I am truly privileged to have had a rational, thoughtful, and funny mentor as I have had in Dr. Lu.

Furthermore, I want to thank the members of my committee, Dr. Richey Davis, Dr. Aaron Goldstein, and Dr. Rong Tong. They provided pragmatic and insightful suggestions during my preliminary exam, and guidance to help me excel in my understanding of core subjects. They have also been a source of stimulating and enjoyable conversation.

I am grateful to the people of Virginia Tech's Department of Chemical Engineering. Prof. David Cox has graciously worked with me to bring changes that provide a wide variety of benefits our graduate students. The office staff, in particular Stacey Radcliffe, Tina Russell, and Andrea Linkous were a source of joy and positivity, and also were

responsible for making possible many of the improvements ChEGSA proposed to benefit graduate students. They often helped us to realize opportunities that we weren't even aware of.

I would like to thank the lab mates who have helped me over the years: Sai Ma, Yan Zhu, Travis Murphy, Mimosa Sarma, Chengyu Deng, Yuan-Pang Hsieh, Bohan Zhu, Qiang Zhang, Jerry Liu, Zirui Zhou, Tom Hadlock, and Gaoshan Li. They each were kind, helpful, and inclusive, allowing us to have a healthy and happy lab environment. In particular, I would like to thank Travis Murphy, Yuan-Pang Hsieh, Bohan Zhu, and Jerry Liu. In addition to being excellent sounding boards and assisting my research, they helped provide valuable insight for my research and my life, and presented me with perspectives that I had not considered before. They helped me look forward to each day, even during difficult times.

Finally, I would like to thank my family and friends for their support in making this possible. My parents, Tom Naler and Andrea MacDonald, provided me with advice and encouragement over the years, and were my most ardent supporters. My friends, who helped me accomplish my personal goals and provided a welcome respite from the stress of graduate school. Last but not least, my partner, Brian Judy, was a significant source of strength during my graduate studies, and made sure to look out for my best interests, especially when I was not.

Table of Contents

List of Figures

List of Tables

List of Abbreviations

BC	Basal cell
BMDM	Bone-marrow derived monocytes
bp	Base pairs
BRCA1	Breast cancer gene 1
BSA	Bovine serum albumin
cDNA	Complementary DNA
ChIP	Chromatin immunoprecipitation
COPD	Chronic obstructive pulmonary disease
Ct	Cycle threshold
DEG	Differentially expressed genes
DNA	Deoxyribonucleic acid
DTU	Differential transcript usage
EDTA	Ethylenediaminetetraacetic acid
EGTA	Ethylene glycol-bis(β-aminoethyl ether)-N,N,N',N'-tetraacetic acid
ER	Estrogen receptor
FACS	Flourescence activated cell sorting
FBS	Fetal bovine serum
FC	Fold change
FDR	False detection rate
FrIP	Fraction of reads in peaks
GO	Gene ontology
GSEA	Gene set enrichment analysis
GWAS	Genome-wide association study
IFN	Interferon
IP	Immunoprecipitation
kb	kilobase pairs
LP	Luminal progenitor
LPS	Lipopolysaccharide
MAPK	Mitogen-activated protein kinase

M-CSF	Macrophage colony stimulating factor
MHC	Major histocompatibility complex
MIA	Maternal immune activation
ML	Mature luminal cells
MOW-ChIP	Microfluidic oscillatory washing-based ChIP
mRNA	Messenger RNA
MUT	Carries the BRCA1 mutation
NC	Does not carry the BRCA1 mutation
NSC	Normalized strand correlation
nt	nucleotide
PBS	Phosphate buffered saline
PDMS	Polydimethylsiloxane
PIC	Protease Inhibitor Cocktail
PMSF	Phenylmethylsulfonyl fluoride
PRR	Pattern recognition receptor
qPCR	quantitative polymerase chain reaction
RFU	Relative fluorescence units
RNA	Ribonucleic acid
RSC	Relative strand correlation
SC	Stromal cells
SCC	Spearman correlation coefficient
SDS	Sodium dodecyl sulfate
SNP	Single nucleotide polymorphism
TE buffer	Tris-EDTA buffer
TF	Transcription factor
Tlr4	Toll-like receptor 4
TRAM	Translocation associated membrane protein 1
TRIF	TIR-domain-containing adapter-inducing interferon β
Tris	Tris(hydroxymethyl)aminomethane
TSS	Transcription start site
UPR	Unfolded protein response

1 Introduction

The epigenome is the means by which our environment and our experiences, or those of our parents, can produce a tangible effect on us. As opposed to our DNA, which is largely stable, our epigenome is in flux and is capable of changing how our DNA expresses itself. It is how two living things, with the same exact DNA, can have very different features or diseases. For example, if an individual who has schizophrenia has an identical twin, their twin will also be diagnosed with schizophrenia only about 50% of the time. Furthermore, our surroundings and our experiences can affect our epigenome in ways that induce, exacerbate, or leave us vulnerable to disease. Even internal changes, such as genetic mutation, can affect the epigenome and lay the foundation for later illness.

1.1 Epigenetics

Epigenetics is the body of inheritable modifications to the genome that do not change the underlying gene sequence.[1] It is responsible for the myriad of cells that are present within a human body, despite the fact that they all share the same exact genome. Furthermore, epigenetics is what allows our bodies to be affected by and adapt to our surroundings. Disruption of the epigenome can be both a cause or contributor of disease as well as a marker. For example, widespread changes in the epigenome are a hallmark of cancer – sometimes as a result of genetic mutation, though not always.[2] Due to its reversible nature, it has become a popular target for medical therapies.[3] The main focus in epigenetics research is on DNA methylation, 3D chromatin structure, histone modification, and non-coding RNA, though there are other epigenetic marks. Here, we will primarily focus on histone modifications.

Chromatin Structure

Within each human cell, there is approximately 2 meters of DNA. In order for it pack tightly in the cell, the DNA is wrapped around an octamer of histones in a unit structure known as a nucleosome.[4] The histone octamer consists of four pairs of H2A, H2B, H3, and H4 histones which are wrapped by ~147bp of DNA. Between each nucleosome, there is ~50bp of DNA, such that the series of nucleosomes mimics 'beads on a string'.[5] The chromatin can then be further coiled and packed in a form known as heterochromatin, which is associated with gene repression.[1] Conversely, the less dense form, euchromatin, is associated with gene activation. The state of chromatin packing is largely determined by either histone modifications or DNA methylation.

Histone Modification

While the location of a nucleosome is relatively stable, each histone has an N-terminal amino-acid tail that can be modified.[4] The number of known modifications has rapidly increased with recent years, though the main modifications studied involve mono-, di-, or tri-methylation or acetylation of one of the amino acids (primarily lysine) present on the tail. In notation, the acetylation of the lysine in the 27th position of the amino acid tail on histone H3 is denoted as H3K27ac. The type and location of the modification can affect whether or not gene expression is promoted or repressed. For example, H3K27ac and H3K9ac are associated with active enhancer and promoter regions, respectively.[6-8] H3K9me3 is associated with densely packed heterochromatin, where gene expression is silenced.[9] Similarly, H3K27me3 is associated with Polycomb silencing of genes.[10] In contrast, H3K79me2 is associated with increased gene expression and H3K4me3 marks promoters.[11,12] In order to determine the locations at which these histone modifications

are occurring across the genome, researchers use chromatin immunoprecipitation followed by high-throughput sequencing.

Chromatin Immunoprecipitation (ChIP)

Chromatin immunoprecipitation (ChIP) is a method of isolating the DNA that is wrapped around nucleosomes that have been modified in a specific way.[13] Generally, superparamagnetic beads are coated in antibody against the histone mark of interest (e.g. anti-H3K27ac). The beads are then incubated with chromatin, which is either fixed with formaldehyde then sonicated (XChIP) or digested through MNase (nativeChIP or nChIP). Smaller fragments of DNA allow for better resolution of a histone's location, however there needs to be an adequate number of DNA bases for the location to be determined. Afterwards, the beads are washed to remove non-specific binding and the chromatin is eluted from the beads. The DNA is then removed from the histone and tagged with sequencer-specific adapters in a process known as library preparation. Once the libraries are prepared, the DNA is sequenced to determine where the modifications are occurring along the genome. While ChIP is an effective means for genome-wide histone mapping, it does not provide data on which one of the two histones are modified, or if both histones share the same or different modifications.[4]

MOWChIP

Unfortunately, traditional ChIP methods generally require on the order of millions of cells to perform the assay.[13] This is particularly difficult in the case of rare cell types or from primary tissues, such as from a biopsy, where sample is severely limited or must be shared.[14-17] In response to this, our lab created a device to perform microfluidic oscillatory washing-based ChIP (MOWChIP) that was capable of effectively isolating ChIP-DNA for

sequencing from as few as 100 cells.[18] By leveraging a packed bed to increase adsorption, we were able to obtain over 25 times more ChIP-DNA from cells than previous methods.[19] Recent optimization has allowed us to perform up to eight MOWChIP assays in parallel.[20] It has also been used to analyze a wide variety of cell types and histone modifications, even some known for their difficulty. Other technologies such as Drop-ChIP[21], CUT&RUN[22,23], and ChIL-seq[24] are also capable of performing low-input ChIP-seq. However, they suffer from either few reads per sample (Drop-ChIP), lower data quality (CUT&RUN), belabored process (ChIL-seq), or low throughput data acquisition (CUT&RUN, ChIL-seq).

1.2 Sequencing Technology

In order to understand how the epigenome is affected, specifically for ChIP-seq, the enriched ChIP-seq DNA must be sequenced. During this process, each nucleotide in a fragment of DNA is identified, and eventually this information can be used to identify the genomic locations at which the histone modification occurs.

Sanger Sequencing

The first major iteration of automated sequencing was Sanger's 'chain-termination' sequencing, developed originally in 1977.[25] Sanger sequencing used amplification of DNA strands using a mix of nucleotides (dNTPs) and dideoxynucleotides (ddNTPs). When incorporated into the complementary strand, the ddNTPs prevent further additions.[26] Many strands of various lengths would be formed and the samples could be sequenced by running the samples on a gel. At first, this required four lanes (one for each ddNTP) but eventually incorporated fluorescent labelling to be run on one. Sanger

sequencing was famously used by the Human Genome Project in sequencing the human genome during the 1990's at a cost of $3 billion dollars over 13 years.[27,28]

Next Generation Sequencing

The second generation of high-throughput sequencing is referred to as next-generation sequencing. The three biggest technologies over the years have been Roche's 454 pyrosequencing, Thermo Fisher's Ion Torrent sequencing, and Illumina Solexa sequencing.[29] The most popular technology by far, and the one we use in our lab, is Illumina's sequencing technology. Developed by Solexa, who was later purchased by Illumina, in 2006, it makes use of a solid-phase amplification technique known as 'bridge amplification'.[30] Adapters are added to DNA fragments, which allows them to bind to complementary anchor points on the flow cell. DNA polymerase fabricates a complementary strand of DNA at the anchor point, and the original fragments are washed away. Then, the DNA strands fold over and attach to a nearby anchor point, forming a bridge. The complementary sequence is generated, the two strands are separated, and the cycle continues. Illumina's production level sequencers are capable of generating billions of reads per run, with reads up to 150-250bp.

Third Generation Sequencing

The third generation of high-throughput sequencing consists of PacBio SMRT and Oxford Nanopore technologies. These technologies are notable for their ability to perform real-time sequencing with significantly longer (~100x) reads.[31] In addition, they are capable of directly sequencing methylated DNA, histone modifications, and other epigenetic marks. Pac-Bio's SMRT (single molecule real-time) sequencing platform was a sequencing-by-synthesis technology released in 2009 that leverages small

wavelengths to perform sequencing and is currently capable of read lengths greater than 10kb and over 350k reads per run.[31,32] Oxford Nanopore, released in 2015, feeds DNA strands through a protein nanopore that is embedded within a charged membrane and changes in voltage are used to determine the sequence.[33,34] While both technologies are better at handling high repeat regions than Illumina, they also suffer from higher error rates, though there are methods of mitigating this such as consensus-based sequencing.[31,34] Furthermore, their focus on long reads makes them less effective in genome-wide analyses such as ChIP-seq.

1.3 Bioinformatics

Once the DNA is sequenced, we are given substantial files with millions of reads denoting the bases sequenced. In order to obtain meaningful underlying biological data, the sequenced data must undergo specific processing methods. This use of computational tools in order to better understand biology is known as bioinformatics. In addition, the analysis can be empowered by combining multiple types of analysis, such as ChIP-seq and RNA-seq, to provide novel and robust insights into the underlying biology.

ChIP-seq Data Analysis

First, the reads are aligned to a reference genome. If there does not exist a reference genome, then one can be created, though it requires deep sequencing (i.e. each location has multiple reads that map it) with long enough reads such that there is sufficient overlap to determine the order of the reads. However, this is beyond the scope

of our work, since ChIP-seq uses short reads and thus requires a reference. Then, reads that map to many locations are removed and the locations of 'peaks' are determined. Peaks are locations of the genome where the ChIP sample has a significant number of reads as compared to a background sample – generally normal DNA that has been sequenced. The peaks denote locations where there is a histone modification present. Once we have determined where the peaks are located, we can isolate peaks unique to a condition, compare the peak height between conditions to analyze differential modification levels, and even map peaks to nearby genes to determine if any biological pathways are enriched.

Furthermore, analysis of a combination of marks can provide additional insight into biology, such as regulatory elements, that is not capable with just one mark. For example, enhancers are a cell-type specific regulatory element that are responsible for activating gene transcription, even at great distances.[35] Specifically, they are regions whose sequences can bind various transcription factors that then facilitate transcription of a target. While H3K27ac marks active enhancers, H3K4me3 levels should be low at enhancer locations.[6,36] Thus, we are able to identify active enhancer regions by determining those regions that have high H3K27ac signal and low H3K4me3 signal. When multiple enhancers are present near one another, the region is deemed a super-enhancer.[37] Seemingly contradictory modifications can also co-occur on the same nucleosome. Promoters are regions of the gene where transcription starts and are distinct from enhancers. Promoters marked with both H3K4me3, which marks active promoters[11], and H3K27me3, which is associated with gene silencing[10], are considered to be bivalent promoters.[38] They are suggested to be silenced regions that are poised for activation.

Altogether, the tools at our disposal enable us to probe the role of epigenetics across many situations.

Transcriptomic Data Analysis

Genes that are actively expressed are transcribed into messenger RNA (mRNA), which is in turn translated into functional proteins[39]. As such, sequencing the mRNA provides insight into gene expression levels, known as RNA-seq[40]. This is done by isolating the mRNA and converting it into complementary DNA (cDNA). Adaptors are ligated onto the cDNA and the cDNA is amplified, before being sequenced. Much like in ChIP-seq, the sequenced reads must be processed. However, there are two main ways this can occur. Traditionally, the reads are aligned to a reference genome, much like in ChIP-seq, before the transcripts are quantified. There are newer, alignment-free methods that associate the reads directly with the transcripts, by breaking them into smaller fragments and matching them to pre-indexed transcripts[41,42]. These methods are faster and are very accurate in the quantification of highly-expressed or long genes, but they have worse performance for small or low-expressed RNAs[42]. In both cases, transcripts with low read counts are removed, before all reads are normalized[40]. Once the RNA-seq data is prepared and determined to be of suitable quality, the data is primarily used for determining genes that are differentially expressed between two conditions.

1.4 Research Topics

Here, we wanted to better understand the role of epigenetics in disease and related changes that occur in gene expression. As such we explore the effects of *BRCA1* mutation, lipopolysaccharide stimulation, and maternal immune activation on the epigenome and transcriptome.

Chapter 2 – Effect of *BRCA1* mutation

Women who have a mutation in the *BRCA1* gene are at high risk of developing breast cancer within their life time. To better understand the effect that *BRCA1* has on the epigenome, we profiled healthy breast tissue for H3K27ac from women with the *BRCA1* mutation and from those without. We show that the *BRCA1* mutation causes widespread changes to the epigenome of four different human breast cell types: basal, luminal progenitor, mature luminal, and stromal. However, there were only substantial differences in the H3K27ac modification levels of basal and stromal cells, despite previous research pointing to luminal progenitors as the source of breast cancer in women with the *BRCA1* mutation. Epigenomic variance at each of these marks were found to be in proximity to genes that were involved in DNA damage, unfolded protein response, and apoptosis, all of which *BRCA1* has been implicated in. In addition, we analyzed NC cell-type-specific transcription factor enrichment in *BRCA1* mutant cell types in conjunction with analysis of differential modification of cell-type specific genes. Together, our data suggests that the epigenomic changes due to BRCA1 mutation may promote the differentiation of cells in the basal compartment into luminal progenitor cells, which may later lead to breast cancer.

Chapter 3 – Immune changes from differential lipopolysaccharide stimulation

Chronic inflammation can facilitate or exacerbate many diseases, and there are many causes of chronic inflammation that we have all experienced, like stress or poor sleep habits. Despite this, the specific process by which low-grade inflammation occurs is not clear. To study this, we stimulated murine bone marrow-derived monocytes at low-doses and high-doses of lipopolysaccharide, a component of Gram negative bacteria that is associated with chronic inflammation, to determine the differences between low-grade and acute inflammation. Analysis of genome-wide H3K27ac binding and gene expression data suggest that low-grade inflammation preferentially uses the TRAM/TRIF-dependent pathway of TLR4 signaling, instead of the MyD88-dependent pathway. Further analysis of gene expression data from TRAM-deficient mice support this conclusion. In addition, key genes were identified that might explain what prevents the resolution of low-grade inflammation.

Chapter 4 – Neural alterations due to maternal immune activation

Activation of the immune system of a pregnant mother, such as due to infection, can have long-term effects on her child. In humans, MIA increases risk for autism and schizophrenia and has been found to be effectively modeled in mice. Here, we analyze the effect of maternal immune activation (MIA) on the epigenome of mouse offspring. Moreover, we analyze how cross-fostering, a common tactic to determine prenatal and postnatal effects, has an effect. Non-fostered MIA offspring show subtle, yet possibly key, differences when compared to non-fostered Mock mice. However, both of these groups of mice were significantly different than their control group, suggesting that even being exposed to MIA-born pups has an effect on the non-fostered Mock mice. Furthermore, cross-fostered Mock offspring and MIA offspring were also different than both non-

fostered offspring and their own control group, and were very similar to one another. These changes suggest that MIA exposure also has an effect on these mice similar to that in the non-fostered groups, but may be somewhat ameliorated as a result of cross-fostering.

Analysis of the epigenome and transcriptome is a powerful means of better understanding the biological mechanisms at play in many diseases. While the research described here advances knowledge into each of the disorders in question, there is still much more research that will be necessary to fully elucidate the etiology of each of these diseases, as well as means of possible treatment. Finally, Chapter 6 describes avenues of future research that can build upon the present work.

2 Cell-type-specific epigenomic variations associated with BRCA1 mutation in pre-cancer human breast tissues

---

Published Work

The work presented in this chapter was adapted from previously preprinted work noted below. Authors retain all copyright of figures.

Hsieh, Y.-P., Naler, L. B., Ma, S., and Lu, C. Cell-type-specific epigenomic variations associated with *BRCA1* mutation in pre-cancer human breast tissues. *bioRxiv* (2020) doi: 10.1101/2020.08.24.265199

Author Contributions

Chang Lu designed and supervised the study. Yuan-Pang Hsieh conducted the epigenomic profiling of the breast tissue samples. Lynette Naler analyzed the data. Sai Ma helped with experimental work and data analysis. Lynette Naler and Chang Lu wrote the manuscript. All authors proofread the manuscript and provided comments.

2.1 Project Summary

BRCA1 germline mutation carriers are predisposed to breast cancers. Epigenomic regulations have been known to strongly interact with genetic variations and potentially mediate biochemical cascades involved in tumorigenesis. Due to the cell-type specificity of epigenomic features, profiling of individual cell types is critical for understanding the molecular events in various cellular compartments within complex breast tissue. We produced cell-type-specific profiles of genome-wide histone modifications including H3K27ac and H3K4me3 in basal, luminal progenitor, mature luminal, and stromal cells extracted from pre-cancer *BRCA1* mutation carriers ($BRCA1^{mut/+}$) and non-carriers ($BRCA1^{+/+}$), using a low-input ChIP-seq technology that we developed. We discovered that basal and stromal cells present the most extensive epigenomic differences between

mutation carriers (*BRCA1*$^{mut/+}$) and non-carriers (*BRCA1*$^{+/+}$) while luminal progenitor and mature luminal cells are relatively unchanged with the mutation. Furthermore, the epigenomic changes in basal cells due to *BRCA1* mutation appear to facilitate their transformation into luminal progenitor cells. Our findings shed light on the pre-cancer epigenomic dynamics due to *BRCA1* mutation and how they may contribute to eventual development of predominantly basal-like breast cancer.

2.2 Background

Breast cancer is the most prevalent cancer in women, and is the cancer women are most likely to die from.[43] In fact, it is the leading cause of death of women between 35 and 55.[44] At least one in ten women get breast cancer at some point in their life.[45] While mortality from breast cancer is decreasing in developed countries, it is steadily increasing in less developed countries. Although only 5% of breast cancer cases are estimated to be due to genetic predisposition, it is believed to be responsible for 25% of cases diagnosed before a woman turns 30.[46] Despite the fact that there are multiple genes that are responsible for familial breast cancer inheritance, almost fifty percent can be attributed to mutations in BRCA1. First identified in 1990 and cloned in 1994, about 1 in 1000 individuals have a mutations in BRCA1 and those who do have a 46% – 87% chance of getting breast cancer in their lifetime.[46-51] Although there appears to be no relation between BRCA1 mutation and decreased odds of survival, women with early-onset breast cancer do have higher rates of metastasis, recurrence, and mortality.[52,53]

BRCA1 encodes a protein responsible for repairing DNA after double-stranded breaks and cell cycle checkpoint regulation; thus, BRCA1 mutations cause genomic

instability which can eventually lead to cancer.[51,54] Approximately 80% of BRCA1 mutation-based breast cancers are basal-like and/or triple-negative.[55] However, BRCA1 is expressed and functional in other tissues so there must be more than just a genetic component to BRCA1-mutation based breast cancer.

While DNA hypomethylation is common in many cancers, BRCA1 mutation breast cancers generally have even lower DNA methylation levels than sporadic breast cancer.[56] In normal tissue, BRCA1 positively regulates the expression of DNMT1, which is responsible for maintenance of DNA methylation levels.[57] Therefore, loss of BRCA1 function causes widespread DNA demethylation and is associated with increases in the gene expression levels of multiple proto-oncogenes. Despite this, BRCA1 mutant breast cancers do exhibit promotor hypermethylation of estrogen receptor alpha, which encodes ER and explains the decreased ER levels that often occurs in BRCA1 mutant breast cancer.[58]

BRCA1 is also capable of affecting histone modifications. BRCA1 has been shown to interact with the histone deacetylases HDAC1 and HDAC2.[59] Since histone acetylation is associated with open and active chromatin, the loss of BRCA1 function leads to activation of other components. For example, normal BRCA1/HDAC2 function is shown to repress the oncogenic microRNA miR-155 and BRCA1's absence increases miR-155 expression.[60] BRCA1 is part of a complex that ubiquitylates histone H2A, which has been shown to be critical for the suppression of satellite transcripts.[61] In the absence of BRCA1, the satellite DNA is transcribed into non-coding RNAs that cause widespread genomic instability and induces breast cancer.[62]

However, how these genetic alterations trigger the molecular cascades that ultimately lead to the pathology of tumorigenesis remains unclear. Breast tissue contains both epithelial and stromal compartments and the former can be further divided into basal (BCs), luminal progenitors (LPs), and mature luminal (MLs) cells based on their surface markers that are indicative of their developmental lineage and/or location in the two epithelial layers of the mammary duct [63]. These various cell types present characteristic gene expression patterns and epigenomic landscapes [64-67]. Recent studies have suggested that *BRCA1*-associated basal-like breast cancers originate from luminal progenitor cells instead of basal stem cells [68,69]. Furthermore, BRCA1 mutation appears to retard the differentiation of luminal progenitors into mature luminal cells.[70-72] Thus it is critical to understand how various cell types within breast tissue are affected by *BRCA1* mutation and how such dynamics in the cellular identity potentially contribute to tumorigenesis.

Epigenomic landscape plays a significant role in defining the cell state and mediating genetic factors into molecular cascades that are eventually involved in disease development. DNA sequence variation is known to impact epigenetic landscape, chromatin structures and molecular phenotypes via influencing the cis-regulatory elements such as promoters and enhancers[73-75]. The changes in the epigenetic landscape may in turn alter gene expression and cellular phenotypes to promote cancer development. *BRCA1* mutation has been recently discovered to significantly alter epigenomic functional elements such as enhancers in our study using breast tissue homogenates[76]. However, due to predominant basal-like characteristic of *BRCA1*-associated tumors, cell-type-specific profiling of tissue samples is needed to decipher

how each cell type within breast tissue is affected by the mutation and contributes to tumorigenesis.

In this study, we profile two important histone marks H3K4me3 and H3K27ac in a cell-type-specific manner in all four major cell types from pre-cancerous human breast tissue samples using a low-input ChIP-seq technology that we developed (MOWChIP-seq [18,20]). We compare the data on *BRCA1* mutation carriers (*BRCA1*$^{mut/+}$) and non-carriers (*BRCA1*$^{+/+}$) and extract epigenomic features that separate the two groups. Such comparison reveals that the extent of epigenomic changes varies among the four cell types. These epigenomic alterations potentially change the cell state and lay the groundwork for future tumorigenesis.

2.3 Methods

Breast tissues

Breast tissues were obtained from adult female cancer-free *BRCA1* mutation carriers (MUT) or non-carriers (NC) who underwent cosmetic reduction of mammoplasty, diagnostic biopsies, or mastectomy. All procedures were approved by the University of Texas Health Science Center at San Antonio. The consent forms were signed by donors to approve the use of the tissue for breast cancer research. Genetic testing of *BRCA1* mutation was conducted by the hospital[77]. Briefly, samples were minced and dissociated

for 18 hours in a 1:1 solution of Hams F12 and DMEM media supplemented with 2% wt/vol BSA, 300 U/mL collagenase, and 100 U/mL of hyaluronidase.

Sorting Cell Populations

To sort the cell populations, first the isolated cell suspension was incubated with 10% rat serum to prevent non-specific binding. Then, the cells were incubated with antibodies to APC-conjugated CD49f, FITC-conjugated EpCAM, Pacific Blue-conjugated streptavidin, and Biotin-conjugated CD45, CD235a, and CD31. Lastly, cells were incubated with 7-AAD. After gating to remove debris and doublets, cells that were live (7-AAD^{neg}) and not hematopoietic or endothelial cells (Lineage^{neg}, PacBlue^{neg}) were then separated into four fractions using FACS: EpCAM^{-}CD49f^{-} stromal cells (SCs), EpCAM^{low}CD49f^{high} basal cells (BCs), EpCAM^{high} CD49f^{+} luminal progenitor cells (LPs), and EpCAM^{high} CD49f^{-} mature luminal cells (MLs).

Chromatin Shearing

The sonication process to generate chromatin fragments is similar to what we described in previous publications[18,20]. A sorted cell sample of a specific type (containing 100K to 3 million cells, depending on the cell type and sample) was centrifuged at 1600 g for 5 min at room temperature and washed twice with 1 ml PBS (4 ˚C). Cells were resuspended in 1 ml of 1% freshly prepared formaldehyde in PBS and incubated at room temperature on a shaker for 5 min. Crosslinking was quenched by adding 0.05 ml of 2.5 M glycine and shaking for 5 min at room temperature. The crosslinked cells were centrifuged at 1600 g for 5 min and washed twice with 1 ml PBS (4 ˚C). The pelleted cells were resuspended in 130 μl of the sonication buffer (Covaris, 10 mM Tris-HCl, pH 8.0, 1 mM EDTA, 0.1% SDS and 1x protease inhibitor cocktail (PIC)) and sonicated with 105 W

peak incident power, 5% duty factor, and 200 cycles per burst for 16 min using a Covaris S220 sonicator (Covaris). The sonicated chromatin samples were shipped to Virginia Tech for MOWChIP-seq assay. The sonicated sample was centrifuged at 16,100 g for 10 min at 4 ˚C. The sheared chromatin in the supernatant was transferred to a pre-autoclaved 1.5 ml microcentrifuge tube (VWR). A fraction of the sonicated chromatin sample was mixed with IP buffer (20 Mm Tris-HCl, pH 8.0, 140 mM NaCl, 1 mM EDTA, 0.5 mM EGTA, 0.1% (w/v) sodium deoxycholate, 0.1% SDS, 1% (v/v) Triton X-100, with 1% freshly added PMSF and PIC) to generate a MOWChIP sample containing chromatin from 50,000 cells with a total volume of 50 μl.

Fabrication of MOWChIP Devices

PDMS devices are fabricated by multi-layer soft lithography and use a master as the mold. Masters are fabricated using photolithography. The device layout is designed using LayoutEditor (juspertor GmbH) and printed on 10k dpi transparencies (Fineline Imaging) to generate the photomasks. A photomask was generated for each of the two layers, fluidic and control. Next, the photoresist SU-8 2025 (MicroChem) is spun onto a 3-inch diameter silicon wafer (University Wafers). For the fluidic master, it was spun at 500 rpm for 10 seconds then at 2500 rpm for 30 seconds. For the control master, it was spun at 500 rpm for 10 seconds then at 1500 rpm for 30 seconds. The coated wafer was then baked at 95 °C for 8 minutes. The wafer was then covered with the appropriate photomask and exposed to UV light (575 mW) for 17 seconds followed by another 95 °C bake for 8 minutes. The wafer was then placed in SU-8 developer and developed for 3-5 minutes. After developing, the wafer was washed with isopropranol and dried with

pressurized air. SU-8 bonding was strengthened by baking the wafer one last time at 150 °C for 15 minutes.

Once the master was prepared, the device was fabricated with polydimethylsiloxane (PDMS) polymer (Momentive, RTV 615). For the fluidic layer, 5 parts of reagent A and one part of reagent B (~36 g total) were thoroughly mixed and poured into a petri dish containing the fluidic master. For the control layer, 20 parts of reagent A and one part of reagent B (~5.25 g total) were thoroughly mixed in a weigh boat. Both PDMS mixtures were then degassed for one hour to remove air bubbles. Once degassed, the PDMS for the control layer was spun onto the control master at 500 rpm for 10 seconds followed by 1100 rpm for 30 seconds. Both PDMS covered devices were baked for ~12 minutes at 80 °C to partially cure the PDMS. Once cooled, the fluidic layer was cut and peeled. Then, it was aligned onto the control layer and baked for an additional two hours. After the bake, the PDMS device was removed from the wafer, inlet holes punched with a 2-mm hole puncher and cut into multi-unit slabs. Each slab was bonded to a cleaned glass slide and bake for an additional hour to strengthen the bond.

MOWChIP-seq

We conducted MOWChIP-seq of the sonicated chromatin samples with 50,000 cells per assay for H3K27ac profiling and 10,000 cells per assay for H3K4me3 profiling, using protocols and microfluidic devices described in our previous publications[18,20]. We used anti-H3K27ac antibody (abcam, cat: ab4729, lot: GR323132-1) and anti-H3K4me3 antibody (Millipore, cat: 07-473, lot: 2930138) in these experiments.

Protein A-coated Dynabeads (Life Technologies) were washed twice with IP buffer (20 mM Tris-HCl [pH 8], 140 mM NaCl, 1 mM EDTA, 0.5 mM EGTA, 0.1% (w/v) sodium doxycholate, 0.1% SDS, 1% (v/v) Triton-100X in Milli-Q water) before being resuspended in 150 µL of IP buffer and 0.5 µg of H3K27ac (Abcam) antibody. The bead solution was then rotated at 4 °C for 2 hours. After incubation, beads were washed three times, resuspended in 5 µL of IP, and placed on ice until use.

For the operation of the MOWChIP device, the on-device valve was actuated by a solenoid valve in conjunction with a compressed air outlet. The solenoid valve was manipulated with a data acquisition card and through the LabVIEW (National Instruments) program. First, the on chip sieve valve is filled with water (30 psi). Once all the air has been expelled, the valve was opened and IP buffer is flowed through the inlet at a flow rate of 200 µL/min by use of a syringe pump connected to PFA tubing. The flow rate was decreased to 1 µL/min, the sieve valve closed, and IP buffer flowed for an additional 2 minutes before the flow was stopped and the tubing removed. The antibody-coated beads were loaded into the inlet by pipette and guided into the main chamber with a magnet. Next, the chromatin sample was flowed through at 1.5 µL/minute and the magnet was used to form the beads into a packed bed after five minutes of flow. Chromatin amount was equivalent to 50k cells for H3K27ac. After the chromatin was finished, IP buffer was flowed for 5 minutes at 1.5 µL/minute. Oscillatory washing was then performed with 50 µL of Low Salt washing buffer (20 mM Tris-HCl [pH 8], 150 mM NaCl, 2 mM EDTA, 0.1% SDS, 1% (v/v) Triton-100X in Milli-Q water) for five minutes at ~0.65 psi (valve open). Another five-minute oscillatory wash was performed with High Salt washing buffer (20 mM Tris-HCl [pH 8], 500 mM NaCl, 2 mM EDTA, 0.1% SDS, 1% (v/v) Triton-100X in Milli-

Q water). The sieve valve was closed and IP buffer flowed for an additional 2 minutes. Finally, the sieve valve was opened and the beads were flowed out at 200 µL/min with IP buffer.

ChIP DNA Isolation

Tubes containing IP beads were placed on a magnet and the supernatant removed. 100 µL of elution buffer (10 mM Tris-HCl [pH 8], 50 mM NaCl, 10 mM EDTA, 0.03% SDS in Milli-Q water) was added to the tube, followed by 4 µL of 20 mg/mL proteinase K. For the input sample, 90 µL of elution buffer and 4 µL of proteinase K were added. Samples were then incubated at 65 °C for 8 hours. Once completed, the samples were vortexed and briefly centrifuged. 100 µL of phenol-chloroform was added into each tube and vortexed for one minute, then centrifuged at 16,000 g for 10 minutes. The upper aqueous phase was carefully removed to a fresh tube. Next, an ethanol precipitation of the DNA was performed by adding 480 µL of 100% ethanol, 60 µL of 5 M ammonium acetate, and 6 µL of glycogen. The mixture was vortexed briefly and placed at -80 °C for two hours. Then, the samples were centrifuged at 16,100 g for 10 minutes at 4 °C and the supernatant removed. 500 µL of cold 70% ethanol was added and the samples were centrifuged for an additional five minutes. The supernatant was discarded and the DNA pellets were air dried for 10 minutes before resuspension in 12 µL of low EDTA TE buffer (Swift Biosciences).

Determining Sample Enrichment

For each sample and sample input, 2 µL of DNA was diluted to 20 µL with low EDTA TE buffer. A 20 µL qPCR reaction was assembled using 10 uL of SYBR Green Master Mix (BioRad), 1.4 µL of combined forward and reverse primers, and 8.6 µL of DNA

in a 96-well plate. Each histone mark was tested with at least one positive and one negative primer (Table 2-1):

Table 2-1 Human H3K27ac Primers

Name	Type	F/R	Primer
KLF6	Positive	F	GCG TTT ACC TGT TGC CAG TA
		R	CCA TGT GCA GCA TCT TCC A
BAZ1A	Positive	F	TCT CAA CTC CGC TCC TCT CT
		R	TGG GCT GGG CTT CGT TT
N-SLC	Negative	F	TTC CCA ACG TCA CAG AGT TAG
		R	GAC AGT ACA GCA CAG AGG TTA G
N-PER	Negative	F	GGT GCT CCC TGA TTG TTA GT
		R	CTT GTG CTT TGG GTC CAT TAA G

The qPCR was then performed by first denaturing the DNA for 2 minutes at 95 °C followed by 45 cycles of 95 °C for 15 seconds, 58 °C for 20 seconds, and 72 °C for 20 seconds. Once the qPCR was completed, the enrichment was determined by the following equation:

$$Enrichment = \frac{Percent\ input\ of\ positive\ locus}{Percent\ input\ of\ negative\ locus}$$

where the positive and negative percent inputs are calculated by:

$$Percent\ Input = 2^{\left(Ct_{input} - \frac{\log(Dilution\ Factor)}{log2} - Ct_{ChIP}\right)} \times 100\%$$

The Ct values of the input and ChIP were taken from the qPCR results and the dilution factor is defined as follows:

$$Dilution\ Factor = \frac{Sample\ vol.of\ input\ DNA + Sample\ vol.of\ ChIP\ DNA}{Sample\ vol.of\ input\ DNA}$$

ChIP-seq Library Preparation

Library preparation was performed using the Accel-NGS 2S Plus DNA Library Kit protocol (Swift Biosciences) with minor modifications as described below. For each library, 8 µL of sample was used. For all steps, we used options that pertained to samples with less than 10 ng of genomic DNA. At the end of the Ligation II clean-up, beads were

resuspended in 22 µL of low EDTA TE buffer. Then, 20 µL of the ChIP sample was used in the PCR-Library Amplification step, along with 2.5 µL of 20X EvaGreen dye (Biotium) to monitor the amplification. Amplification was stopped when the fluorescent intensity of a sample had increased by 3000 RFU over its baseline (typically ~13-14 cycles). After the library bead clean-up, samples were resuspended in 10 µL of low EDTA TE buffer and the library enrichment was determined. Libraries were quantified using a KAPA Library Quantification kit (KAPA Biosystems) and fragment sizes were verified using the High Sensitivity DNA Analysis kit on a TapeStation (Agilent). Libraries were pooled to a final concentration of 10 nM and sequenced with an Illumina HiSeq 4000 using single-end 50 bp reads.

Data Quality Control

ChIP-seq data sets that had fewer than 10,000 called peaks were discarded. After quality control, the technical replicates of the same cell sample were combined for the data analysis. As the result, we obtained 3 biological replicates for MUT H3K27ac samples, 4 biological replicates for NC H3K27ac samples, 2 biological replicates for MUT H3K4me3 samples, and one biological replicate for the NC H3K4me3 sample. The fraction of reads in peaks (FrIP) was calculated using the number of mapped reads within peak regions divided by total mapped reads. Normalized-strand correlation (NSC) and relative-strand correlation (RSC) was calculated using phantompeakqualtools[78,79].

Data Processing

Unless otherwise mentioned, all data analysis was performed with Bash scripts or with R (The R Foundation) scripts in RStudio. Sequencing reads were trimmed using default settings by Trim Galore! (Babraham Institute). Trimmed reads were aligned to the

hg19 genome with Bowtie[80]. Peaks were called using MACS2 ($q < 0.05$)[81]. Blacklisted regions in hg19 as defined by ENCODE were removed to improve data quality[82]. Mapped reads from ChIP and input samples were extended by 100 bp on either side (250 bp total) and a normalized signal was calculated.

$$Normalized\ Signal = \left(\frac{ChIP\ Signal}{No.of\ ChIP\ Reads} - \frac{Input\ Signal}{No.of\ Input\ Reads}\right) \times 10^6$$

For Pearson's correlation, the signal was calculated around the promoter region (TSS +/- 2 kb) and plotted with the corr and levelplot functions. For visualization in IGV (Broad Institute), the signal was calculated in 100 bp windows over the entire genome and output as a bigWig file.

Differential Analysis

To determine peak regions with differential signal, the Bioconductor package DiffBind was used[83,84]. A 'majority-rules' consensus peak set was generated for each experimental group and combined to make a master set for analysis. Peaks were considered to be valid if they were present in the majority of biological replicates. Counts were generated using default conditions and compared using the DESeq2 option. Normalized signal counts were extracted and plotted in heatmaps and boxplots using ggplot2[85]. Gene ontology analysis was performed using the web-based tool GREAT 4.0.4[86] with default settings for hg19. For the SC analysis, the top 6,000 regions (by smallest FDR value) were used.

Enhancers Analysis

To call enhancers, we considered H3K27ac^{high} regions that did not intersect with promoter regions to be enhancer regions. First, consensus H3K27ac peak sets were

generated for NC and MUT samples for each cell type after determining the set of peak regions present in NC and/or MUT samples. Peak widths were expanded to be 1000 bp long (summit +/-500 bp). Promoters were defined as TSS +/- 500 bp. Any H3K27ac 1 kb regions that intersected with a promoter region was removed and the remaining regions were designated as enhancers. Motif analysis was performed to determine enriched transcription factor binding motifs among the enhancer regions with HOMER[87] (with options –size 1000 –mask –p 16 –nomotif). Functional classification of transcription factors was performed using Panther v15.0.0[88]. Enhancers were mapped to genomic regions with ChIPSeeker[89]. Enhancers were considered associated with ER-negative SNPs (obtained from NHGRI-EBI GWAS Catalog[90]) if the SNP was within 150 kb up- or downstream.

2.4 Results

Breast tissues from *BRCA1* mutation carriers (MUTs, n = 3) and non-carriers (NCs, n = 4) were collected during breast reduction or mastectomy surgery, dissociated, and sorted into the basal, luminal progenitor, mature luminal, and stromal cell (SC) types (Fig. 2-1a)[91]. We profiled H3K4me3 and H3K27ac using MOWChIP-seq with at least two technical replicates for each cell sample (Tables 2-2 and 2-3). All samples had a fraction of reads in peaks (FrIP), normalized-strand correlation (NSC), and relative-strand correlation (RSC) that fell within ENCODE guidelines [79]. H3K4me3 is an activating mark that is associated with transcriptional start sites of genes [92,93] and H3K27ac labels active enhancers [6]. Our ChIP-seq datasets are highly correlated between technical replicates with an average Pearson correlation coefficient r of 0.962 for H3K4me3 and 0.950 for H3K27ac. We also observed very high genome-wide correlations among biological replicates in a group (MUTs or NCs), with an average r of 0.960 for H3K4me3 and 0.918 for H3K27ac (Fig. 2-1b). Generally, H3K4me3 is not a strong differentiating mark for separating MUTs and NCs. The correlation r between NCs and MUTs H3K4me3 data is high for all cell types (0.962 for BCs, 0.960 for LPs, 0.962 for MLs and 0.960 for SCs) (Fig. 2-2). In contrast, when genome-wide H3K27ac is examined, many more differential peaks are observed between MUTs and NCs and among various cell types (Fig. 2-1c). BCs and SCs show large difference between MUTs and NCs (with an average r of 0.739 and 0.877, respectively). In comparison, LPs and MLs have similar H3K27ac profiles between MUT and NC (with an average r of 0.914 and 0.888, respectively).

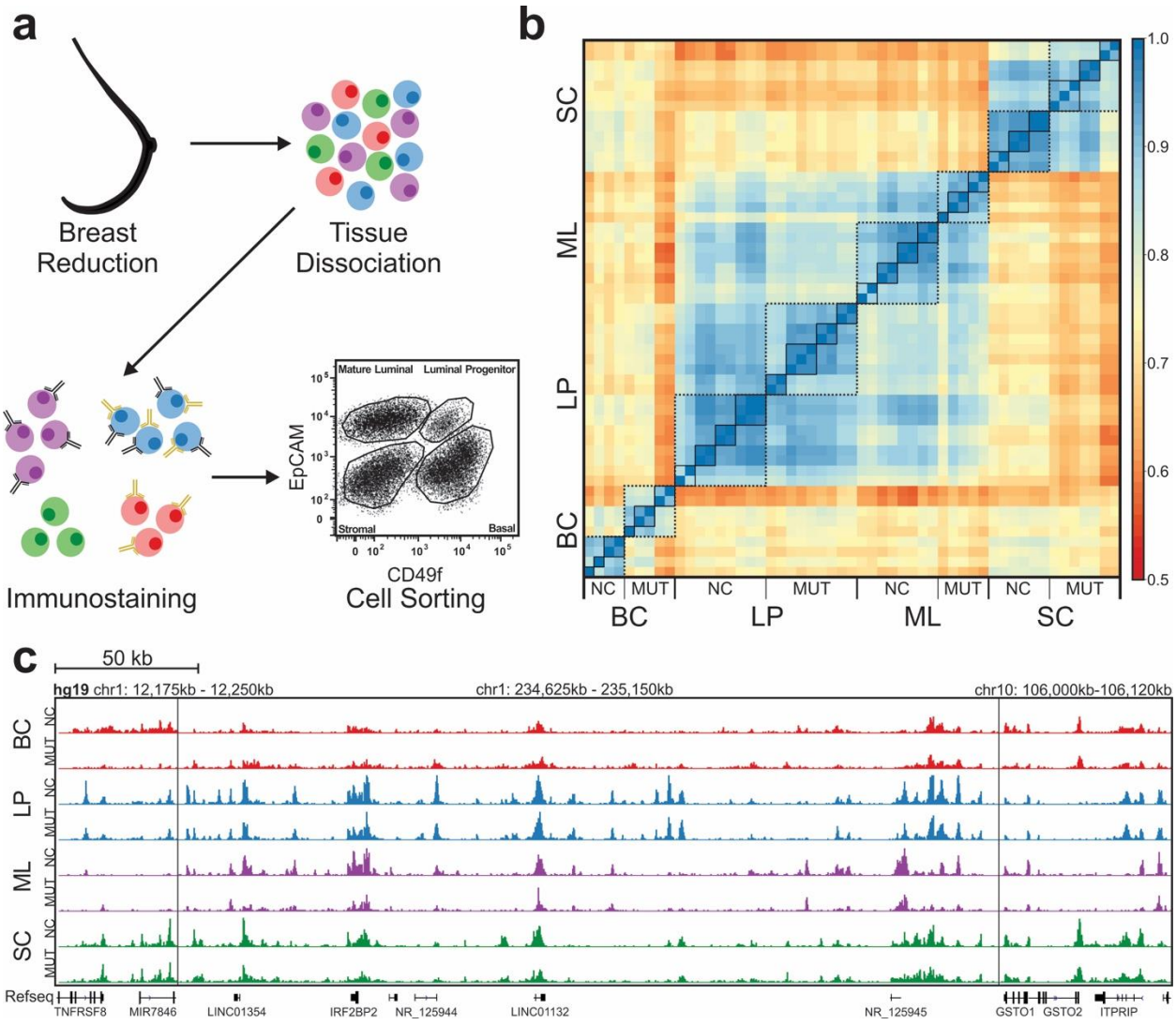

Figure 2-1 Cell-type-specific ChIP-seq data on human breast samples from BRCA1

(a) Breast tissue samples of mutation carriers (MUTs) and non-carriers (NCs) were separated into the basal cells (BCs), luminal progenitor cells (LPs), mature luminal cells (MLs), and stromal cells (SCs) by FACS. (b) Pearson correlations among H3K27ac ChIP-seq data sets of various cell types from NCs and MUTs around promoter regions (TSS +/- 2 kb). Each solid-line frame circles the technical replicates on one cell sample and each broken-line frame circles the data on a specific cell type. (c) Representative tracks of normalized H3K27ac signal for each of the cell types from NCs and MUTs. Three regions in the genome are presented and separated by vertical lines.

Table 2-2 H3K27ac Metadata

Cell Type	Sample	Total Reads (millions)	Trimmed Reads (millions)	Aligned Reads (millions)	Alignment (%)	Duplication (%)	Peaks	FrIP (%)	NSC	RSC
BC	NC1	19.6	19.5	18.8	96.3	10.3	13,581	3.2	1.03	1.52
	NC2	16.4	15.4	14.2	92.2	38.3	19,319	4.2	1.11	4.23
	NC4	10.1	10.1	9.6	95.5	7.9	5,910	1.4	1.03	1.57
		17.7	17.4	16.7	95.7	9.3				
	NC Input	9.0	8.8	8.1	91.1	7.1	-	-	-	-
	MUT1	19.8	19.7	18.9	96.0	16.4	20,883	3.2	1.03	2.92
	MUT2	18.6	18.6	18.0	97.1	32.1	42,252	7.4	1.02	1.86
		16.2	16.1	15.7	97.1	30.0				
	MUT3	18.6	18.6	18.1	97.7	14.4	18,718	2.6	1.02	1.82
		13.6	13.6	13.2	97.2	13.1				
	MUT Input	16.7	16.7	15.3	91.6	11.7	-	-	-	-
LP	NC1	14.1	14.1	13.3	94.2	68.0	37,362	8.1	1.14	4.00
		16.9	16.8	15.9	94.6	71.0				
	NC2	22.8	22.3	21.2	95.2	14.3	53,218	23.3	1.18	1.41
		13.6	13.5	12.9	95.8	11.5				
	NC3	13.8	12.8	13.2	95.6	13.3	51,651	17.7	1.10	1.46
		22.1	21.9	21.0	96.0	13.2				
	NC4	5.2	5.2	5.0	96.4	6.0	49,647	21.9	1.15	1.48
		23.3	23.0	22.2	96.5	13.8				
		31.2	30.3	28.7	94.9	13.5				
	NC Input	15.3	15.2	14.0	92.0	11.7	-	-	-	-
	MUT1	14.6	14.6	14.0	96.3	13.7	52,641	15.7	1.07	1.55
		15.2	15.1	14.4	95.7	16.5				
		20.6	20.5	19.7	96.0	13.3				
	MUT2	13.0	13.0	12.7	97.2	30.1	70,990	21.1	1.08	1.63
		21.4	21.4	20.8	97.1	31.6				
	MUT3	14.8	14.7	14.3	97.0	12.8	40,357	9.2	1.05	1.82
		13.3	13.3	13.0	97.2	13.5				
	MUT Input	19.4	19.4	17.7	91.4	9.5	-	-	-	-
ML	NC1	12.1	11.7	11.0	93.8	66.5	21,702	5.8	1.14	3.83
		14.0	13.8	13.0	94.6	55.3				
	NC2	12.2	12.1	11.4	94.8	12.7	16,062	5.0	1.06	1.66
		16.2	16.0	15.2	95.1	16.5				
	NC3	19.6	19.5	18.9	96.8	10.6	31,709	12.2	1.08	1.45
		16.7	16.7	16.1	96.6	8.0				
	NC4	41.9	41.7	40.6	97.2	17.9	32,428	11.8	1.08	1.45
		44.3	43.7	42.4	97.0	14.1				

	NC Input	8.5	8.5	7.8	91.9	7.0	-	-	-	-
	MUT1	15.6	15.5	14.8	95.5	17.8	14,831	2.8	1.03	2.50
	MUT2	18.3	18.3	17.7	96.9	34.5	49,674	17.5	1.11	1.82
		17.9	17.9	17.4	97.1	33.5				
	MUT3	13.5	13.5	13.1	96.9	12.4	17,262	4.7	1.04	1.76
		14.0	14.0	13.6	97.1	15.6				
	MUT Input	11.5	11.5	10.5	91.4	10.5	-	-	-	-
SC	NC1	13.9	13.8	13.1	94.4	61.6	51,558	16.3	1.20	2.50
		13.6	13.5	12.9	95.6	59.8				
	NC2	17.3	17.2	16.6	96.7	12.8	44,403	15.8	1.13	1.58
		11.7	11.7	11.2	96.4	11.7				
	NC4	38.5	38.5	37.0	96.2	13.6	52,229	22.7	1.11	1.59
		28.4	28.4	27.5	96.8	9.6				
	NC Input	11.5	11.5	10.6	92.0	9.6	-	-	-	-
	MUT1	14.0	14.0	13.5	96.3	11.8	13,028	2.1	1.02	1.82
		13.1	13.0	12.4	95.8	12.1				
		13.0	13.0	12.2	93.7	12.7				
	MUT2	22.5	22.5	21.9	97.6	32.9	51,265	12.9	1.06	2.08
		16.7	16.7	16.3	97.4	27.9				
	MUT3	12.4	12.4	12.0	97.4	11.7	16,566	2.3	1.02	1.84
		13.4	13.3	13.0	97.5	12.6				
	MUT Input	16.5	16.5	15.1	91.8	8.7	-		-	-

Table 2-3 H3K4me3 Metadata

Cell Type	Sample	Total Reads (millions)	Trimmed Reads (millions)	Aligned Reads (millions)	Alignment (%)	Duplication (%)	Peaks	FrIP (%)	NSC	RSC
BC	NC5	17.3	17.0	16.1	94.8	19.0	27,186	16.1	1.14	1.66
		13.8	13.7	13.0	95.3	16.6				
	NC Input	9.0	8.8	8.1	91.1	7.1	-			
	MUT2	16.3	16.3	15.4	94.4	24.6	29,507	10.1	1.07	1.93
		15.8	15.8	14.9	94.5	24.4				
	MUT3	13.6	13.6	13.0	95.8	15.8	28,811	13.3	1.10	1.64
		14.7	14.7	14.0	95.5	16.4				
	MUT Input	16.7	16.7	15.3	91.6	11.7	-			
LP	NC5	18.4	18.4	17.4	94.6	26.5	33,050	16.0	1.14	1.80
	NC Input	15.3	15.2	14.0	92.0	11.7	-			
	MUT2	12.7	12.6	11.7	93.1	27.4	29,066	10.1	1.06	1.60
		13.3	13.3	12.4	93.4	20.9				
		12.9	12.9	12.0	93.3	23.1				
	MUT3	13.9	13.7	12.8	93.4	15.6	24,822	8.1	1.06	1.87
		12.6	12.5	11.9	94.9	15.5				
	MUT Input	19.4	19.4	17.7	91.4	9.5	-			
ML	NC5	13.1	12.9	12.3	96.9	17.6	22,748	11.9	1.12	1.67
		13.6	13.5	12.8	95.0	16.5				
	NC Input	8.5	8.5	7.8	91.9	7.0	-			
	MUT2	13.0	11.9	11.2	94.0	27.7	27,980	14.9	1.14	1.67
		15.4	14.2	13.1	92.8	26.8				
		13.8	12.8	12.0	93.6	25.8				
	MUT3	15.1	14.4	13.9	96.5	16.0	19,290	7.3	1.07	1.84
		12.6	12.0	11.6	96.6	15.0				
	MUT Input	11.5	11.5	10.5	91.4	10.5	-			
SC	NC5	11.3	11.3	10.7	94.8	18.5	25,504	15.3	1.16	1.82
		15.1	14.9	14.2	94.9	20.3				
	NC Input	11.5	11.5	10.6	92.0	9.6	-			
	MUT2	16.0	16.0	15.1	94.3	25.2	27,806	10.4	1.08	1.90
		13.8	13.8	13.0	94.2	21.4				
	MUT3	14.4	14.4	13.6	95.0	16.4	23,838	9.3	1.07	1.86
		12.3	12.3	11.7	95.3	13.5				
	MUT Input	16.5	16.5	15.1	91.8	8.7	-			

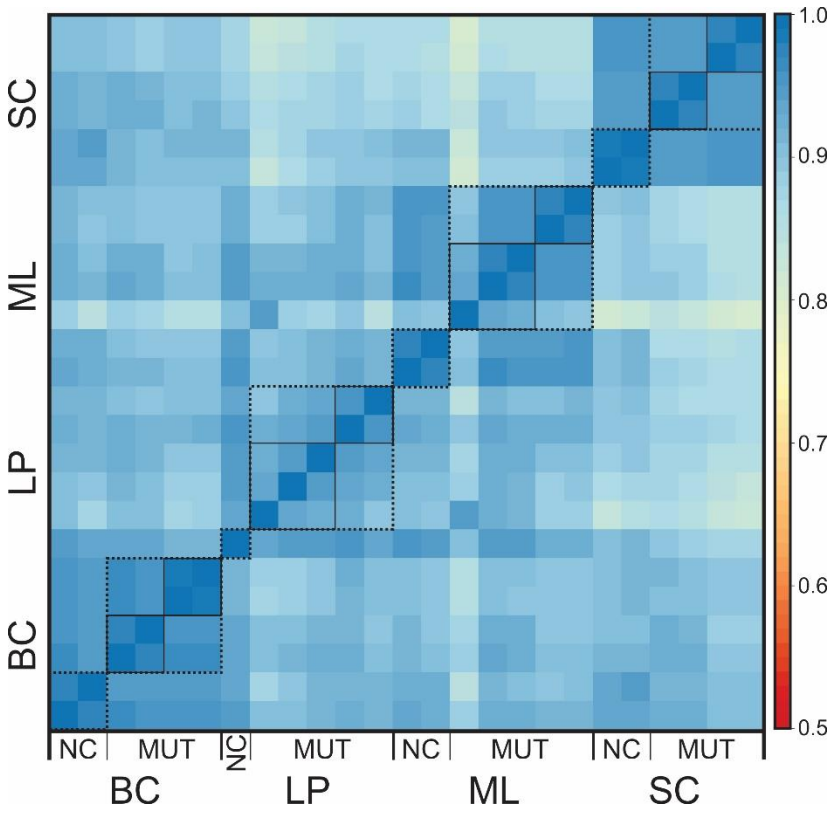

Figure 2-2 Correlation of BRCA1 H3K4me3 ChIP-seq data sets

Pearson correlation of various cell types from NCs and MUTs around promoter regions (TSS +/- 2 kb). Each solid-line frame circles the technical replicates on one cell sample and each broken-line frame circles the data on a specific cell type.

In terms of differences among various cell types, BCs, LPs, and MLs have very similar H3K4me3 profiles (average r of 0.926 among MUTs and 0.946 among NCs) and SCs show some differences from LPs and MLs (average r of 0.881 and 0.915 between SCs and LPs, 0.875 and 0.919 between SCs and MLs in MUT and NC, respectively). With H3K27ac data, LPs and MLs correlate with each other fairly well (average r = 0.832 and 0.872 in MUTs and NCs, respectively) while the other pairs have much lower correlation (with average r in the range of 0.668-0.794).

We carefully examined differentially modified H3K27ac peak regions (fold-change ≥ 2, FDR < 0.05) between MUTs and NCs (Fig. 2-3a). We found very few differential regions in LPs and MLs (518 and 2, respectively). However, there were a substantial number of differential peaks present in BCs (3,545) and a large number of different peaks in SCs (19,946). BCs had a mix of regions that showed either higher or lower H3K27ac signal in MUTs than in NCs (1,497 and 2,048, respectively), while the vast majority of differential regions in SCs (19,367 out of 19,946) had lower H3K27ac signal in MUT samples. We then compared the normalized H3K27ac signal at all peak regions (Fig. 2-3b). The median values were similar between NC and MUT patients in all epithelial cell types (with MUT values within ± 5% of NC ones), while there was a marked decrease in H3K27ac median signal in MUT SCs (by 13.5% compared to NC SCs).

The differentially modified H3K27ac regions were then mapped to their nearest genes. These differential regions were associated with 783, 3,972, and 12,160 genes in LPs, BCs, and SCs, respectively. We also conducted gene ontology enrichment analysis on these three cell types. The analysis on LPs did not bring out any GO terms. Thus our focus was on BCs and SCs which had the largest numbers of differential

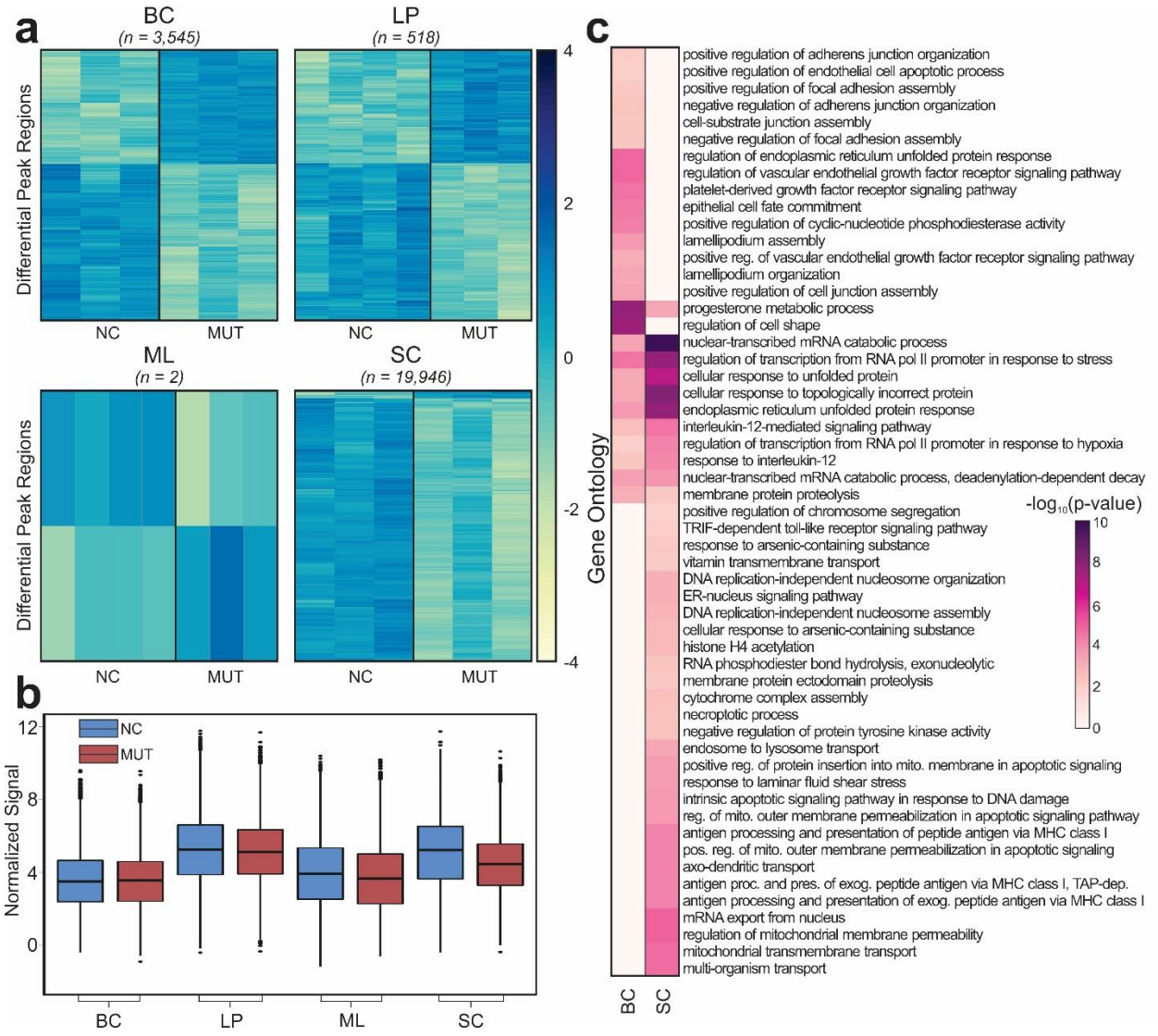

Figure 2-3 Differential H3K27ac peak regions between NCs and MUTs

(a) Heatmaps of differentially modified H3K27ac peak regions found to be significant (fold-change ≥ 2, FDR < 0.05) between NCs and MUTs. (b) Boxplots of normalized H3K27ac signal at all peak regions. (c) Gene ontology enrichment analysis using GREAT of significant differentially modified peak regions between NCs and MUTs.

H3K27ac regions between NCs and MUTs (Fig. 2-3c). A number of BRCA1-associated processes, including progesterone metabolism [94-97], RNA polymerase II transcription [98-100], and unfolded protein response (UPR) [101], were enriched in both BCs and SCs. BRCA1 has been shown to inhibit progesterone signaling [97] and reduction in BRCA1 level has been shown to increase expression of GRP78, a key UPR regulating gene [101]. Moreover, BRCA1 is part of the RNA polymerase II holoenzyme [98]. Ontologies related to apoptosis [102,103], antigen processing [104-106], and DNA damage response [107,108] are only significant in SCs. BRCA1 has extensive association with apoptosis, including those due to endoplasmic reticulum stress that is related to UPR [109]. For example, BRCA1 binding at the endoplasmic reticulum leads to a release of calcium that causes apoptosis. Furthermore, reduction in BRCA1 level has been shown to increase activation of $CD8^+$ tumor-infiltrating lymphocytes. There are also several ontologies associated with DNA damage response significant in SCs. For instance, DNA replication-independent nucleosome assembly and organization can only occur with histone variant 3.3, which is part of the DNA repair pathway [110,111]. In addition, histone H4 acetylation also opens up the chromatin for easier access to damaged regions [112]. In contrast, we largely see ontologies associated with cell motility and adhesion in BCs. *BRCA1* mutations have been shown to increase cell motility in cancer cells [113-115]. However, epithelial cell fate commitment is also present only in BCs. Cells within the BC compartment have been previously shown to have the potential to differentiate into LPs[116].

Next, we predicted enhancers present in each of the cell types for both NC and MUT samples (Fig. 2-4a). Enhancers were determined by finding H3K27ac^{high} regions

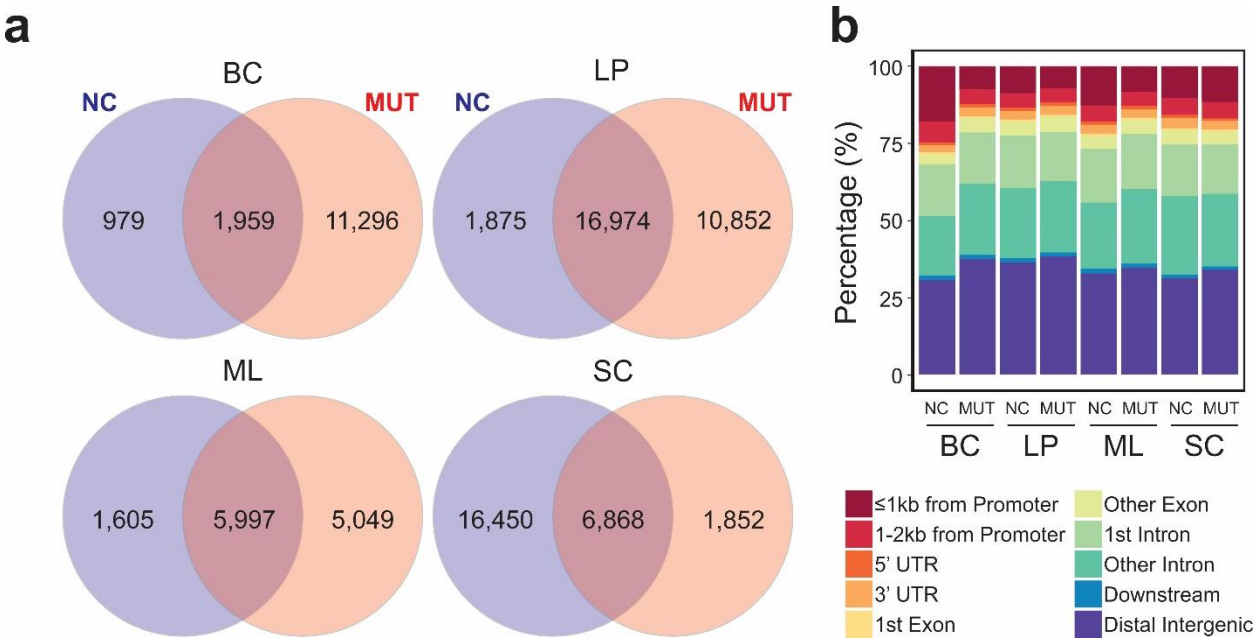

Figure 2-4 Enhancers predicted in various cell types from NCs and MUTs

(a) Venn diagrams of overlap between NC and MUT enhancers. (b) Genomic locations of the enhancers in various cell

that did not intersect with areas nearby transcription start sites (+/- 500 bp from TSS). Using the NCs as the reference, MUTs covers 67%, 90%, 79%, and 29% of the NC enhancers in BCs, LPs, MLs, and SCs, respectively. The enhancers were then mapped to genomic regions (Fig. 2-4b). The most exaggerated differences due to *BRCA1* mutation were seen in BCs, including a 6.9% increase in the distal intergenic fraction and 12.3% decrease in the promoter vicinity fraction (i.e. < 2 kb from promoters). It is clear that *BRCA1* mutation plays a different role in enhancer activity that is unique to each cell type.

Enhancer regions were then scanned to determine the transcription factor (TF) binding motifs significantly enriched in each cell population (Fig. 2-5). BCs had substantially more differentially enriched TF motifs than any other cell type, likely due to the smaller overlap between NC and MUT enhancers for BCs. In MUT samples, BCs primarily have many additional TFs, while SCs mainly lacked TFs. In all cases, over 50% of differentially enriched TFs were found to have no known link to *BRCA1* mutation. However, some TFs were found to be differentially enriched between MUT and NC in multiple cell types with known association with *BRCA1* mutation. These include *PAX5* [117] (BCs, MLs, and SCs), *CHOP* [101] (BCs and SCs), *EGR1* [118,119] (BCs and LPs), and *P73* [120] (BCs and SCs). Some TFs found were not associated with *BRCA1* yet were associated with breast cancer. These include *EGR2* [121,122](BCs, LPs, and SCs), *HOXC9* [123,124](BCs, MLs, and SCs), *HSF1* [125-127](BCs, LPs, and SCs), *NPAS2* [128](BCs, LPs, and MLs), and *USF1* [129](BCs, LPs, and MLs). We then used PANTHER to classify the differential TFs in each cell type into pathways, and found that Gonadotropin-releasing hormone (GnRH) receptor pathway, Wnt Signaling pathway, apoptosis pathway, and p53 pathways were

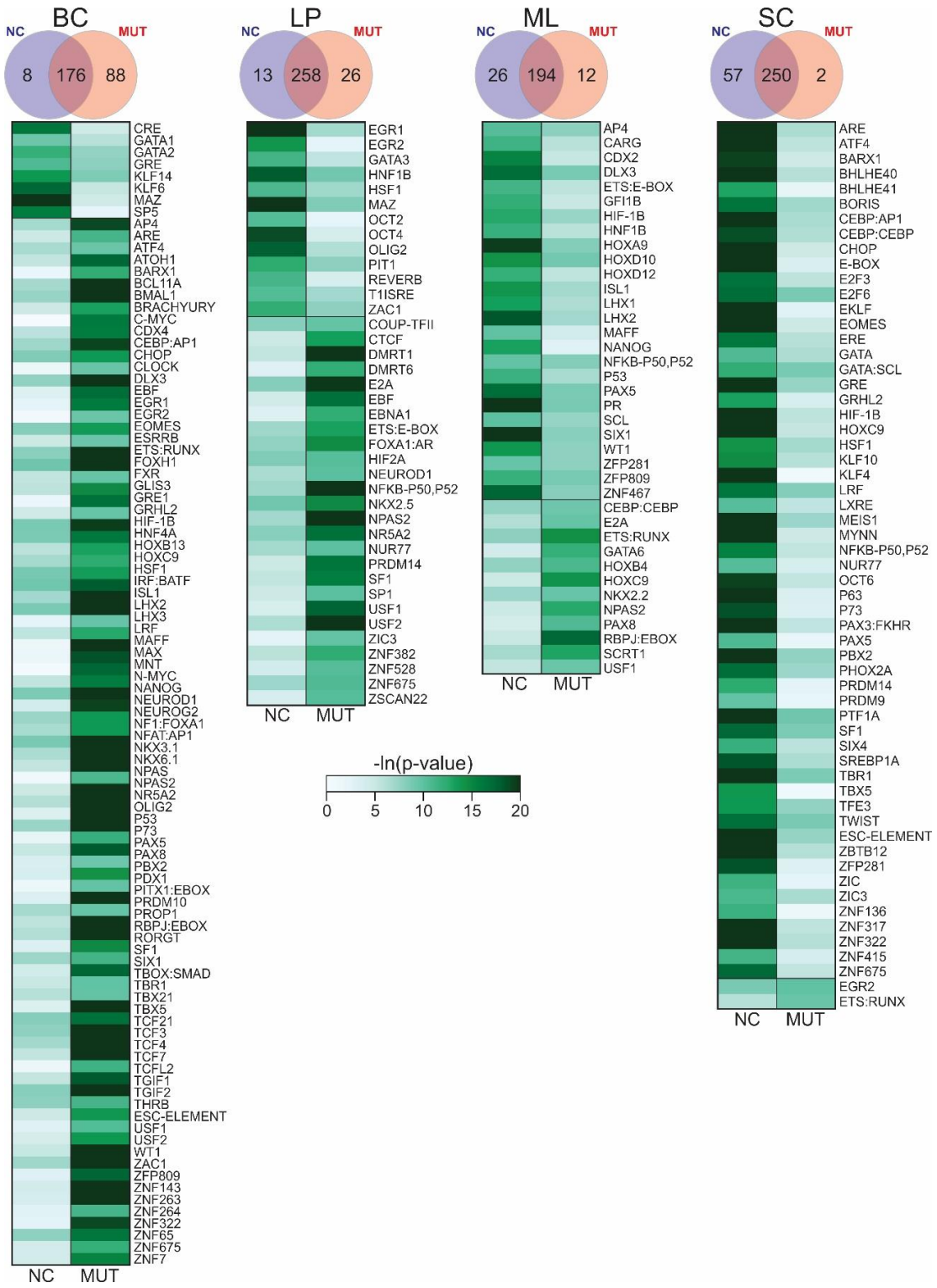

Figure 2-5 Heatmaps of motifs significant in either NC or MUT cell types

Heatmaps of motifs found to be significantly enriched in either NC or MUT but not both for various cell types. Color represents the level of significance. Venn diagrams of overlap between motifs enriched in NCs or MUTs are also presented.

enriched in all four cell types. *BRCA1* has a key role in the Wnt signaling pathway[130,131], regulates apoptotic responses[102,103], and has been shown to interact with *P53* [132-135]. As for the GnRH pathway, while there is not a direct link to BRCA1, GnRH agonists have been shown to be effective in the treatment of breast cancer [136].

Overall, we see the most significant epigenomic changes in BCs and SCs due to *BRCA1* mutation among the four cell types from these pre-cancer breast tissue samples, while much fewer variations were see in LPs. This is unexpected as LPs have been implicated as the driver in the onset of *BRCA1*-mutation associated breast cancer[70]. Thus we examine the possibility of basal cells differentiating into luminal cells, as proposed in previous literature [116]. First, we examined the cell-type specific genes identified for the three epithelial cell types (BCs, LPs, and MLs) in the literature [65]. The expression of these genes largely defines the identity of specific cell types. By comparing NC and MUT BCs, we found that 6% (44/712) of the BC-specific genes experiences significant changes in H3K27ac state due to the mutation, compared to 1% (4/305) for LPs and 2% (23/444) for MLs. Of these differentially marked basal genes, 95% had lower H3K27ac signal in MUT, suggesting that there is primarily a loss of basal gene expression in MUT basal cells. In the same fashion, we also examined cell-type-specific TFs in the three cell types and how they vary due to the mutation. Enriched TFs in each cell population were predicted based on motif analysis of enhancers profiled using H3K27ac data [137]. By examining NC samples, we extract 8, 55, and 6 cell-type-specific TFs (p-value < 0.0001) for BCs, LPs, and MLs, respectively (Fig. 2-6). In comparison, MUT BCs, LPs, and MLs preserved 6, 44, and 5 of these TFs, respectively. Interestingly, MUT BCs also enriched 28 of the LP-specific TFs and 3 of the ML-specific TFs, compared to MUT LP enriching 1 BC-specific

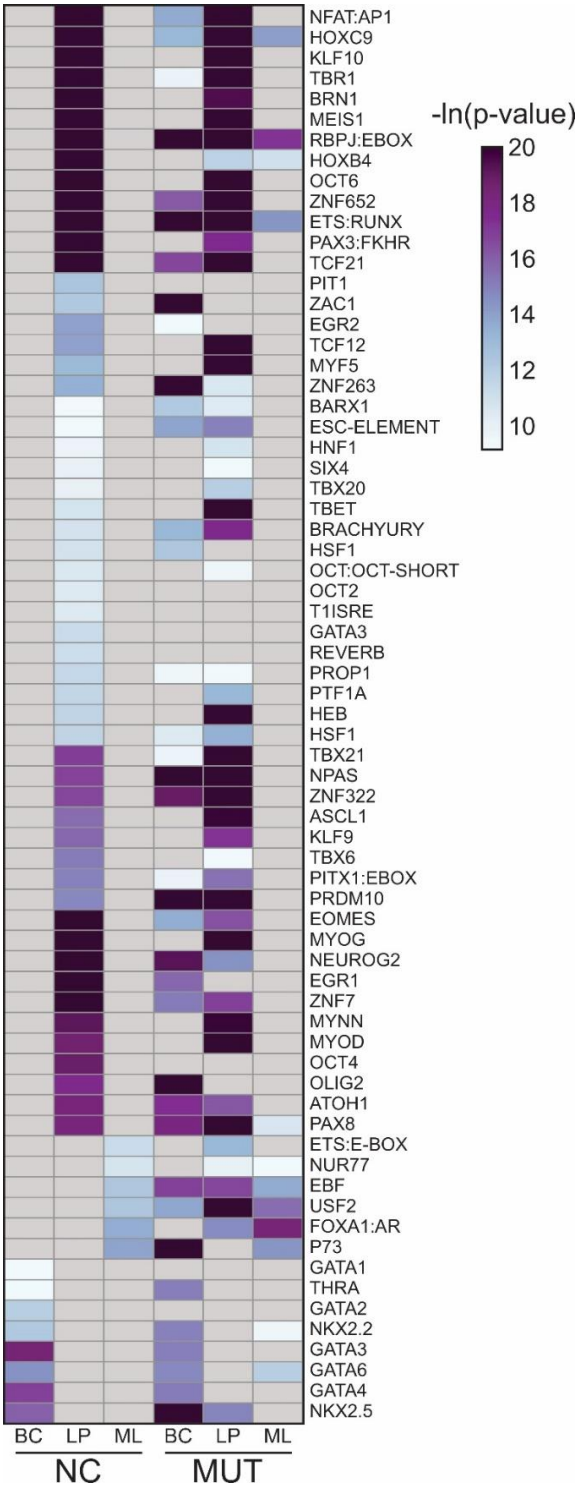

Figure 2-6 Enrichment of NC cell-type-specific motifs in NC and MUT

Heatmap of p-values for motifs found to be significantly enriched (p-value < 0.0001) in only one of three cell types (BCs, LPs, or MLs) from NCs and their enrichment in MUTs. Color represents the level of significance. All p-values that are insignificant are colored gray.

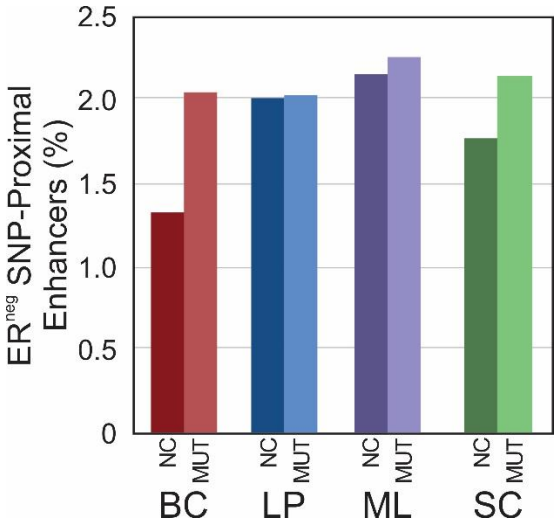

Figure 2-7 Proximity of enhancers to ER-negative breast cancer SNPs

Percent of enhancers that are within +/- 150 kb of SNPs significantly associated with ER-negative breast cancers through GWAS for all 4 cell types.

TFs and 5 ML-specific TFs, and MUT ML enriching 2 BC-specific TFs and 5 LP-specific TFs. These results indicate that the BC state experiences more substantial change than LPs and MLs due to *BRCA1* mutation, consistent with the notion of BC differentiation into LPs.

To further validate the possibility of the basal compartment being a significant contributor in *BRCA1*-mutation associated breast cancer, we determined the number of enhancers that were in proximity to 123 SNPs involved in ER-negative breast cancer as discovered by GWAS [90] (Fig. 2-7). ER-negative breast cancer is a term that effectively covers both basal-like and triple-negative breast cancers [138,139]. In a cohort of 3,797 BRCA1 mutation carriers diagnosed with breast cancer, 78% had ER-negative breast cancers [140]. Overall, we saw increases in the percent of enhancers that were proximal to ER-negative SNPs in each cell type due to BRCA1 mutation, suggesting an overall increase in breast cancer risk. However, we see the largest increase (~55%) between NC

and MUT BCs followed by SCs (~21%). This further supports that the BRCA1 mutation leads to profound epigenetic changes in BCs and that these changes have the potential to increase breast cancer risk.

2.5 Discussion

The interactions between genomics and epigenomics are well-recognized events. Gene mutation may alter epigenomic landscape in a significant way and such alternation may carry important implications on cancer development. Several lines of evidence support the feasibility of sorting out epigenomic differences between BRCA1 mutation carriers and non-carriers using a cell-type specific approach. First, we found very high correlations among biological replicates in both H3K4me3 and H3K27ac within either MUT or NC group. When we compare across the two groups (MUT vs. NC), H3K27ac is more differentiating than H3K4me3, which is consistent with previous findings by us [137] and others [141]. Second, we compared our NC data with published results obtained by examining normal breast tissues pooled from multiple individuals [65]. Each of the top 5 significantly enriched transcription factors in BCs, LPs, and MLs were also significantly enriched in our respective NC cell populations. Basal-associated transcription factors [65] such as TP53, TP63, STAT3, and SOX9 were also enriched in NC BCs. Similarly, luminal-associated transcription factors [142-144] CEBPB, GATA3, ELF5, and FOXA1 were all significantly enriched in our NC LP and MLs. Third, we found that three members of the GATA family (GATA1, GATA2, and GATA3) were enriched in either NC BCs or LPs, but not in MUT epithelial cells (Fig. 2-5 and 2-6). This agrees with our earlier study conducted using breast tissue homogenates [76]. GATA3 is known to be critically involved in the

regulation of luminal cell differentiation [145,146]. Finally, we also compared our cell-type-specific data with our published data on breast tissue homogenates obtained using a separate patient cohort and conventional ChIP-seq technology [76] (Fig 2-8). The H3K27ac data taken using the breast tissue homogenate (mix) do not differentiate MUT and NC. The homogenate data show a similar degree of correlations with all individual cell types (Pearson correlation in the range of 0.741-0.890). This also underscores the importance for cell-type-specific profiling to pinpoint specific roles for each cell type. These comparisons suggest that although epigenomic differences exist among individual humans [147,148], careful cell-type-specific ChIP-seq profiling captures important genome-wide epigenomic differences due to *BRCA1* mutation.

Epigenetic profiles define cell identity by regulating cell-type-defining genes and transcription factors. The difference in the epigenomic landscape between *BRCA1* mutants and non-carriers may be important for explaining the high propensity of *BRCA1* mutation carriers for breast cancer. Our data on a sensitive mark H3K27ac are the most different in BCs and SCs when MUTs and NCs are compared. In comparison, very few changes were observed in LPs and MLs due to the mutation. Furthermore, our analysis of the cell-type-specific genes and TFs also reveal that MUT BCs resemble LPs. Such resemblance was in accordance with previous reports on the presence of LP-fated cells and bi-potent mammary stem cells in the basal compartment [116,149]. Thus we propose that the precancerous process within *BRCA1* mutation carriers may start with substantial epigenomic changes in basal cells among all epithelial cell types and these basal cells share similarity with luminal progenitor cells. These findings provide new insights into epigenomic factors involved in BRCA1 cancer biology.

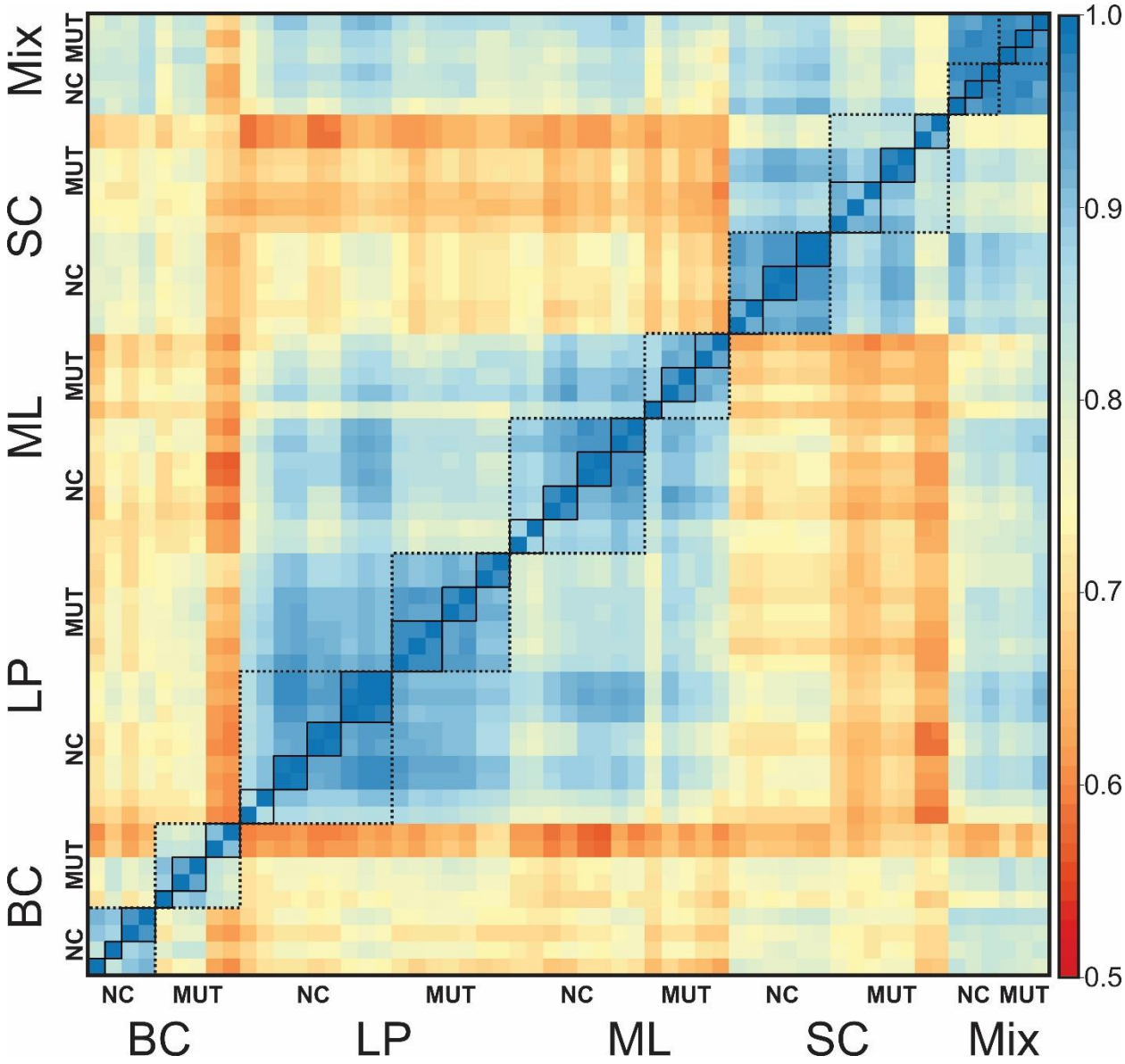

Figure 2-8 Correlation of cell-type-specific data and homogenate H3K27ac data

Pearson correlations among cell-type-specific and homogenate H3K27ac data. “Mix” refers to H3K27ac data (GSE121229 from GEO) obtained using human breast tissue homogenates containing epithelium-enriched cell population.

3 Epigenomic and transcriptomic differences between low-grade and acute inflammation in LPS-induced murine immune cells

---

Published Work

The work presented in this chapter was adapted from previously preprinted work noted below. Authors retain all copyright of figures.

Naler, L. B., Hsieh, Y.-P. Geng, S., Zhou, Z., Li, L., and Lu, C. Epigenomic and transcriptomic differences between low-grade and acute inflammation in LPS-induced murine immune cells. *bioRxiv* (2021) doi: 10.1101/2021.03.28.437377

Author Contributions

Chang Lu and Liwu Li designed the experiments and supervised the research. Shuo Geng conducted the animal experiments and produced the cell samples. Yuan-Pang Hsieh and Zirui Zhou conducted the ChIP-seq and RNA-seq assays. Lynette Naler analyzed the data. Lynette Naler, Yuan-Pang Hsieh, Shuo Geng, Liwu Li, and Chang Lu wrote the manuscript.

3.1 Project Summary

Chronic, low-grade inflammation has a widespread and significant impact on health, especially in Western-society. While inflammation is beneficial for the removal of microbes, low-grade inflammation never resolves and can cause or worsen other diseases. However, the process by which low-grade inflammation occurs is poorly understood. As lipopolysaccharide (LPS) is associated with chronic inflammatory diseases, we exposed murine bone-marrow derived monocytes to chronic LPS-stimulation at Low-dose (100 pg/mL) or High-dose (1 µg/mL), as well as a PBS control. The cells were profiled for H3K27ac expression and gene expression. The gene expression of TRAM-deficient and IRAK-M-deficient mice with LPS exposure was also

analyzed for mechanistic insight. We determined that many of the differences between the Low-dose and High-dose conditions are related to the TRIF-dependent pathway of TLR4 signaling. Furthermore, these changes are also seen in the epigenome, suggesting the epigenome may be what leads to the differential response. These findings further characterize the different means utilized in low-grade conditions, and how it might lead to a damaging, non-resolving state. Moreover, our data provide potential targets for future mechanistic or therapeutic studies.

3.2 Background

Low-grade, or chronic inflammation, plays a large role in the onset or exacerbation of many mental and physical diseases, including Alzheimer's disease[150], depression[151], diabetes[152], and some cancers[153]. Despite this, there still are no canonical markers for low-grade inflammation, partly due to a correlation of inflammatory activity with age[154,155]. Some recent studies in humans have attempted more sophisticated integrated approaches that show promise, but more research is required to identify key biomarkers and how they should be interpreted[155-157].

Low-grade inflammation is often associated with certain lifestyle choices, like Western-style eating practices[158], sedentary behavior[159,160], sleep deprivation[161], and social stress[162]. In fact, individuals who underwent major childhood stressors have elevated mortality and morbidity of immune or chronic diseases later in life, and epigenetic programming has been proposed[163]. This is further supported by twin studies that showed most variation in the immune system is due to non-heritable (e.g. epigenetic) influences[164].

In a bacterial infection, components of the pathogen[165] are recognized by pattern-

recognition receptors (PRRs) that are found on immune and non-immune cells[166-169]. This, in turn, leads to a signaling cascade that is used to recruit immune cells, such as neutrophils and monocytes/macrophages, which ingest the microbes or release anti-microbials[170,171]. Once the threat is eliminated, pro-inflammatory macrophages uptake spent neutrophils, which reprogram the macrophages to an anti-inflammatory state[172,173]. Anti-inflammatory macrophages help promote healing by protecting against tissue damage, clearing out debris, and producing growth factors[173]. However, when macrophage and monocyte inflammatory activity is not resolved then it can lead to low-grade inflammation and chronic diseases[76,174-178].

Lipopolysaccharide (LPS) is an endotoxin and component of the cell wall of Gram-negative bacteria, such as *Escherichia coli*, that also has been found at low levels in individuals who have chronic diseases or detrimental lifestyle choices as mentioned previously[179,180]. It has been used to study inflammation both *in vivo* and *in vitro*, although more often with high-doses of LPS. While persistent low-dose LPS has been shown to lead to a low-grade inflammatory state, the mechanism by which it does so is still not entirely known, though it could be due to sustained activity of the inflammatory NF-κB[180-183].

LPS stimulation activates two different pathways, which both have pro- and anti-inflammatory aspects. First, LPS binds to Toll-like receptor 4 (TLR4) and activates the MyD88-dependent pathway[180,184,185]. The MyD88-dependent signaling cascade activates mitogen-activated protein kinases (MAPKs), NF-κB translocation to the nucleus, transcription factors CREB and AP-1, as well as induces expression of pro-inflammatory genes such as TNF-α, IL-6, and COX-2[185]. However, it is also involved in the production

of anti-inflammatory cytokines like IL-10. In addition, MyD88-dependent signaling leads to an increase in glycolysis, synthesis of acetyl-CoA, and synthesis of fatty acids. Next, TLR4 is endocytosed, ending the MyD88-dependent pathway and triggering the TRIF-dependent pathway[185]. The TRIF-dependent pathway activates IRF3 and IRF7 to induce expression of type I interferons (IFN), CCL5, and CXCL10. It is also involved in anti-inflammatory cytokine IL-10 production and is important for TNF-α expression[185,186]. Furthermore, in macrophages, the TRIF-dependent pathway also upregulates cell-surface CD40, CD80, and CD86 which are necessary for antigen presentation for T lymphocytes, bridging the gap between the innate and adaptive immune system[185,187]. Finally, both pathways are involved in the canonical activation of the NRLP3 inflammasome, which is responsible for the activation of the inflammatory cytokine, IL-1β, and can cause pyroptosis, a form of programmed cell-death[185].

The epigenome plays a large role in the behavior and identity of macrophages. For example, the epigenome of tissue-resident macrophages is affected by their local microenvironment and they can even be reprogrammed by transplanting them to a different location[188]. They also have varied transcriptional signatures during efferocytosis, a process where apoptotic cells are cleared[189]. LPS-stimulation has also been shown to have a significant, and sometimes lasting, effect on the histone modifications of macrophages[190]. LPS-induced tolerance affects the epigenome of macrophages by inhibiting induction of inflammatory genes while leaving antimicrobial genes unaffected[191]. Research into means of targeting and altering the epigenome of inflammatory macrophages into an anti-inflammatory state has also increased in recent years, with studies showing possible therapeutic potential[192]. Despite this, there is little research on

how low-doses of LPS affect the epigenome[193-196] or transcriptome[196-200] of monocytes or macrophages differently compared to high-doses of LPS.

In this study, we profiled the histone mark H3K27ac and performed RNA-seq analysis of murine bone marrow-derived monocytes that are exposed to low and high-dose levels of LPS, as would be seen in low-grade and acute inflammation, respectively. H3K27ac marks active enhancers which, in conjunction with RNA-seq, allows us to determine how the epigenome affects gene expression. Low-input technologies including Microfluidic Oscillatory Washing ChIP-seq (MOWChIP-seq[20,201]) and Smart-seq2[202,203] were used for the epigenomic and transcriptomic profiling. We compared the conditions to extract the effects of LPS-dosage on the epigenome and, in turn, the transcriptome of immune cells. Furthermore, we also analyzed the effects of TRAM deletion, necessary for the TRIF-dependent pathway[185], and IRAK-M deletion, which suppresses TLR-signaling and is associated with endotoxin tolerance[204]. Altogether, this analysis could help elucidate the means by which subclinical concentrations of endotoxin can lead to low-grade inflammation as opposed to acute inflammation.

3.3 Results

Bone marrow-derived monocytes (BMDMs) were isolated from mice and dosed with PBS, low-dose LPS (100 pg/mL), or high-dose LPS (1 µg/mL). We profiled H3K27ac using MOWChIP-seq[18] and performed RNA-seq with two replicates per condition (Tables 3-1 and 3-2). We found very high average correlation between ChIP-seq replicates of 0.9858 (Fig. 3-1a). Between conditions, the highest correlation is between PBS and low-dose (0.9572) and the lowest correlation between PBS and high-dose (0.8959), with low-dose and high-dose falling in-between (0.9385). This suggests that the increasing LPS dosage causes a concomitant change to H3K27ac signal. When looking at genome-wide H3K27ac signal, we see that increasing the dose of LPS tends to reduce the H3K27ac signal (Fig. 3-1b). In fact, the overall H3K27ac signal at peaks also tends to go down with increasing LPS-dosage (Fig. 3-1c). Furthermore, the number of peaks present in each sample as decreased with increasing dosage (PBS = 25,679, Low = 21,597, High = 14,659).

As such, many of the peaks that were present in PBS samples were not present in Low-dose samples (6,566) and even more (12,602) were not present in High-dose (Fig. 3-1d). However, Low-dose samples gained a small number of peaks (2,484) while High-dose samples gained even fewer (1,582). In addition, the fraction of peaks near promoters increased with increasing LPS dosage, yet, this primarily was due to a reduction of distal peaks, rather than an increase of proximal peaks (Fig. 3-1e). However, some of the peaks gained by Low-dose and High-dose conditions were proximal to gene promoters. Since H3K27ac also localizes to active promoters, this suggests that dosage of LPS leads to the activation of genes that are not active under normal conditions[205].

Table 3-1 WT H3K27ac Metadata

Sample	Total Reads (millions)	Trimmed Reads (millions)	Aligned Reads (millions)	Alignment (%)	Peaks	Consensus Peaks
PBS – 1	13.8	13.8	12.0	87.1	34,372	25,679
PBS – 2	15.9	15.9	14.0	88.0	46,067	
Low – 1	21.4	21.3	18.2	85.4	34,967	21,597
Low – 2	19.4	19.4	16.8	86.8	28,091	
High – 1	19.4	19.4	16.6	83.5	20,685	14,659
High – 2	21.0	21.0	18.1	86.2	23,775	

Table 3-2 RNA-seq Metadata

Genotype	Sample	Total Reads (millions)	Trimmed Reads (millions)	Aligned Reads (millions)	Alignment (%)
WT	PBS-1	18.0	18.0	15.0	83.4
	PBS-2	16.9	16.9	14.3	84.7
	Low-1	15.6	15.6	12.9	83.2
	Low-2	15.1	15.1	12.6	83.8
	High-1	16.8	16.8	14.2	84.5
	High-2	14.0	14.0	11.9	85.3
TRAM$^{-/-}$	PBS-1	13.7	13.7	10.9	79.5
	PBS-2	14.2	14.2	11.7	82.2
	Low-1	14.0	14.0	11.3	80.7
	Low-2	15.0	14.9	11.8	79.1
	High-1	30.4	30.4	25.2	83.1
	High-2	14.2	14.2	11.0	77.9
IRAK-M $^{-/-}$	PBS-1	13.4	13.4	11.1	82.7
	PBS-2	17.7	17.7	14.8	83.8
	High-1	16.2	16.2	13.8	85.4
	High-2	18.3	18.3	14.7	80.7

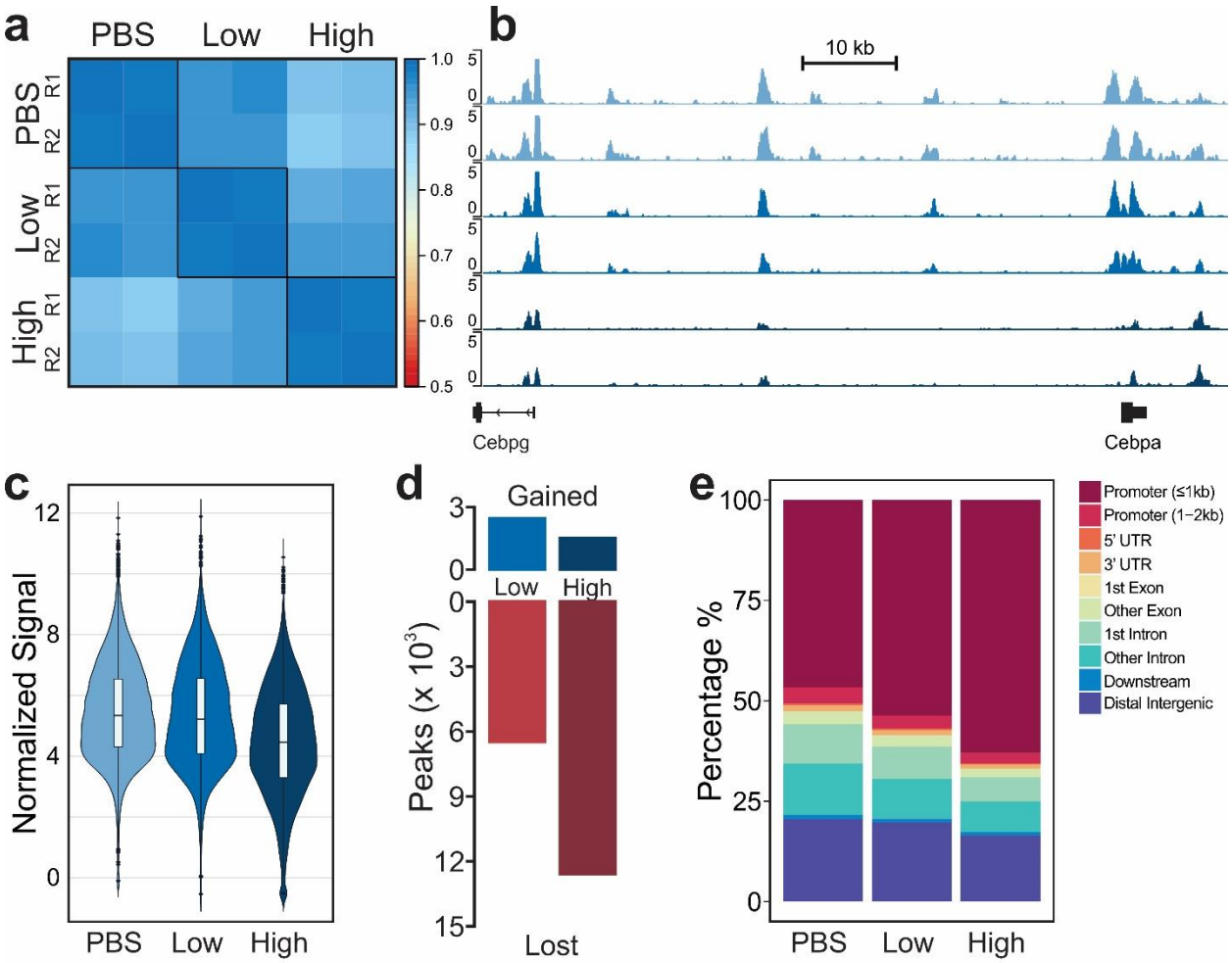

Figure 3-1 Overview of ChIP-seq data for murine BMDMs dosed with PBS or LPS

(a) Pearson's correlation of normalized H3K27ac signal around promoter regions (TSS +/- 2 kb). (b) Tracks of normalized H3K27ac signal for replicates dosed with PBS, low-dose LPS, or high-dose LPS. Add vertical scale. (c) Distribution of normalized H3K27ac signal at peaks. (d) Number of peaks gained or lost in low-dose or high-dose conditions compared to PBS. (e) Percentage of peaks at genomic locations.

Although H3K27ac does mark active transcription, it plays a more pivotal role in long-range gene regulation at enhancer regions. Therefore, we determined the locations of enhancers, which were defined as H3K27ac^{high} regions that do not overlap with regions near transcription start sites and can be linked to genes in conjunction with RNA-sequencing data (see Methods). The number of enhancers also decreased with increasing LPS-dosage (PBS=5,738, Low=4,400, High=2,711). Normalized H3K27ac signal for the conditions at each enhancer was clustered with k-means clustering (Fig. 3-2a). The genes linked to the enhancers in each of the clusters were analyzed for overrepresentation of Gene Ontology biological process gene sets (Fig. 3-2b). We then separated these into three groups: dosage correlated, acute inflammation and low-grade inflammation.

The dosage correlated group, including clusters I, II, and III, had either increased or decreased H3K27ac signal with increased LPS-dosage. Due to the binary nature of histone modifications, this means that increased LPS dosage leads to a higher fraction of cells with either presence or absence of H3K27ac at enhancers linked to the genes in these clusters. Most obviously, we see that Cluster I, which increases in expression from PBS to High-dose, is filled with leukocyte-related (which include monocytes and macrophages) gene ontologies, which play a key role in inflammation[206,207]. As such, it is reasonable that with increased LPS-dosage we would see a stronger inflammatory response. In Clusters II and III, which decreased from PBS to High-dose, we see several pathways related to autophagy and endocytosis. It has been shown in literature that LPS-stimulation induces autophagy as a means of mediating the inflammatory response[208-211]. Upon further investigation into the enhancer-linked genes in these autophagy-related

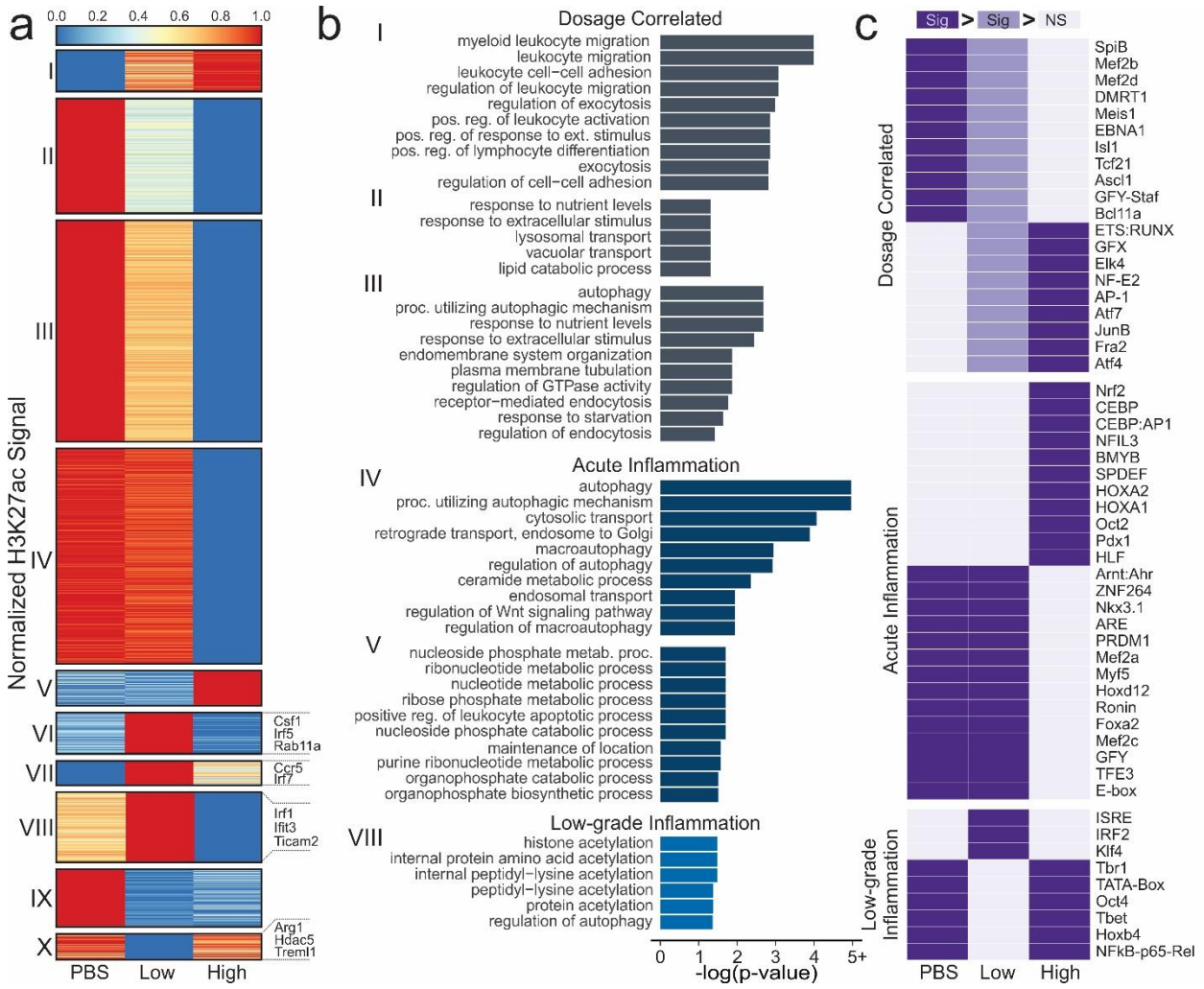

Figure 3-2 Effect of LPS dosage on enhancers

(a) K-means clustering of enhancers present in PBS, Low-dose, or High-dose samples (b) Significant (FDR < 0.05) Gene Ontology biological process gene sets for clusters from (a). (c) Significantly enriched motifs ($p < 1 \times 10^{-6}$) that are different in two comparisons. One purple cell denotes enrichment over the two gray cells and two denotes enrichment over the third cell. One light and one dark purple signifies dark is enriched over light, and light is enriched over gray.

processes, we find genes such as Trem2[212], Sesn1[213], and Nrbf2[214], all of which inhibit the inflammatory effect of macrophages. Differential H3K27ac expression at gene promoters also shows that increased LPS-dosage reduces expression at genes that negatively regulate components of the TLR4 signalling pathway, such as the MAPK cascade (Fig. 3-3, Cluster III)[185,215,216]. This suggests that LPS stimulation may lead to the inhibition of anti-inflammatory genes, allowing for the pro-inflammatory aspects of the TLR4 signalling pathway to be freely utilized.

The acute inflammation group, where the signal was either substantially lower or higher in High-dose LPS compared to Low-dose LPS and PBS, consists of clusters IV and V. These enhancers are recognized as highly characteristic of the High-dose condition and associated acute inflammation. In Cluster IV, we once again see autophagy-related pathways. Gene promoters with substantially lower H3K27ac signal in High-dose cells were enriched in pathways for Il-6 and Il-8 production, which can have anti-inflammatory effects (Fig. 3-3, Cluster IV)[215,216]. In Cluster V, we see many nucleotide-associated metabolic and catabolic processes, which have been shown to be increased with LPS stimulation in literature[217,218]. It is unclear why these processes are not increased in Low-dose cells.

The low-grade inflammation group, in which signal was either substantially increased or decreased in Low-dose LPS when compared to High-dose LPS or PBS, consists of clusters VI, VII, VIII, IX, and X. These enhancers are recognized as highly characteristic of the Low-dose condition and associated low-grade inflammation. Only Cluster VIII had any significantly enriched terms, most of which were related to histone and protein acetylation, primarily acetylation at lysines. LPS stimulation has been shown

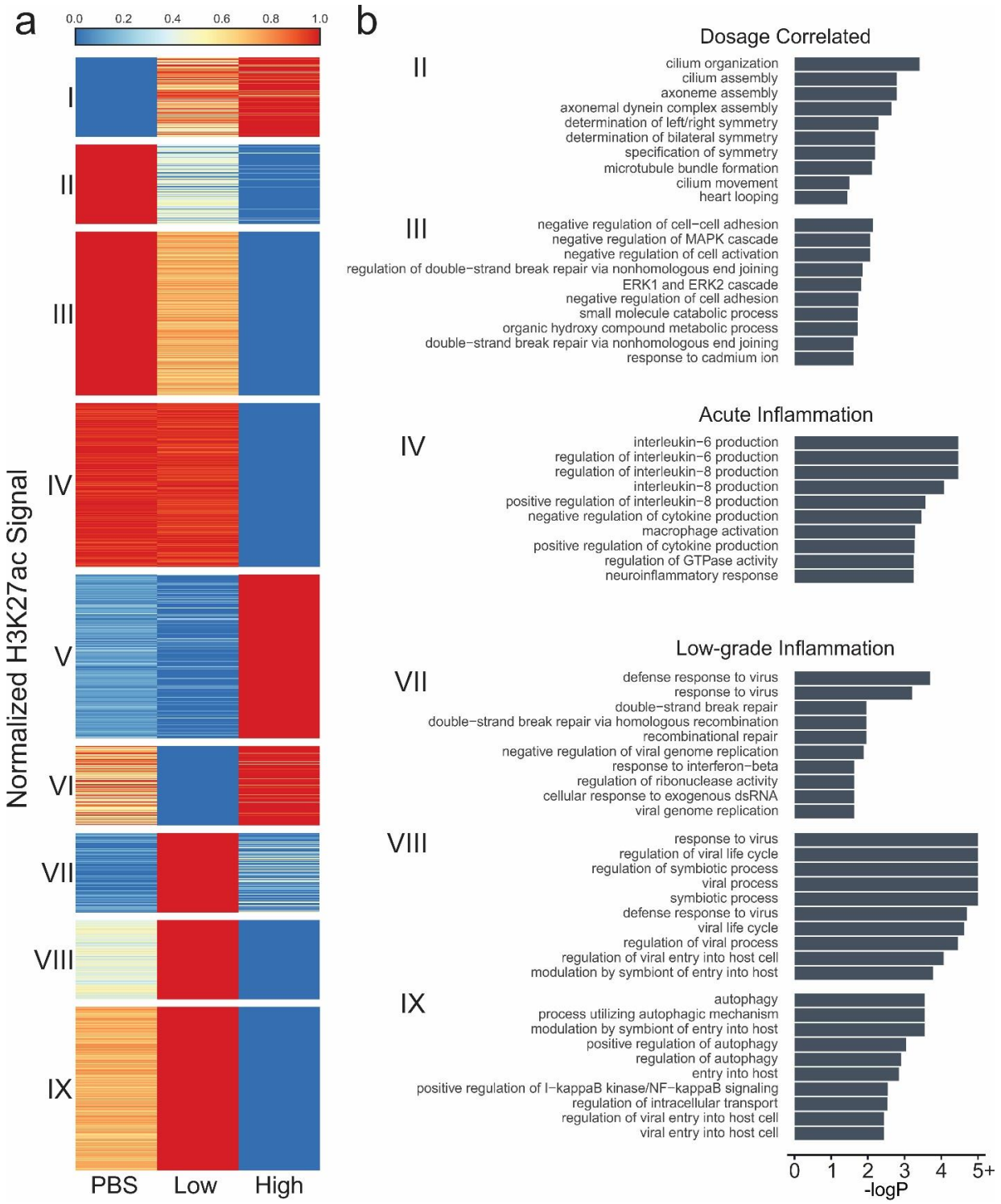

Figure 3-3 H3K27ac signal at promoters for murine BMDMs

(a) Normalized H3K27ac signal around promoter regions (TSS +/- 2 kb) with differential marking (FDR < 0.05, fold-change >= 2) clustered using k-means clustering. (b) Gene ontologies that are significantly enriched (FDR < 0.05) in the associated clusters from (a).

in literature to affect histone acetylation[219], but we do not have enough information to determine which modifications (other than H3K27ac) are affected uniquely by Low-dose LPS, though aberrant histone acetylation has been found in multiple chronic inflammatory diseases[220,221]. However, the enhancers within this grouping were linked to some interesting genes within the immune system. For example, enhancers that had higher signal in Low-dose were linked to genes like Csf1, Irf5, Rab11a, Ccr5, Irf7, Ticam2, Ifit3, and Irf1, while enhancers with lower signal in Low-dose were linked to genes like Arg1, Hdac5, and Treml1. Rab11a is responsible for transporting TLR4 from the endocytic recycling compartment to forming phagosomes[185]. This transport triggers the TRIF-dependent signalling pathway, which requires TRAM (Ticam2). TRIF-dependent signalling leads to increases in interferon-alpha and interferon-beta production which, in turn, activate interferon-induced genes such as Ifit3. Hdac5[222] and Treml1[223] both regulate the inflammatory response. Furthermore, reduction of Hdac5 expression was also associated with an increase of Irf1 and transcription of interferon-beta[222]. In addition, Arg1, which is a typical marker of anti-inflammatory macrophages[197], is reduced in Low-dose while Irf5, shown to promote pro-inflammatory macrophage polarization[224], is increased in Low-dose. Together, these suggest that, while the Low-dose cells are markedly different from High-dose cells, they do have a pro-inflammatory phenotype, which is consistent with previous studies[181]. It is interesting to note that Csf1, which is associated with anti-inflammatory macrophages, is highly increased in Low-dose cells, however, previous studies have shown an association between Csf1 and chronic inflammation[225].

Since enhancers are hotbeds of transcription factor binding activity, the enhancer

regions were then scanned for transcription factor binding motifs that were separated into motifs uniquely and significantly enriched or diminished in low-grade inflammation, acute inflammation, or if the enrichment was correlated to LPS-dosage (Fig. 3-2c). Among the dosage-dependent affected motifs, we see multiple immune-related transcription factors that are increased with increasing LPS-stimulated inflammation such as JunB[226], AP-1[227,228], Atf4[229], and NF-E2[199].

In acute inflammation, we see several transcription factors that are important in the TLR-signaling pathway such as Nfil3[230,231], Hoxa2[232], Nrf2[233], CEBP:AP1[234,235], and OCT2[236,237], all of which are activated with LPS stimulation in literature. In fact, the differential enrichment of Nrf2 between High-dose and Low-dose is also supported by previous research. Nrf2 is activated by LPS stimulation via the reduction of the protein Keap1, however, Keap1 protein has been shown to accumulate in Low-dose conditions[181,233]. The Mef2 family (Mef2a, Mef2b, Mef2c, Mef2d) of transcription factors motifs are significantly deficient in High-dose cells, but are present in Low-dose cells. It has been show that the Mef2 family is initially upregulated by LPS-stimulation but are soon downregulated[199]. It is possible that, in the Low-dose condition, the LPS-stimulation is not enough to lead to the downregulation of the Mef2 family.

Low-grade inflammation leads to fewer enriched motifs than deficient motifs. Motifs that are enriched only in Low-dose are ISRE, Irf2, and Klf4. Irf2[238,239] and Klf4[240] are both inflammation regulators while ISRE is an IFN-I stimulating response element which, when bound, activates genes in the inflammation pathway[241]. This is consistent with previously discussed upregulated enhancer-linked genes such as Irf7. Additionally, Irf2 has been shown to positively regulate the non-canonical inflammasome pathway, which, in turn,

leads to increased GSDMD expression[242]. In fact, we do see increased GSDMD expression in our enhancer data, where it is located in Cluster VI. Low-dose also has reduced p65 motifs, a NF-κB subunit that is part of the canonical pathway involved in inflammation[243] . However, in monocytic cells that have already been stimulated with a gram-negative bacteria, a second stimulation shows reduced p65 activity[244,245]. There is a possibility that sustained low-dosage of LPS may lead to such a reaction. Furthermore, it appears that reduced p65 expression can be somewhat compensated for[246].

We analyzed RNA-sequencing data to further understand the effect of LPS on murine immune cells. We see a similar pattern of RNA-seq data correlation as was in the ChIP-seq data (Fig. 3-4a). Average replicate correlation was 0.9964 and the correlation between PBS and low-dose was similarly high (0.9873). The high-dose replicates had approximately similar correlations with either PBS (0.8922) or low-dose (0.9142). Unlike the H3K27ac signal, there was not a decrease in RNA-signal with increasing LPS-dosage (Fig. 3-5a). Much like the differential peaks, the number of differentially expressed genes (DEGs) was lowest between PBS and Low-dose (155) with much greater differences between PBS and High-dose (3,249) closely followed by Low-dose and High-dose (3,061) (Fig. 3-5b). However, differentially expressed genes were largely equally split into up- and down-regulated genes for each comparison, except between PBS and Low-dose, where there were more genes upregulated in Low-dose than PBS samples. Many genes (~63%) that are differentially expressed in one comparison, are differentially expressed in multiple comparisons (Fig. 3-5c).

The normalized RNA-sequencing expression data of differentially expressed genes were visualized in a heatmap (Fig. 3-4b). Each of these clusters were analyzed for

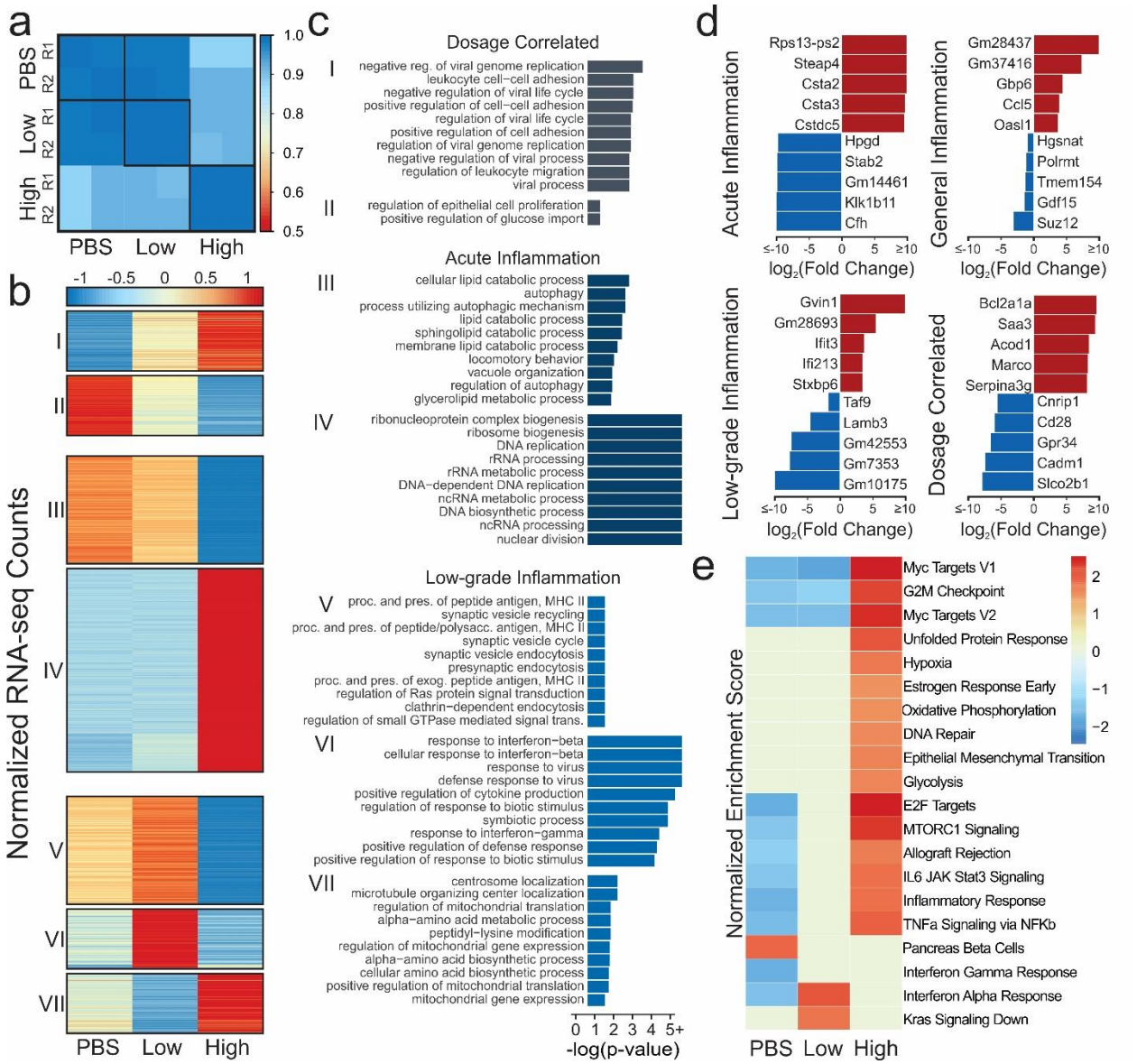

Figure 3-4 Effect of LPS dosage on gene expression

(a) Pearson's correlation of normalized RNA-seq counts at genes (b) Heatmap of normalized gene expression of DEGs present in more than one comparison. (c) Significant biological process gene ontologies for genes that are differentially expressed in more than one comparison. (d) Top upregulated and downregulated genes for each condition. (e) Gene-set enrichment analysis. Color denotes normalized expression score if that pathway was significant (FDR < 0.05) in sample vs. rest.

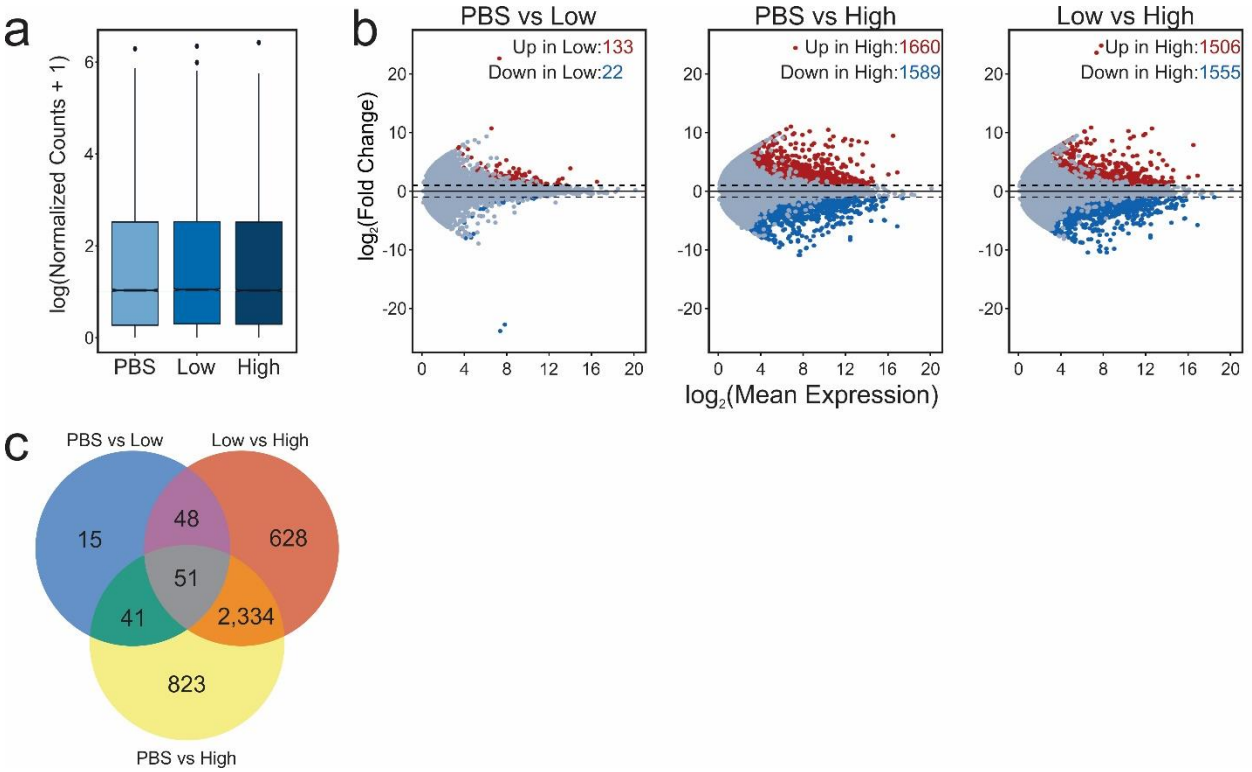

Figure 3-5 Overview of gene expression changes due to LPS

(a) Boxplots of normalized RNA-seq counts at genes (b) MA-plots of the fold change between two samples of a comparison versus the mean gene expression of that gene. Color denotes significance (FDR < 0.05, FC >= 2) (c) Overlap of differentially expressed genes.

enrichment of Gene Ontology biological process gene sets (Fig. 3-4c). Dosage correlated Clusters I and II, which increased or decreased with added LPS-dosage, are consistent with enhancer analysis. Both analyses identified leukocyte-related pathways were increased with increasing dosage. In addition, negative viral process was also increased with additional LPS. While LPS is from a bacteria, TLR4 can also be activated by viral ligands, thus there is large overlap in the genes in each of these ontologies[247]. We also see an reduction of glucose import with increased LPS-dosage, which is also consistent with literature[248]. Clusters specific to acute inflammation, Clusters III and IV, had similar autophagy and nucleic acid-related processes as the corresponding enhancer clusters. However, Cluster III also had more lipid metabolic processes that were down-regulated in High-dose conditions, which is consistent with previous research showing LPS-stimulation to decrease lipid catabolism[249].

Finally, Clusters V, VI, and VII were specific to Low-dose. In Clusters V and VI, we see ontologies that are significantly upregulated in Low-dose compared to High-dose or PBS. These include MHC II antigen processing and response to interferon-beta. MHC II antigen processing is the means by which an exogenous antigen is prepared and presented on the cell surface for the activation of CD4+ T cells. These cell surface molecules that present the antigen are only upregulated in the TRIF-dependent pathway. Furthermore, what the macrophage secretes can also affect CD4+ T cell function and aberrant CD4+ T cells have been implicated in inflammatory diseases[250,251]. Interferon-beta related genes and motifs were also found to be enriched or have increased enhancer expression in Low-dose cells compared to High-dose or PBS. This suggests that epigenetics play a notable role in the etiology of low-grade inflammation. This is further

supported by the peptidyl-lysine modification process in Cluster VII, which is down in Low-dose and high in High-dose. With closer inspection, Hdac2 and Hdac4 are included within this clusters. Hdac2 is considered to be crucial to the LPS inflammatory response while also mediating it, and decreased Hdac2 levels have been found in COPD patients[252-254]. Hdac4 is necessary for LPS-stimulated production of pro-inflammatory cytokines, and degradation leads to secretion of HMGB1, which is believed to play a significant role in sepsis[255,256].

The fold-changes of the top genes significantly expressed or repressed in Acute Inflammation (High-dose vs. rest), Low-grade inflammation (Low-dose vs. rest), General Inflammation (PBS vs. rest), and Dosage-specific (increasing or decreasing from PBS to High-dose) were inspected (Fig. 3-4d). In each, we see some genes that have been pointed out in literature before as affected by inflammation or LPS in some way, such as Steap4[257], Bcl2a1a[258], Saa3[259], Marco[260], CFH[261], Ifit3[262], Lrrc14b[263], Ccl5[264], and CD28[265]. We also see multiple predicted genes that might be worth further *in vivo* or *in vitro* functional investigation.

Gene-set enrichment analysis was then performed using each of the conditions compared to the rest (Fig. 3-4e). The first aspect of note is that High-dose is significantly enriching many pathways that have been found to be enriched by LPS-stimulation in literature such as Myc[266,267], hypoxia[268], glycolysis[269], and unfolded protein response[270]. We also see oxidative phosphorylation, which is generally believed to be reduced in LPS-stimulation as the cell transfers to glycolysis, though there is some conflicting evidence[271]. Yet, there are two reasons that it might be enriched in High-dose. First, oxidative phosphorylation is necessary for inflammatory resolution[272]. Or, it could be as a result of

glucose starvation, which can cause cells to shift back towards oxidative phosphorylation[273]. In addition, there are also pathways that seem to be somewhat dosage-dependent, such as E2F targets[274], MTORC1[275], IL6 JAK Stat3 signaling[276,277], and TNF-α[278,279] that are hallmarks of inflammation. However, it is interesting to note that it appears low-dose cells are not undergoing as much replication, as seen in the reduced G2M checkpoint and glycolysis. Furthermore, it appears that, while slight interferon-gamma enrichment[280,281] occurs in both Low-dose and High-dose (seen by deficiency in PBS), that low-dose has stronger enrichment of interferon-alpha and Kras Signaling down. Interestingly, interferon-alpha overexpression, which studies suggest can lead to chronic inflammation[282], is a characteristic of systemic lupus eruthematosus, an autoimmune disease[283,284]. The reduction in Kras Signaling, which is part of the Ras/MAPK pathway, would also point to reductions in the cell-cycle of Low-dose cells[285].

As differential transcript usage (DTU), such as alternative splicing, has been shown to be affected in the macrophage inflammatory response[286], we also chose to examine DTU among the three experimental conditions as differential transcript usage can effect the function of the genes involved. There were a total of 309 genes that had significant DTU with predicted functional consequences across the three comparisons (PBS vs. Low-dose = 82, PBS vs. High-dose = 171, Low-dose vs. High-dose = 172) (Fig. 3-6a). Genes with DTUs in PBS versus High-dose were entirely associated with RNA-splicing ontologies (data not shown), as well as many in Low-dose vs High-dose (Fig. 3-6b). However, Low-dose versus High-dose did have several immune related ontologies, suggesting that DTU may play a role in the differing responses. In particular, we see response to interferon-beta and one of the DTU genes that was involved, IFI204, plays a

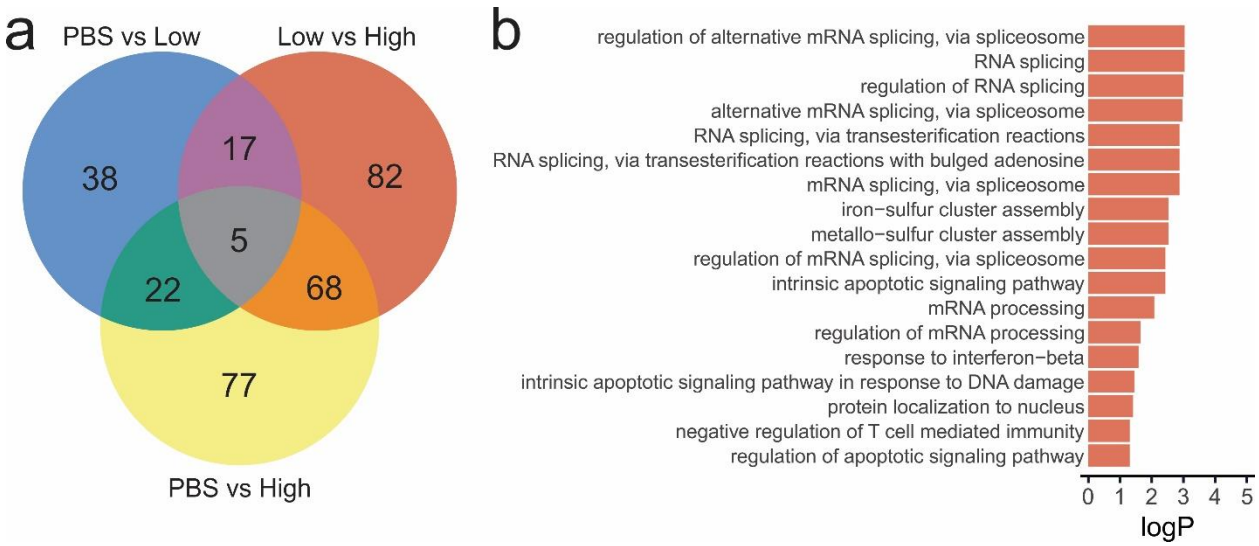

Figure 3-6 Effect of LPS on differential transcript usage

(a) Overlap of genes with significant differential transcript usage among the three conditions. (b) Gene ontologies significantly overrepresented in genes with DTUs in High-dose compared to Low-dose.

key role in interferon-beta release[287]. We also found that, of the 172 DTUs in Low-dose vs. High-dose, 111 had (FDR<0.05) differential H3K27ac signal at their promoters (expected = 40) and 38 were linked to enhancers (expected = 22) for a total of 121 DTUs associated epigenetic regulation. This further suggests that epigenetic regulators may be playing a role in the differences between acute and low-grade inflammation.

The increase that we see of type I interferons-alpha and beta-related processes in Low-dose cells, both epigenetically and transcriptomically, as well as increased epigenetic enhancement of TRAM (RNA-seq FDR < 0.05, FC ≈ 1.8) led us to postulate that low-dose LPS might lead to more use of the TRIF-dependent pathway (which requires TRAM), while high-dose might lead to more use of the MyD88-dependent pathway (Fig. 3-2a and Fig. 3-4c,e)[185]. In order to better understand the mechanistic pathways that might be differentially affected by low-dosage of LPS, we performed additional experiments using TRAM-deficient and IRAK-M-deficient BMDMs (Fig. 3-7a). TRAM-deficient cells are incapable of utilizing the TRIF-dependent pathway and IRAK-M-deficient cells have an unregulated MyD88-dependent pathway. We see that WT-high-dose cells correlate the strongest with TRAM-deficient-high (r = 0.9614) followed by the low-dose and PBS conditions (r = 0.8663 – 0.9149), while the two IRAK-M samples had the lowest correlation (High = 0.8150, PBS = 0.7623). Average correlation between the WT and TRAM-deficient low-dose and PBS samples was very high at r = 0.9859. IRAK-M-deficient PBS was most highly correlated with the other two PBS samples, but IRAK-M-deficient high-dose had lower correlation with all samples (r = 0.8090 – 0.9035). When we perform principle component analysis of the most variable genes, we see fairly similar results (Fig. 3-7b). Due to the significant differences in IRAK-M-deficient cells, we chose

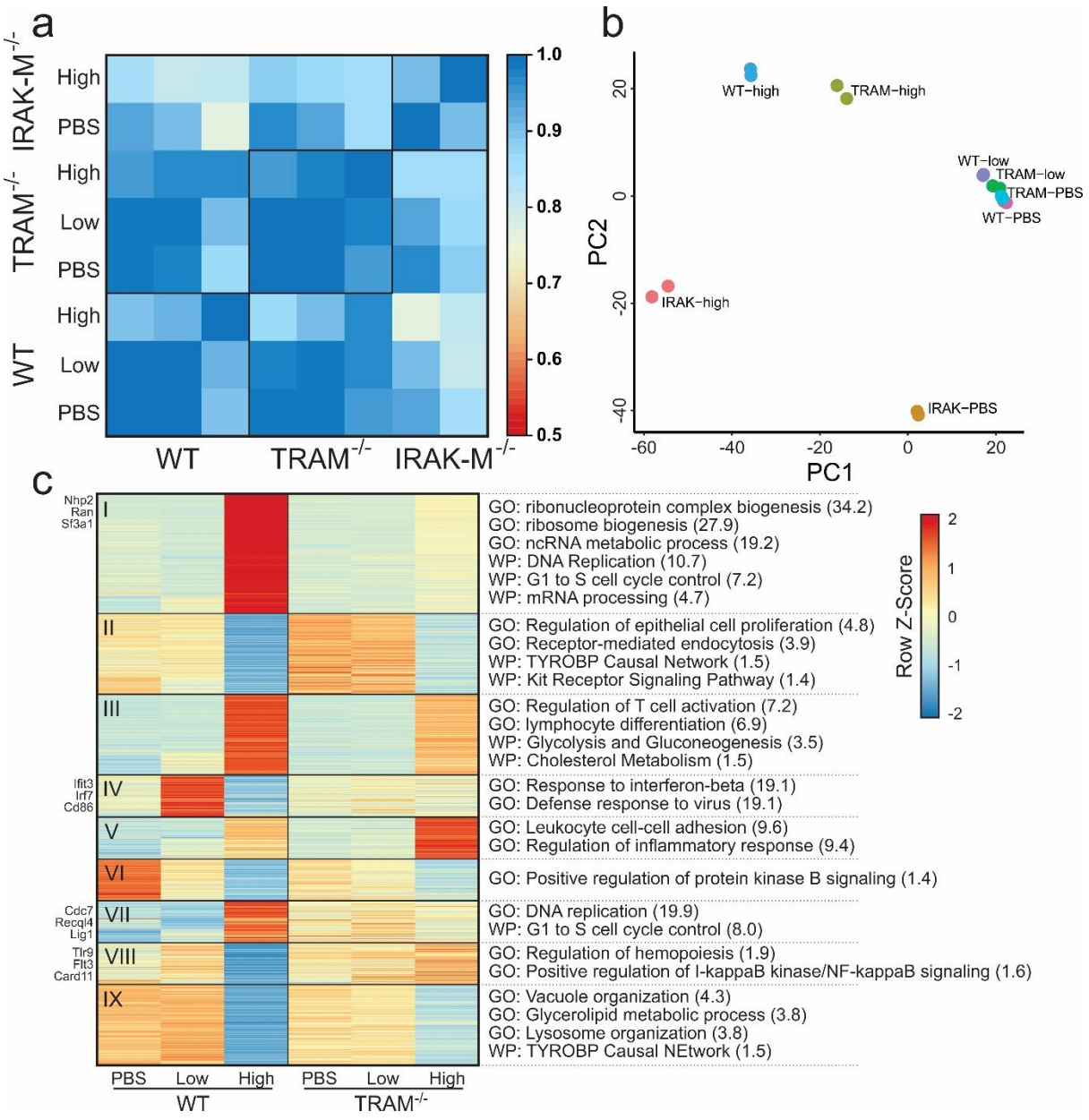

Figure 3-7 Effect of TLR4 pathway on LPS-dosage response

(a) Pearson's correlation of RNA-seq signal between conditions. (b) Principle Component Analysis of replicates using top 500 variable genes. (c) Heatmap of WT and TRAM-deficient gene express at varied LPS-dosage using DEGs from the WT comparisons. Significant pathways on right are from Gene Ontology or WikiPathways. Log(FDR) for each in parentheses.

to limit their inclusion in further analysis.

We then analyzed gene expression across the three dosing conditions for both WT and TRAM-deficient cells, though we restricted the analysis to genes that were differential expressed between the WT conditions (Fig. 3-7c). A decent number of genes were moderately affected by TRAM-deletion, but most maintained a similar expression pattern to WT. Despite this, there are 4 clusters of interest (Clusters I, IV, VII, and VIII) that stand out. Clusters I and VII both show a failure to upregulate DNA replication pathways in TRAM-deficient high-dose cells. While there is evidence of macrophage renewal due to inflammatory insult, it is not well understood, but it is possible that it is TRIF-dependent[288,289].

On the other hand, Clusters IV and VIII both have a pattern of low-dose having the highest expression and high-dose the lowest in WT. There appears to be little to no change in TRAM-deficient cells. In Cluster VIII, TLR9 is an intracellular toll-like receptor that recognizes unmethylated CpG motifs in bacterial or viral DNA[290]. However, TLR9 has been shown to occur after LPS stimulation[291] and TLR9 inhibition helps suppress excessive inflammation in bacterial sepsis[292-294]. Furthermore, it helps regulate antigen presentation in macrophages[295] and participates in interferon-alpha production through IκB kinase signaling[296]. Interestingly, TLR9 is found to be activated through the NF-κB, Erk, Jnk, and p38 Mapk pathways which are not TRIF-dependent, so it is unclear why there is not an increase in TRAM-deficient cells as well[291,297].

Another critical gene is Irf7, which is upregulated in WT-low but not in TRAM-low, that is important for the production of type I interferons[298]. Furthermore, Irf7 expression can lead to a feed-forward loop of type I interferon production, much like we see in WT-

low[299,300]. However, research has shown that Irf7 is necessary for the Il-1β and the type I interferon response elicited through TLR4, and that Irf7 is induced through the TRIF-dependent pathway, consistent with the lack of Irf7 increase in TRAM-deficient cells. Yet, Irf7 is not overwhelming in WT-high cells, so there must an additional factor in low-dose conditions. Trim28 is a negative regulator of Irf7[298] and is significantly reduced in WT-low compared to WT-high cells (FDR < 0.05, FC < 2), while remaining unchanged across the TRAM-deficient cells. If Trim28 is phosphorylated at serine 473 through a PKR/p38 MAPK/MSK1 signaling cascade, it is no longer capable of inhibiting Irf7[301]. Although knockdown of activated MSK1 does increase production of some inflammatory cytokines in neuroinflammation, Trim28 is responsible for regulating a staggering number of genes, so it is unclear if it is involved[301,302]. In addition, phosphorylation of Trim28 is not necessarily equivalent to reduced gene expression. Foxo3[303] and Cflar[304] have also been shown to inhibit Irf7 but neither had notable differences in gene expression.

3.4 Discussion

Our study of gene expression and histone modification changes due to LPS-dosage suggest that a low dosage of LPS leads to cells preferentially utilizing the TRAM/TRIF-dependent TLR4 signaling pathway. First, we found that these changes are seen in the expression of enhancers, the regulators of gene expression. Enhancers with increased signal in Low-dose samples were linked to genes related to the TRAM/TRIF-dependent pathway. In addition, promoters and motifs enriched in Low-dose samples were also associated with the interferon-beta response. Second, we showed genes with increased expression only in Low-dose LPS, such as Stat1, Irgm1, Ifit3, and BST2, were significantly involved in interferon-beta and interferon-alpha responses. Furthermore,

genes with differential transcript usage between Low-dose and High-dose were also associated with interferon-beta response. Finally, we compared the gene expression of WT samples to TRAM-deficient mice to determine that TRAM-deficiency abrogates the interferon-beta associated genes, indicating that the Low-dose increases in interferon-beta specifically rely on TLR4-associated TRAM/TRIF-dependent pathway, as opposed to MyD88 pathway. This preference for the TRIF-dependent pathway also prevented Low-dose samples to not alter nucleotide replication and metabolic pathways that were changed in High-dose samples preferentially going through the MyD88 pathway.

There is increasing appreciation for signal-strength dependent programming of both innate and adaptive immune systems, enabling complex and dynamic host responses to changing landscapes of infectious and inflammatory conditions[305,306]. Although much progress has been made with the dynamic programming of T helper cells exhibiting multi-staged activation and exhaustion under signal-strength and history dependent challenges[307], the similar scenario of innate immune cell adaptation is still less understood. Due to limited systems approaches, even the most well-known concept of endotoxin tolerance regarding innate cell adaptation to repeated LPS challenges fails to clarify the complex innate immune adaptation dynamics. Past studies regarding endotoxin tolerance overly focus on dampened gene expression of limited inflammatory mediators[180], and fails to address augmented induction of diverse immune-; metabolic-; and proliferative related genes involved in complex adaptation to higher dosages of endotoxin. Much less is known about innate responses to pathologically relevant subclinical low dose LPS, highly prevalent in humans with chronic conditions due to mild leakage of mucosal barriers[308]. The lack of systems and clear understanding of signal

strength and history-dependent adaptation to LPS underlies our limited translational success in treating related diseases ranging from acute sepsis to chronic cardiovascular diseases. Our current study provides a comprehensive assessment of gene expression dynamics as well as corresponding epigenetic variations in monocytes challenged with rising dosages of LPS.

Confirming limited previous studies, our collected data reveal that higher doses of LPS not only cause suppression of certain subsets of inflammatory genes, but also potently induce wide arrays of genes involved in altered immune metabolism and proliferative potential. Further characterization of these altered gene expression landscape may help better explain the compound phenotypes of pathogenic inflammation and immune-suppression observed in septic leukocytes collected from human sepsis patients and model murine septic animals[309,310]. In contrast, low dose LPS preferentially induces inflammatory interferon responsive genes, recently shown to be expressed in inflammatory monocytes collected in vivo from various chronic inflammatory disease models including lupus and atherosclerosis[284,311,312].

Our integrated analysis of epigenomic changes at enhancer and promoter regions complements our gene expression data, in further revealing the preferential usage of TRAM/TRIF pathway by low dose LPS. Our finding is consistent with limited previous studies showing that the TRAM/TRIF-dependent pathway is favored in Low-dose LPS conditions and critical for lesion development in atherosclerosis[181]. In addition, we identified signature transcription factors involved in monocyte activation by Low-dose LPS such as IRF1, 5 and 7, with IRF5 previously reported to be involved in monocyte priming by Low-dose LPS[313]. The preferential enrichment of additional transcription factors such

as IRF2 and KLF4 is also interesting, and may provide additional insight regarding the regulation of low-grade inflammatory monocytes. Low-dose LPS also enhanced the expression of Rab11a, a molecule involved in endocytic recycling of TLR4, providing a further mechanistic explanation for our previous observation that internalization of TLR4-LPS complex and the activation of TRAM/TRIF pathway are required for sensing Low-dose LPS[183].

Collectively, our integrative systems study further clarifies the highly complex and dynamic adaptation of macrophages to rising dosages of LPS, and reveals more of the inner workings of underlying mechanisms, yet much more research will be required to fully understand how immune pathways and components interact in the dynamic ontogeny of macrophage activation states related to the etiology of low-grade inflammation. Studies that utilize time courses, additional LPS concentrations, and other transgenic mice all would be beneficial for truly unveiling low-grade inflammation. Additional epigenomic studies may also reveal the causal relationships at play and possible therapeutic targets. Together, this could lead to identification of relevant molecular targets in human immune cells for future clinical applications.

3.5 Methods

Mice

C57/BL6 mice purchased from the Jackson Laboratory were bred and maintained in pathogenic-free conditions. Male 8-12 week old mice were used in this study. The Institutional Animal Care and Use Committee (IACUC) approved all procedures performed on the mice.

Cell Culture

Crude BM cells were pooled from multiple (~6-7) mice and cultured as previously published[181]. Briefly, the pooled cells were split across three plates and cultured in RPMI complete media (RPMI 1640 with 10% FBS, 2 mM L-glutamine, and 1% penicillin/streptomycin) along with M-CSF (10 ng/mL) and either PBS, low-dose LPS (100 pg/mL), or high-dose LPS (1 µg/mL). Fresh LPS was added every two days and the cells were harvested after 5 days.

Chromatin Shearing

Samples containing 10^6 cells were centrifuged at 1600 g for 5 minutes at 4 °C. Each sample was washed twice with cold 1 mL PBS and resuspended in 9.375 mL of PBS. Then, 0.625 mL of 16% formaldehyde was added and the samples were incubated on a shaker for 5 minutes at room temperature. The samples were then quenched with 0.667 mL of 2 M glycine and incubated for 5 minutes at room temperature on a rotator. The cells were then centrifuged at 1600 g for 5 minutes and washed twice with 1 mL cold PBS. The pellet was resuspended in 130 µL of Covaris sonication buffer (10 mM Tris-HCl, pH 8.0, 1 mM EDTA, 0.1% SDS and 1x protease inhibitor cocktail (PIC)) and sonicated with a Covaris S220 sonicator using 75 W peak incident power, 5% duty factor, and 200 cycles per burst for 16 minutes at 4 °C. Sonicated samples were centrifuged at 16,100 g for 10 minutes at 4 °C before the supernatant containing sheared chromatin was removed to a fresh tube. Finally, 2.4 µL of sheared chromatin was then mixed with 46.6 µL of IP buffer (20 mM Tris-HCl, pH 8.0, 140 mM NaCl, 1 mM EDTA, 0.5 mM EGTA, 0.1% (w/v) sodium deoxycholate, 0.1% SDS, 1% (v/v) Triton X-100, 1% freshly added PMSF and

PIC) to generate a 50 µL sample containing chromatin from 20,000 cells for MOWChIP-seq.

MOWChIP-seq

Sonicated chromatin samples of 20,000 cells per assay were profiled for H3K27ac (abcam, cat: ab4729, lot: GR312651-2) with MOWCHIP-seq as described in our previous publications[18,20]. Libraries for sequencing were prepared using the Accel-NGS 2S Plus DNA Library Kit (Swift-Bio) and samples were sequenced using an Illumina HiSeq 4000 with single-end 50 nt reads.

RNA-seq

10,000 cells were used to produce each RNA-seq library, with two replicates for each genotype and experimental condition. RNA was extracted into a 30 µL volume using the RNeasy Mini Kit (74104, Qiagen) and RNase-Free DNase Set (79254, Qiagen), following the manufacturer's instruction. The extracted mRNA was then concentrated by ethanol precipitation and resuspended in 4.6 µL of RNase-free water. Next, we used the SMART-seq2 protocol[202], with minor modifications, to prepare cDNA. 2 µL of oligo-dT primer (100 µM) and 2 µL of dNTP mix (10 mM) were added to 2 ng of mRNA in 4.6 µL of water. The mRNA solution was denatured at 72 °C for 3 min, then immediately placed on ice. Next, 11.4 µL of reverse transcription mix [1 µL of SuperScript II reverse transcriptase (200 U/µL), 0.5 µL of RNAse inhibitor (40 U/µL), 4 µL of Superscript II first-strand buffer, 1 µL of DTT (100 mM), 4 µL of 5 M Betaine, 0.12 µL of 1 M $MgCl_2$, 0.2 µL of TSO (100 µM), 0.58 µL of nuclease-free water] was added to the mRNA solution. For

the reverse transcription reaction, the solution was incubated at 42 °C for 90 min, followed by 10 cycles of 50 °C for 2 min, 42 °C for 2 min, then inactivation at 70 °C for 15 min. 20 μL of the resulting solution (first-strand mixture) was then mixed with 30 μL of PCR mix [25 μL KAPA HiFi HotStart ReadyMix, 0.5 μL IS PCR primers (10 μM), 0.5 μL Evagreen dye, and 4 μL nuclease-free water] and amplified using the program 98 °C for 1 min, followed by 9-11 cycles of 98 °C 15 s, 67 °C 30 s, 72 °C 6 min. Finally, the cDNA was purified using 50 μL of SPRIselect beads. RNA-seq libraries were generated with the Nextera XT DNA Library Preparation kit (FC-131-1024, Illumina) and manufacturer's protocol, using approximately 600 pg of purified cDNA from each sample. Samples were sequenced using an Illumina HiSeq 4000 with single-end 50 nt reads.

Data Processing

Unless otherwise mentioned, all data analysis was performed with Bash scripts or with R (The R Foundation) scripts in RStudio. Sequencing reads were trimmed using default settings by Trim Galore! (Babraham Institute). Trimmed reads were aligned to the mm10 genome with Bowtie[80]. Peaks were called using MACS2 ($q < 0.05$)[81]. Blacklisted regions in mm10 as defined by ENCODE were removed to improve data quality[82]. Mapped reads from ChIP and input samples were extended by 100 bp on either side (250 bp total) and a normalized signal was calculated.

$$Normalized\ Signal = \left(\frac{ChIP\ Signal}{No.of\ ChIP\ Reads} - \frac{Input\ Signal}{No.of\ Input\ Reads}\right) \times 10^6$$

For Pearson's correlation, the signal was calculated around the promoter region (TSS +/- 2 kb) and plotted with the corr and levelplot functions. For visualization in IGV (Broad

Institute), the signal was calculated in 100 bp windows over the entire genome and output as a bigWig file. RNA-seq data was quantified using Salmon[41] against the mm10 transcriptome using a full decoy and normalized counts were calculated with DESeq2[314].

Enhancers Analysis

To call enhancers, we considered H3K27ac^{high} regions that did not intersect with promoter regions to be enhancer regions. First, consensus H3K27ac peak sets were generated for each of the experimental conditions. Peak widths were expanded to be 1000 bp long (summit +/-500 bp). Promoters were defined as TSS +/- 2000 bp. Any H3K27ac 1 kb regions that intersected with a promoter region was removed and the remaining regions were designated as putative enhancers. The signal at each of the putative enhancers was then correlated (Spearman) to RNA-seq gene expression values within the same topological domain. Putative enhancers were linked to the gene with the highest correlation, however, links were only considered significant if the Spearman correlation coefficient (SCC) > 0.25 and if the correlation was considered significant if both empirical and quantitative p-values were less than 0.05. For both p-values, the SCC was calculated between the given putative enhancer and all genes on the same chromosome. The empirical p-value was then calculated as the fraction of genes on the same chromosome that has a higher correlation than the currently linked gene. The quantitative p-value was calculated by treating the calculated SCC values as a distribution and using the R function pnorm to calculate a significance. Motif analysis was performed to determine enriched transcription factor binding motifs among the enhancer regions with HOMER[87] (with options –size 1000 –mask –p 16 –nomotif).

RNA-seq Analysis

Differential gene expression analysis was performed using DESeq2, where genes with a fold-change >= 2 and FDR < 0.05 were considered to be significantly differentially expressed. Boxplots and MA plots were done in R using ggplot and ggpubr. Clustering was performed using clusterProfiler. Gene-set enrichment analysis was performed with GSEA[315,316] using the Hallmark gene set and gene-set level permutation. Gene sets were considered significant if the FDR < 0.05. Significant differential transcript usage ($p < 0.05$, dIF > 0.1) was determined using IsoformSwitchAnalyzeR[317,318] with the default DEXSeq[319]. Data output was then ran through CPAT[320], PFAM[321], SignalP[322], NetSurfP-2.0[323], and results were combined back into IsoformSwitchAnalyzeR to determine genes that might have functional consequences as a result of the DTUs. Genes were analyzed for gene ontologies with clusterProfiler.

4 The effect of maternal immune activation and cross-fostering on the murine brain epigenome and transcriptome

---

Published Work

The work presented in this chapter has not yet been published.

Author Contributions

Chang Lu and Javier González-Maeso designed the experiments and supervised the research. Justin Anderson conducted the animal experiments and produced the tissue samples. Bohan Zhu conducted the ChIP-seq and RNA-seq assays. Lynette Naler analyzed the data. Lynette Naler, Bohan Zhu, Justin Anderson, Javier González-Maeso, and Chang Lu wrote the manuscript.

4.1 Project Summary

Activation of the maternal immune system (MIA) during pregnancy can significantly increase the lifetime risk of neurodevelopmental disorders, such as schizophrenia or autism, in the unborn child. Although this risk has been linked to increased exposure of the fetus to immune cytokines, it is unclear exactly how this exposure affects the brain and why that might predispose disorders like schizophrenia. Here, we activate the immune system of pregnant mice with exposure to influenza virus or a mock solution. In order to separate prenatal and postnatal effects, half of the litter was then swapped, such that, regardless if the mother was exposed to the virus or not, each mother would be raising both Mock-born and MIA-born pups. This was also done with Mock-only mice as a control. Widespread changes associated with schizophrenia or neurological disorders were found in all mice that were raised with MIA co-siblings, yet reduced effects suggested a protective effect on those that were removed from their own parent and fostered.

4.2 Background

Activation of the maternal immune system (MIA), such as by viral or bacterial infection, has been shown to be a risk factor in the development of neurodevelopmental disorders, such as schizophrenia[324-337] and autism[338-341]. Worldwide, schizophrenia has a lifetime risk of 0.4%, although risks are higher in developed and developing countries.[342] Schizophrenia is a heterogeneous condition diagnosed clinically by determining an individual's mental state and personal or familial history.[343] Symptoms of schizophrenia include delusion, hallucinations, and disorganized speech, impaired motivation, social withdrawal, and reduction of spontaneous speech. In addition to these, there are can also be cognitive impairments, particularly in memory, though this seems to vary widely between individuals.[344] Differences are not just limited to symptoms either. For example, there is evidence that the brains of schizophrenics born to mothers who had an infection during pregnancy are physically distinct from those that were not a result of MIA.[332]

While the lifetime risk of schizophrenia is low in the general population, having family diagnosed with schizophrenia can significantly increase an individual's risk of developing schizophrenia, leading to a heritability rate of 80%.[345,346] However, pinning down common genetics has been difficult and results have been inconsistent due to the heterogeneity of the disease, environmental aspects, and study limitations.[347,348] In fact, the genetic component of schizophrenia could stem from multiple genetic faults concurrently.[349-351] Genes from neurodevelopment and cognition[352,353], the immune system[350,353,354], glutamatergic neurotransmission[355], and postsynaptic signaling[351,356] have all been implicated. Yet, schizophrenia risk is also affected by environmental (i.e. epigenetic) factors.[349,357,358] For example, concordance rates of schizophrenia between

twins is only about 40-50%.[346] Unfortunately, it is not always possible to separate epigenetic changes that are due to disease and those from treatment with anti-psychotics.[359] In addition, most work has primarily looked at specific regions instead of genome wide analysis.[347] Studies have found differential methylation in the promoter regions of genes associated with serotoninergic[360-363], dopaminergic[364], glutamatergic[365], and GABAergic (particularly reelin)[365-367] neurotransmission systems as well as neurodevelopment[365,368,369] and other genes associated with schizophrenia[370-372]. Far less work has been done looking at histone modifications in schizophrenia, which has primarily focused on either specific genes or on overall histone modification levels[347,373-377].

In order to model the effect of MIA with more constrained environmental factors, research has turned to animal models. Three main rodent models are used to study maternal infection: influenza, poly(I:C), and lipopolysaccharide (LPS).[378,379] Influenza infection is performed intranasally during the first or second term of pregnancy and leads to several physical and behavioral changes in the offspring that strongly resemble neurodevelopmental disorders like schizophrenia. For example, the offspring show deficits in social interaction, exploratory behavior, and prepulse inhibition (PPI), which measures how resistant an individual is to being startled after being primed.[378] Physically, offspring have a localized deficit in Purkinje cells[380], more densely packed pyramidal cells[381], localized brain atrophy, and white matter thinning of male offspring.[382,383]

Although intranasal influenza infection provides the most complete immune response, most research into how MIA affects offspring instead utilizes poly(I:C) and LPS injections to activate the maternal immune response.[384] These models have shown

increased levels of immune cytokines such as IL-1β, IL-6, IL-10, and TNFα occur in the placenta and amniotic fluid of immune-activated mothers, and further studies suggested that these cytokines might lead to the neurodevelopmental changes in offspring.[378,385-396]

Cross-fostering studies have shown that just being raised by mothers who underwent immune activation was enough to confer some changes on the pups, despite being born to unaffected mothers[397]. In fact, cross-fostering is a powerful means of isolating prenatal and postnatal effects[398]. Despite this, little research has been done into how prenatal and postnatal MIA conditions affect offspring differently[399]. A cross-fostering experiment that utilized maternal stress, instead of infection, as a means of inducing schizophrenic-like symptoms, suggested that postnatal effects had little to no effect on neuropsychological changes[400]. Maternal care has been shown to not be significantly different between biological and cross-fostered pups, however these studies did not include maternal immune activation[401,402]. Furthermore, the maternal care behavior of mice has been shown to be significantly affected by immune activation during gestation, and aberrant maternal care can affect the neurobiology of their offspring[403,404]. Thus, the effect postnatal care has on neurodevelopmental changes due to maternal immune activation is unclear. This, in conjunction with a lack of genome-wide data profiling the transcriptome and epigenome, led us to perform the experiments and analysis described in this manuscript.

In this study, the histone marks H3K27ac and H3K4me3 were profiled through the use of our low-input Microfluidic Oscillatory Washing ChIP-seq (MOWChIP-seq[20,201]) technology, and performed RNA-seq analysis with Smart-seq2[202,203] of neurons isolated from the prefrontal cortices of mice. Our goal was to understand the effect of maternal

immune activation on offspring, and to determine if these changes are prenatal, postnatal, or a mix of the two through cross-fostering. This led us to seven experimental groups. We chose to then separate our analysis into three main parts. First, we analyze groups that were not born to or raised by an MIA mother to determine what effect cross-fostering has on both the fostered pups and the adopting pups in a mock setting. Then, we analyze the effect of MIA on pups in the adopting family. Finally, we investigate the effect of MIA on the fostered pups.

4.3 Results

The prefrontal cortices were isolated from mice to understand the effect of maternal immune activation and elucidate the roles of prenatal and postnatal effects. There were seven experimental groups (Fig. 4-1a). Groups A, B, C, and D followed standard cross-fostering procedure to study pre-natal versus post-natal effects. Groups A and C were born to a Mock mother, while B and D were born to a MIA mother. Within 24 hours of birth, B and C were swapped such that a Mock mother raised groups A and B and a MIA mother raised groups B and C. Groups E and F underwent a similar cross-fostering procedure, but using only Mock mice, while group G had no cross-fostering of any form. We profiled H3K27ac and H3K4me3, as well as performed RNA-seq, for each mouse in all of the conditions. The mice were clustered with tSNE utilizing gene expression and histone modification signal at peaks, and colored according to their experimental group (Fig. 4-1b). Interestingly, we see that groups A and D cluster together, separate from groups B and C, and from groups E, F, and G. This was unexpected, as from literature we expected that B and C would fall between A and D. However, we did see that groups A, B, C, and D, which had some form of exposure to MIA or to MIA pups, did cluster away from groups E, F, and G, suggesting that MIA does have an effect, even on pups in the adopting family. Each of the groups can be cleanly distinguished from one another, except for B and C. We then correlated the mice according to their normalized H3K27ac and H3K4me3 signal at promoter regions, or according to their gene expression (Fig. 4-1c). H3K27ac had the most variable correlations, which is consistent with previous work done using murine neurons[405], with an average in-group correlation of 0.922 and average inter-group correlation of 0.843.

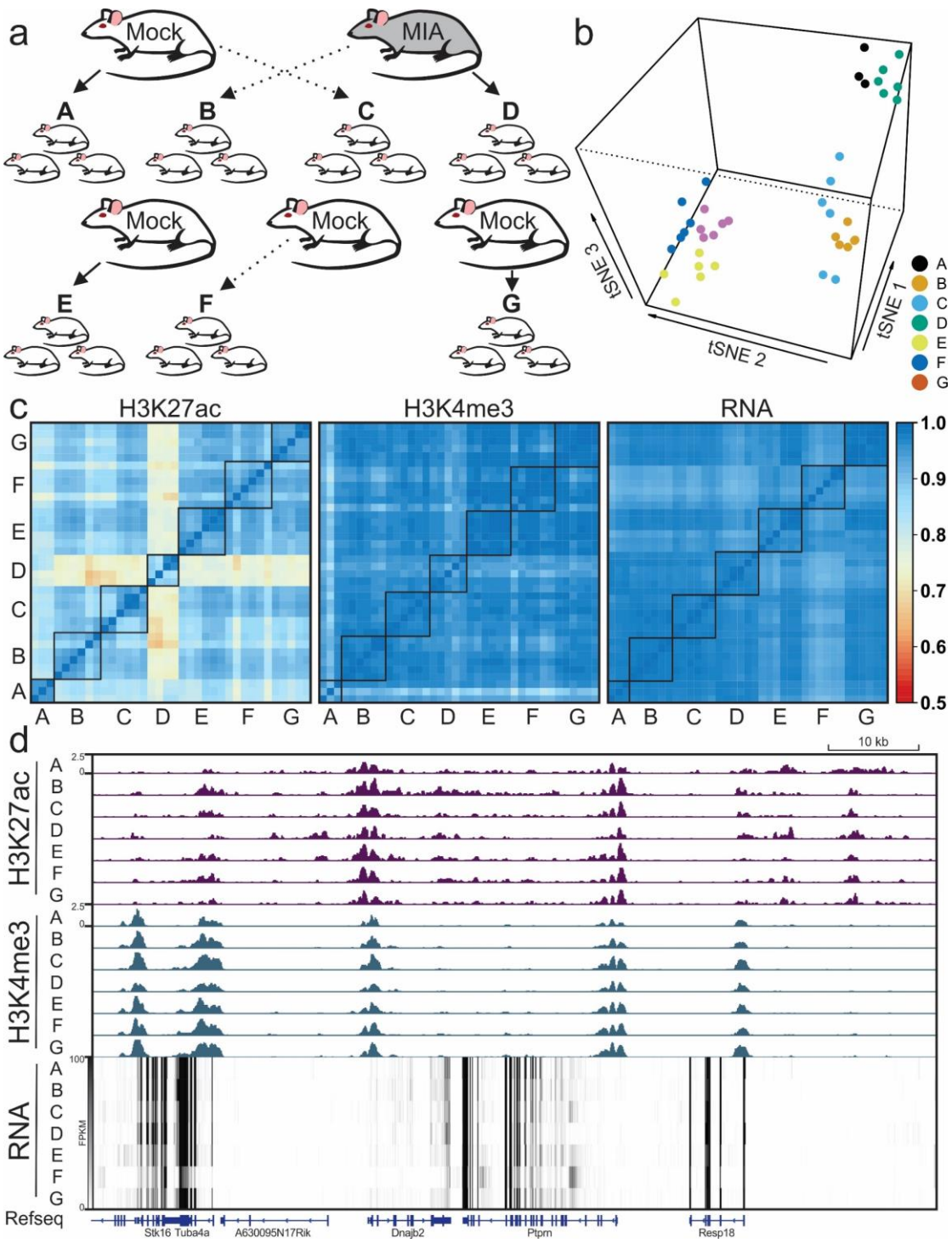

Figure 4-1 Histone modification and gene expression data from MIA and Mock mice

(a) Overview of the experiment and labels of experimental groups. (b) tSNE of histone modification and gene expression data. Each point represents a unique mouse. (c) Pearson's correlation of histone modification signal at promoters or of gene expression. (d) Visualized tracks displaying ChIP-seq peaks and RNA-seq signal.

We do see that group D, has largely poor correlation with every other group (0.772) but is slightly higher with group A (0.802)**.** In contrast, H3K4me3 and RNA expression had much higher in-group correlations (0.970 and 0.952, respectively) and inter-group correlations (0.951 and 0.918, respectively), even with group D. The similarity of these groups are shown in visualization of the ChIP-seq tracks and RNA-seq values (Fig. 4-1d).

To better understand the effect of cross-fostering on murine pups, we compared the epigenomic and transcriptomic data of groups E, F, and G through the use of weighted gene correlation network analysis (WGCNA) (Fig. 4-2). WGCNA was performed on gene expression (denoted R), H3K27ac signal at gene-linked enhancers (denoted E), and H3K4me3 signal at gene promoter regions (denoted P), before the modules from each were clustered together into clusters I - IV. Clusters with similar trait correlation and module eigengene values, which represent gene expression or histone signal, were grouped. It should be noted that, using cluster I as an example, the clusters include genes that are substantially higher in E and F than G (positively correlated), as well as genes that are substantially lower in E and F than G (negatively correlated). Significance for ontologies was determined separately using the positively correlated genes (ontologies in red) and the negatively correlated genes (ontologies in blue).

Cluster I involved genes that correlated with being fostered or being in a mixed family (as groups A – F would be), and groups E and F generally had more similar expression to one another than to group G. The genes with positive correlation in these modules were almost entirely enriched in the oxidative phosphorylation or other related ontologies. It is not clear if these ontologies are upregulated or downregulated, however oxidative phosphorylation is considered to be the primary means of fueling neuronal

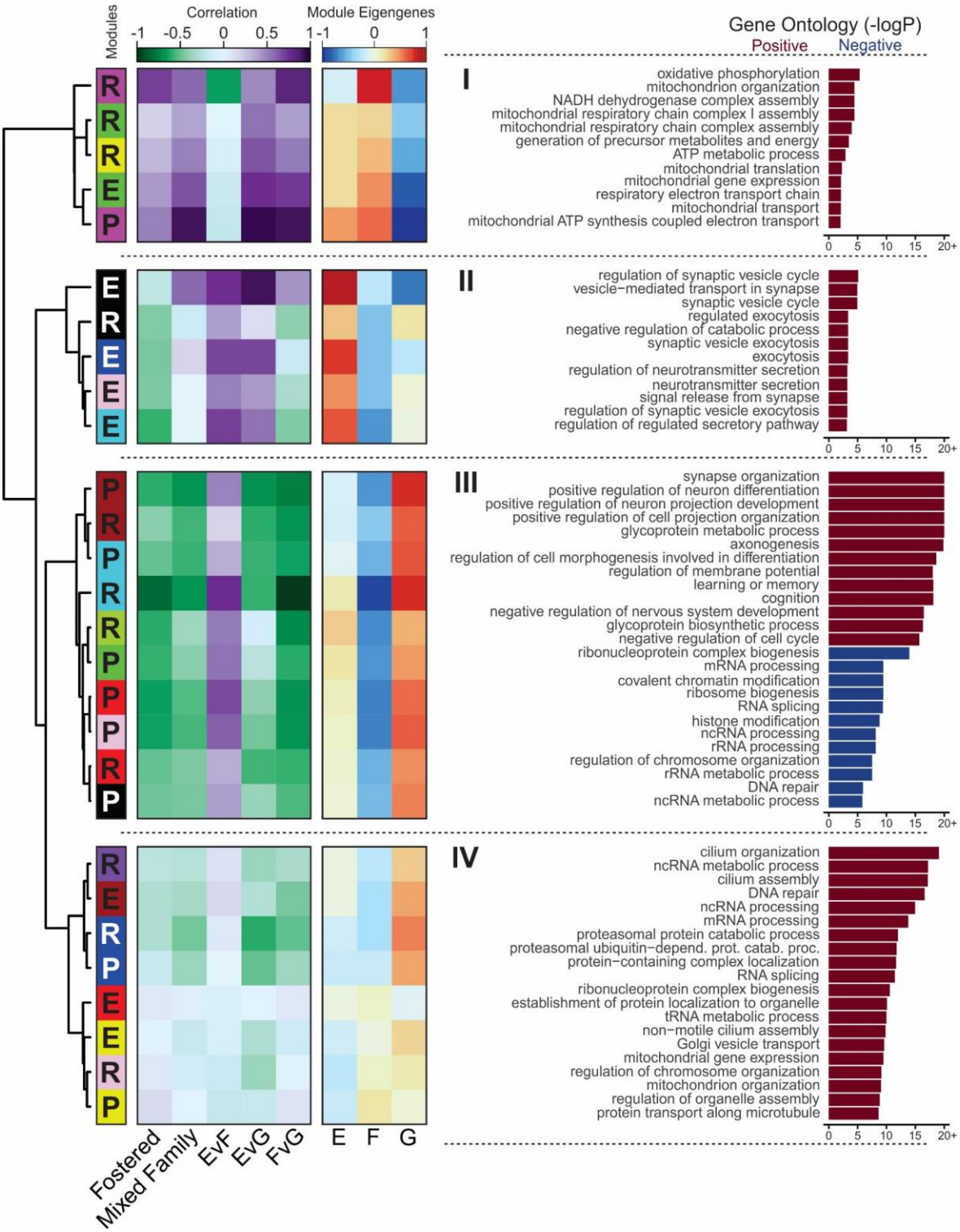

Figure 4-2 Effect of cross-fostering on RNA, enhancer, and promoter expression

Letters and colors denote the modules calculated using WGCNA. Modules are correlated against traits and module eigengenes are shown. Significantly enriched ontologies for genes that positively correlate (red) or negatively correlate (blue) with the eigengenes of the cluster.

stimulation[406].

Cluster II involved genes that correlated with being fostered, but not correlated with being in a mixed family. In this cluster, group E generally had the highest eigengene value and group F had the lowest. Genes in these modules that positively correlated with the eigengenes were largely enriched in the related group of ontologies such as synaptic vesicle cycle, exocytosis, and neurotransmitter secretion. While many of these ontologies did not achieve significance in their sub-ontologies to determine positive or negative regulation, there were a few that did. We see negative regulation of catabolic process in the top ontologies listed in the figure, but other significant directional ontologies include positive regulation of binding, neuron differentiation, and neuron projection development. The negative catabolic ontology is of interest because protein catabolism is critical for healthy neuronal function[407]. Too little degradation, as suggested in this cluster, prematurely ages the brain and is associated with diseases such as Alzheimer's[407], as well as memory and cognitive decline[408]. On the other hand, too much degradation has been linked to disorders like schizophrenia[409]. As for the positive ontologies, although the anti-NeuN antibody used to isolate the cells generally is used to isolate mature neurons, post-mitotic neuroblasts which differentiate into neurons also can express NeuN[410]. Thus, it is possible that this change in gene expression is due to recent or upcoming differentiation.

Cluster III was correlated with both being fostered and being in a mixed family, with highest eigengene value in group G and lowest in group F. Genes that positively correlated with the eigengenes (i.e. highest in group G) were enriched in ontologies associated with positive regulation of neuron differentiation, neuron projection

development, catabolic process, axonogenesis, Wnt signaling, and ion transport. In addition, there are also ontologies for negative regulation of nervous system development, cell cycle, neurogenesis, apoptotic signaling, and locomotion. Wnt signaling has been found to regulate neuron differentiation and axon growth[411], consistent with the positive ontologies we see. Genes that negatively correlated with the eigengenes were enriched in ontologies associated with RNA processing, epigenomic modifications, and DNA repair. Of all significant ontologies, negatively correlated genes were found to positively regulate chromosome organization, cell cycle, DNA repair, dendritic spine formation, and histone modification. Changes in the epigenome are high in mixed families, which is reasonable due to their altered living conditions, but it is surprising that such changes are so long lasting. The fostered mice in particular, group F, also had more cell proliferation and increased dendritic spine formation, which is associated with increased neural plasticity, memory, and learning[412]. These negatively correlated genes were also found to negatively regulate translation of mRNA to proteins and telomere maintenance. Reduced mRNA translation has been associated with neurodegenerative disorders[413] while postmitotic neurons with reduced telomere maintenance have been found to have increased DNA repair response (as we see here) and were more likely to become apoptotic[414]. Cluster IV has the mildest differences between the three groups. The genes that positively correlated with the eigengene values were enriched in many ontologies associated with core cellular functions, some of which were seen in other clusters. As there was not significant correlation with any of the traits, these ontologies do not seem to have experimental significance.

To elucidate the effect of MIA on the pups from the adopting family, we compared

groups A and D with group E (Fig. 4-3). Comparing A to E informs on the effect of being host to pups born to an MIA mother, and D to E informs on the effect of being born to an MIA mother while hosting Mock-born pups. Cluster I is the sole cluster in which groups A and D had higher eigengene values, and these modules generally correlated with being born to a MIA mother, having MIA co-siblings (like in groups A and C), or coming from a mixed family. Genes that positively correlated with this cluster were enriched in similar ontologies as in cluster I of the EFG comparison, where E and F were also higher than in G. In addition, these genes were also significantly associated with positive regulation of mitochondrial translation, which suggests that, in both this cluster and cluster I of Figure 5-2, oxidative phosphorylation is indeed being increased. Genes that negatively correlated with cluster I (i.e. generally higher in E and G) were enriched in ontologies such as positive regulation of neuron projection development, neuron differentiation, posttranscriptional gene silencing, synapse assembly, dendrite development, neuron migration, and axonogenesis. The only negatively regulated ontology was the negative regulation of translation. Together, these ontologies suggest that groups A and D have reduced numbers of newly differentiated neurons, in addition to possible reductions in neural plasticity, yet seem to have increased neural stimulation.

Cluster II had mild negative correlation to being in a mixed family or being born to an MIA mother. Group G had the highest eigengene values, with the remaining three groups having lower values. Correlated genes were associated with ontologies for the positive regulation of peptidyl-serine phosphorylation of STAT, and for the negative regulation of lipid biosynthetic processes and steroid biosynthetic processes.

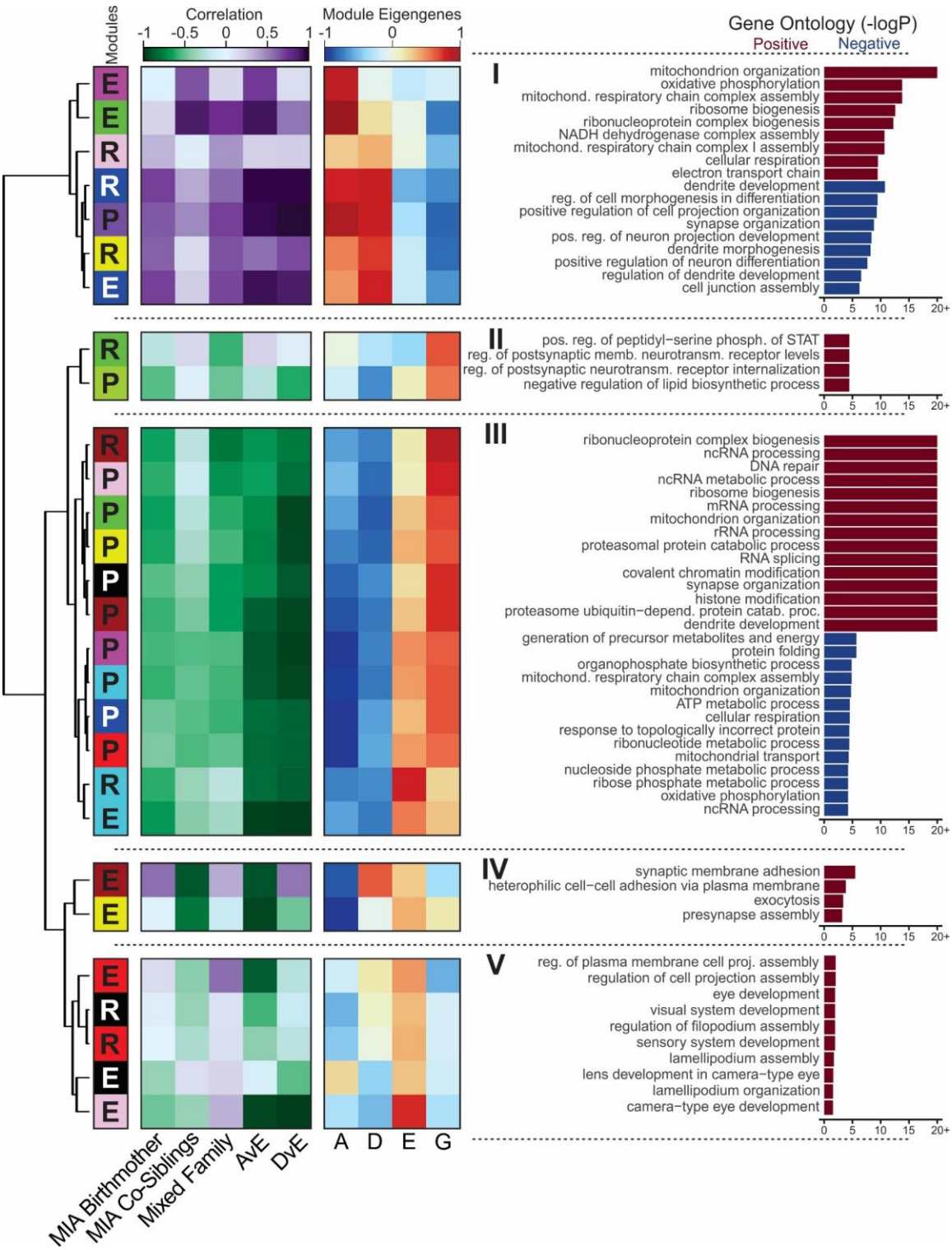

Figure 4-3 Effect of MIA on RNA, enhancer, and promoter expression of adopting pups

Letters and colors denote the modules calculated using WGCNA. Modules are correlated against traits and module eigengenes are shown. Significantly enriched ontologies for genes that positively correlate (red) or negatively correlate (blue) with the eigengenes of the cluster.

Phosphorylation of the serine in STAT proteins has been found to be involved in and highly beneficial for the survival of neurons, particularly during prolonged activation[415]. The regulation of lipid synthesis, in conjunction with the steroid synthesis, suggests the lipids synthesized are sterol lipids, such as cholesterol. Cholesterol synthesis is high in developing neurons, particularly during the process of myelination, and is key part of a neuron's cell membrane[416,417]. Since genes that negatively regulate the synthesis are reduced in groups A and D, this suggests that A and D have increased cholesterol synthesis. In addition, mature neurons gradually lose their ability to synthesize cholesterol, which may be reflected by the negative regulation seen in G, yet can be increased during stimulation[418]. However, reactive oxidation species due to sustained increases in oxidative phosphorylation can lead to increases in neuronal lipid synthesis[419,420]. While research determining if hyperlipidemia occurs in schizophrenia has been mixed[421,422], schizophrenia has been associated with oxidative stress[423].

Cluster III, in opposition to cluster I, are generally negatively correlated with the three traits and lower expression of groups A and D. Positively correlated genes in cluster III resemble the negatively correlated genes of cluster I, with positive regulation of neuron projection development, neuron differentiation, and catabolic process, as well as negative regulation of cell cycle and the apoptotic signaling pathway. Similarly, ontologies of negatively correlated genes of cluster III overlapped with those of the positively correlated genes in cluster I. In addition, they also demonstrated positive regulation of establishment of protein localization to telomere, plus negative regulation of response to endoplasmic reticulum stress and proteolysis in catabolic process. Since endoplasmic reticulum stress is highly intertwined with oxidative stress, and is considered to be a key component of

schizophrenia, this suggests that there is no means of ameliorating likely ER-stress in A and D[424].

Cluster IV had substantially reduced eigengene values in group A, with mixed expression in the remaining three groups, thus these modules had a strong correlation with having MIA co-siblings. The genes in these modules were significantly enriched in ontologies for the positive regulation of synapse assembly and cell projection, and for the negative regulation of substrate adhesion-dependent cell spreading. Substrate-based adhesive methods are primarily used during neuroblast migration, suggesting perhaps that group A has a higher proportion of recently migrated cells, and would explain the reductions in synapse assembly[425,426]. Since damaged neurons can stimulate the migration of neuroblasts to replace them, it is possible that oxidative stress is causing group A to replace their damaged neurons. If this is the case, it is unclear why group D is not.

Cluster V had variable expression among the four groups, but group E largely had the highest expression. There was only mild correlation to experimental conditions, and many of the enriched ontologies did not appear to be experimentally relevant.

In a similar, yet distinct analysis, we wanted to understand the effect of MIA on the pups that are being fostered, so we compared groups B and C with group F (Fig. 4-4). Comparing B to F determines the effect of being fostered in a Mock host family on an MIA-born pup, while C to F reveals the effect of being fostered in an MIA host family on a Mock-born pup.

Cluster I had mild correlation with being born to an immune-activated mother. Expression was largely similar across all groups, except for group B, which was lower

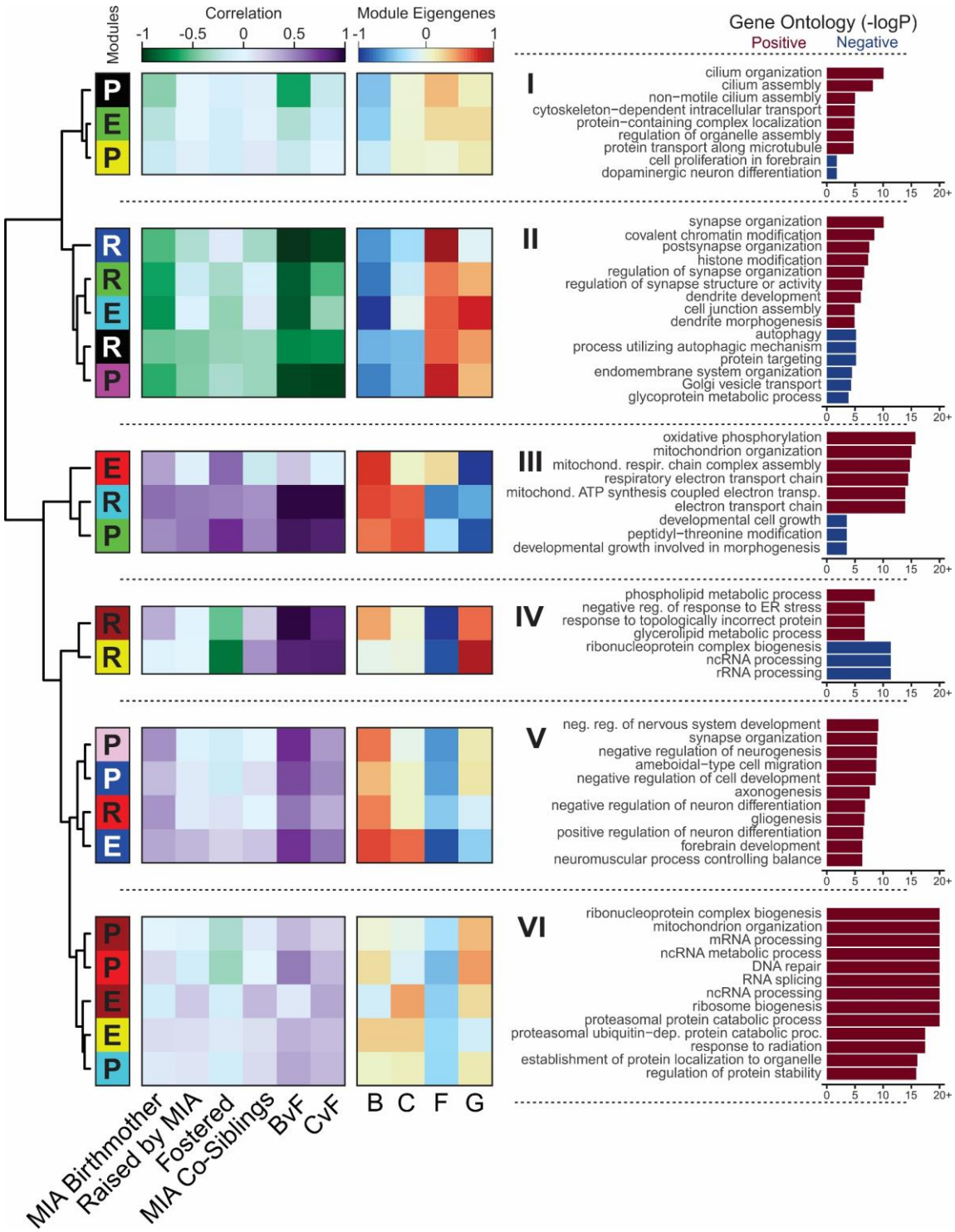

Figure 4-4 Effect of MIA on RNA, enhancer, and promoter expression of fostered pups

Letters and colors denote the modules calculated using WGCNA. Modules are correlated against traits and module eigengenes are shown. Significantly enriched ontologies for genes that positively correlate (red) or negatively correlate (blue) with the eigengenes of the cluster.

than the rest. Genes that positively correlated with the eigengene values were enriched in ontologies for the positive regulation of cellular projection, protein ubiquitination, and neuron differentiation. Meanwhile, gene that negatively correlated (i.e. were highest in group B) were enriched in ontologies associated with cell proliferation in the forebrain and dopaminergic neuron differentiation, and positive regulation of Wnt signaling. Since Wnt signaling is involved in the differentiation into dopaminergic neurons, we believe that the dopaminergic neuron differentiation is also positively regulated[427]. Furthermore, this is of interest since increased dopaminergic neuron activity in the prefrontal cortex has been implicated in schizophrenia[428,429].

Cluster II had more substantial correlation with each of the traits, and groups B and C both had lower eigengene values than groups F and G. Genes that positively correlated with the eigengenes were enriched in ontologies that positively regulated neuron projection development, neuron differentiation, synapse assembly, and CREB transcription factor activity. The CREB transcription factor family is an important part of many aspects of neuronal health and function, from neuronal survival to neural plasticity to memory formation[430,431]. In addition, altered or deficient CREB function has been implicated in schizophrenia[432]. Genes that negatively correlated with the eigengenes (i.e. higher in B and C) were significantly enriched in ontologies for the positive regulation of protein dephosphorylation, response to ER stress, and mTOR signaling. As CREB is activated through phosphorylation, the positive regulation of protein dephosphorylation is consistent with the above[431]. In addition, over-activation of mTOR signaling has been suggested to play a part in schizophrenia, and mTOR inhibitors have been found to be beneficial in neurodevelopmental disorders[433]. There were also enriched ontologies in the

negative regulation of long-term synaptic potentiation and MAP kinase activity. Long-term synaptic potentiation has been found to be impaired in schizophrenia[434], while, after inspecting the genes involved, it appears that ERK signaling is the primary affected MAPK pathway. ERK signaling has been found to be reduced in schizophrenia[435] and a previous study has shown that clozapine, an effective anti-psychotic for the treatment of schizophrenia, does upregulate the ERK signaling pathway[436].

Cluster III is the antithesis of cluster II, with positive correlation with each of the traits and higher eigengene values in groups B and C than in F and G. Much like in Figure 3, we see ontologies associated with oxidative stress enriched in genes with higher expression in groups B and C. Similarly, genes with increased expression in F and G were also enriched in ontologies seen previously, such as positive regulation of neuron differentiation, axonogenesis, and neuron migration. Again, we see that exposure to MIA in some form leads to increased oxidative stress, with reduced neural plasticity.

Cluster IV had correlation with being fostered, though groups B and C did have different expression from group F. Genes that positively correlated with the eigengene values were enriched in ontologies for the positive regulation of neuron projection organization, neuron differentiation, and synapse assembly. There were also ontologies for the negative regulation of response to endoplasmic reticulum stress and neuron apoptotic process. While this is generally consistent with our other results, there has not yet been any association of group F with ER stress. In negatively correlated genes, there was positive regulation of cell cycle, as well as some conflicting ontologies, such as both negative and positive regulation of DNA metabolic process or telomere maintenance. We were able to ascertain that this is likely due to specific aspects of each being changed.

For example, in telomere maintenance there was positive regulation of telomere capping, yet negative regulation of telomere lengthening through telomerase. Although neuron precursor cells transition from telomerase to telomere capping as they become neurons[437], it is not entirely clear what this means for the cells of group F. It is possible that group F cells are dividing more and as such have fewer fully differentiated cells, or the changes may be a malignant result of being fostered.

Cluster V had some correlation with being born to a MIA mother, and eigengene values were highest in group B, and lowest in group F. Positively correlated genes were enriched in ontologies such as positive regulation of GABAergic synaptic transmission, JNK signaling cascade, neuron death, cell cycle, and transcription by RNA polymerase I. Upregulation of the JNK cascade upregulation, in conjunction with the neuron death ontology, points to its function as an inducer of programmed cell death in this case[438]. In contrast, there are also aspects of proliferation (cell cycle, RNA pol I) at the same time. However, it has been shown that excitotoxicity (i.e. from sustained activity, see cluster I) or hypoxia (e.g. from increased oxidative phosphorylation, see cluster III) can cause mature neurons to re-enter the cell cycle, though it is almost guaranteed to end in cell death[439]. This may also explain why there are enriched ontologies for the negative regulation of growth, locomotion, and protein phosphorylation, as there is not enough energy available. Furthermore, genes with increase expression in group B that were enriched in the JNK signaling cascade also included multiple immune genes which have been implicated in neuroinflammation[440], and uncontrolled neuroinflammation is another component of schizophrenia[441]. Lastly, the inclusion of GABAergic signaling within this group of apoptotic cells could elaborate on previous evidence of deficient GABAergic

signaling in schizophrenia[442].

Cluster VI has very mild correlation with the traits, with group F having lower expression than the other three groups. Genes that positively correlated with these modules were enriched in ontologies that positively regulated protein catabolic process, neuron projection development, response to DNA damage stimulus, and translation. They were also enriched in ontologies that negatively regulated the cell cycle and organelle organization. These are generally healthy neural ontologies, and suggest that these genes are probably not experimentally relevant, but the widespread reduction in group F might warrant further investigation.

In order to have a better understanding of how each group relates to one another, we wanted to look at the overall picture. To do so, we continued with analyzing each group against their respective control, but looked at differences across the six treatment groups. First, we performed gene set enrichment analysis of gene expression from groups A – F to determine significantly over- and under-expressed pathways (Fig. 4-5a). There were the most significant changes in groups A and D, with increases in many pathways that we have mentioned previously in this manuscript, such as oxidative phosphorylation, cholesterol homeostasis, mTORC1 signaling, and adipogenesis. Between A and D, group D had reduced G2M checkpoint, suggesting reductions in the cell cycle. It also had reductions in apoptosis and TNFα signaling, though increased allograft rejection. Although there were no grafts, there was an immune response and it might be worth further investigation as to the differences in the immune response between A and D. Many of the pathways in A and D were also upregulated in groups B and C, though group B and C did not have increased expression of DNA repair, Myc targets subgroup V2, and

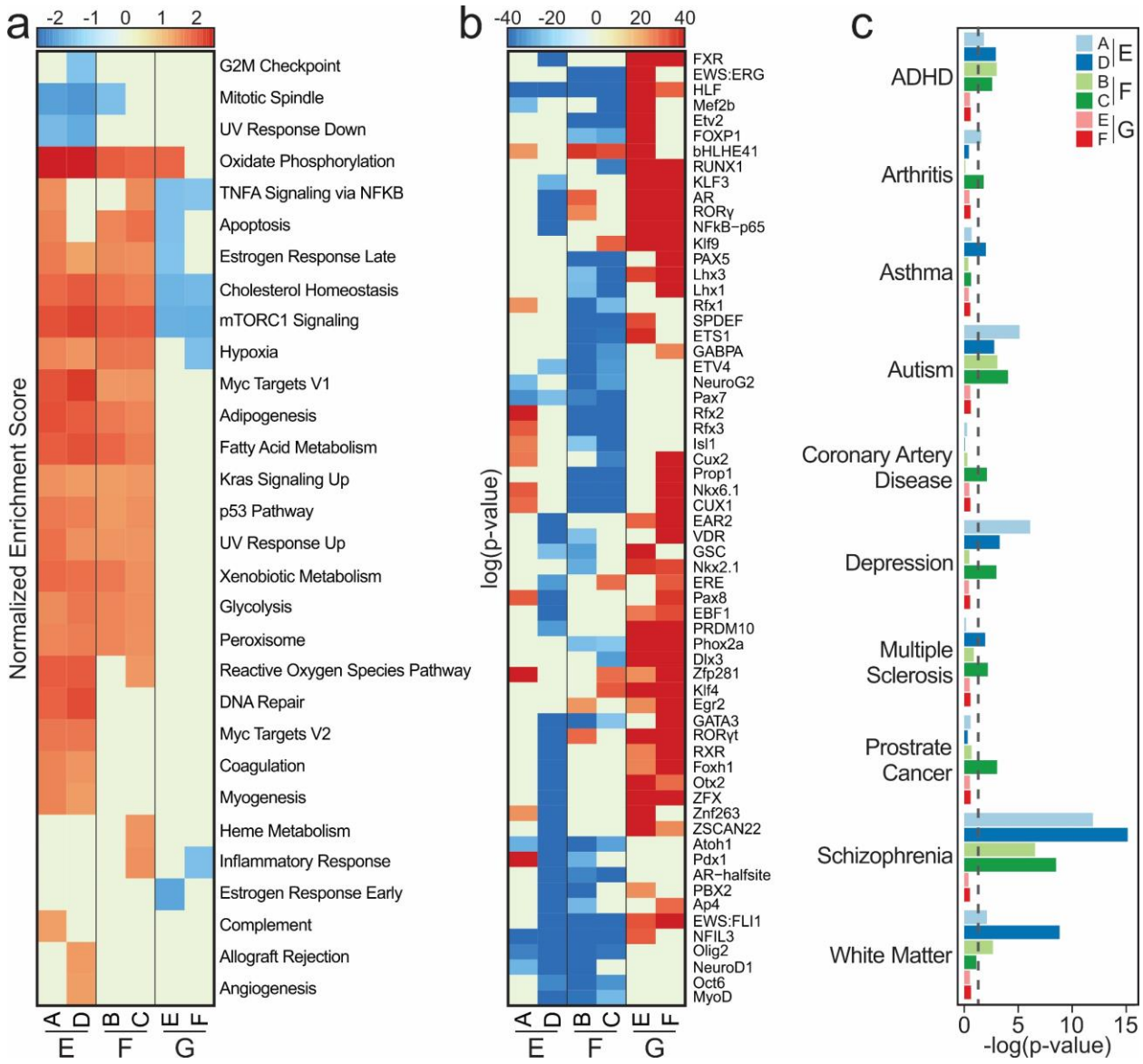

Figure 4-5 Changes in pathways, transcription factors, and SNP susceptibility

(a) Gene-set enrichment analysis of gene expression data of groups A-F, compared against their respective controls. Significant pathways are colored. (b) Significantly enriched (red) or deficient (blue) transcription factors. (c) Significance of overlap between differential enhancers and SNPs from GWAS datasets. Dashed line representative of significance cutoff ($p < 0.05$).

myogenesis. Myogenesis is the formation of skeletal muscle cells, so it is unclear why it is enriched in groups A and D, but may be related to motor neurons in the brain. Interestingly, both groups B and D did not have enrichment of TNFα signaling, and perhaps is an aspect of being born to an MIA mother. In addition, TNFα signaling has been found to not have a role in abnormal behavior as a result maternal immune activation[443]. Finally, groups E and F had far fewer changes than A-D, and the ones they had were under-expressed in E and F, except for oxidative phosphorylation. Altogether, we see that MIA has widespread changes in groups A to D, with even more changes in "hosting pups".

Next, we scanned the enhancers of each groups to determine if there are enriched or deficient transcription factor motifs present in each experimental group (Fig. 4-5b). Here, we see the first major difference between groups A and D. Group D only had deficits in transcription factor motifs, while A had a mix. Transcription factors in group D were involved in several pathways including hippo signaling (FDR=3.1E-4), oxidative stress response (FDR=0.015), and noradrenergic neuron development (FDR=0.0085), SMAD protein complex assembly (FDR=0.023). Dysregulation of hippo[444], the SMAD[445], and noradrenergic[446] signaling pathways have all been implicated in schizophrenia. Group A did not have significant enrichment of any of these pathways, and instead had pathways like axon guidance (FDR=0.0036), glucose metabolic process (FDR=0.034), and histone acetylation (FDR=0.012). Groups B and C had far more overlap and were deficient in transcription factors part of pathways such as somatic motor neuron differentiation (FDR=0.0056), norepinephrine biosynthetic process (FDR=0.016), and neuron migration (FDR=0.0096). Norepinephrine is part of the noradrenergic signaling pathway, while

motor neuron dysfunction has been found in schizophrenic patients[447]. Finally, groups E and F only had enriched transcription factors in comparison to group G, and only a couple of these were enriched in even one other group.

Finally, we analyzed differential enhancers for overlap with single nucleotide polymorphisms (SNPs) from a variety of genome-wide association study (GWAS) diseases sets to see if there any of the experimental conditions confer additional vulnerability (Fig. 4-5c). To do this, we analyzed if the enhancers overlapped with SNPs more than would be expected, and we included non-neurological disorders as well as non-psychiatric diseases of the central nervous system. We largely see significance ($p < 0.05$, denoted by the dashed line) in disorders like ADHD, Autism, depression, with a significant spike in schizophrenia. Interestingly, it appears the significance is higher in the hosting pups than in the fostered pups. Furthermore, group D had increased significance in white matter changes in the brain, a core trait of schizophrenia[448].

4.4 Discussion

While there is a clear role of epigenetics in the etiology of schizophrenia, the exact means or mechanism by which the epigenome confers these changes is not well understood. In addition, the heterogeneity of schizophrenia makes it difficult to study in humans, particularly due to the confounding effects of anti-psychotics, and so many researchers have turned to animal models. The link between maternal immune activation and resulting neurodevelopmental disorders is shared between rodents and humans, providing an ideal means of elucidating the means by which to study what brain functions are affected by fetal exposure to immune cytokines. In order to study the pre- and

postnatal effects of maternal immune activation on the resulting offspring, we utilized a cross-fostering method such that a Mock mother would raise both Mock-born and MIA-born pups, and a MIA mother would do the same. While Mock-born and Mock-raised would normally constitute a control in such studies, we included additional controls were no MIA pups were included.

We found that even being host to MIA siblings can have a significant effect on Mock-born, Mock-raised pups (group A). We see significant similarities between groups A and groups D, with increases of oxidative phosphorylation, ER stress, and cholesterol synthesis, all of which suggest a prolonged neuron stimulation, and decreases in processes that suggest reductions in neural plasticity and is consistent with previous studies of schizophrenia[423,424,449]. They even both had higher susceptibility to schizophrenia GWAS SNPs. Similarly, we also see that fostered pups, groups B and C, had significant overlap with one another, to the point that they were the only inseparable groups in a t-SNE distribution. Groups B and C also had increases in oxidative phosphorylation and reduction of neural plasticity. However, they also had increases in dopaminergic neurons and possible reduction of GABAergic neurons that was not readily seen in A and D, both of which are seen in schizophrenia[428,429,442]. Comparisons across the groups suggest the B and C had less significant oxidative phosphorylation than A and D, and also less impairments of the cell cycle. In our comparisons of Mock-only cross-fostering, the fostered mice showed improved neural plasticity, suggesting that being fostered might ameliorate the condition (for group B) or induce milder symptoms (for group C). While maternal care has not been shown to be significantly different in cross-fostering of non-MIA mice[401,402], postnatal maternal interactions can still have a

substantial effect on the physiology of developing pups[450,451]. Although A and D were largely similar, they did have notable differences in their active transcription factors and in association with SNPs implicated in white brain matter changes. In both of these, D demonstrated further schizophrenic-specific changes.

There are several avenues for future research that would address the limits within this study. First, epigenomic and transcriptomic analysis of MIA-only cross-fostering (akin to groups E, F, and G in this study) would provide some insight on if just the act of cross-fostering has an effect on the severity of changes in MIA mice. Secondly, as it clearly appears that mixing families has an effect on the hosting Mock pups (group A), there may need to be future changes to experimental structure to better study pre- and postnatal effects. Despite the use of cross-fostering as a method for pre/postnatal analysis, there has been little study of cross-fostering itself outside of animal husbandry, which has different goals in their research. Thus, the complex effects cross-fostering has on both the mother and pups is not well understood, so care must be taken to ensure each pup and each mother undergoes the same experience. For example, all mice should probably be fostered to a new mother, with no co-siblings from a different condition. This means MIA-born mice would be raised by a different MIA mother. As such, multiple litters must be included to avoid litter effects. Third, additional behavioral and physiological studies of mice that undergo the experimental conditions listed here to better understand this co-fostering effect. This study was performed in adult mice, but would also benefit from a time course study from fetus to adult brain, including the epigenome and transcriptome, to really understand the etiology of these changes. Finally, it would be interesting to

investigate the mechanism by which Mock pups are affected by their foster MIA-born co-siblings.

Despite the unexpected effect of cross-fostering in this analysis, maternal immune activation has clear effects on the epigenome and transcriptome that could help elucidate how the brain is changed as a result. This study also provides potential target pathways for future study that could lead to potential therapies. In addition, it also provides valuable insight on how to improve such experiments, to even better understand the role of MIA.

4.5 Methods

Animal handling

Pregnant CD-1 dams were purchased from Charles River Laboratory by our collaborator, Dr. Javier González-Maeso of Virginia Commonwealth University (VCU). The animal protocol was approved by the Institutional Animal Care and Use Committee (IACUC) of VCU. On day 9.5 of gestation, they exposed two female mice to the influenza virus intranasally. After the birth of the pups, half of the male pups were cross-fostered to a mother of opposite experimental condition (e.g. pups of control mother fostered by influenza-exposed mother) and weaned once appropriate. Ten week-old male pups were then sacrificed and their prefrontal cortices harvested and snap frozen. Tissues were shipped overnight to our lab and processed within an hour of arrival. A total of six mice per experimental condition was obtained, although there was removal of samples for quality control if there were less than 10,000 peaks.

Nuclei isolation

Neuronal nuclei were isolated by placing 100 mg of frozen tissue in a 7 mL glass dounce tissue grinder. Lysis buffer consisting of 5 mL of NE buffer (0.32 M sucrose, 5 mM $CaCl_2$, 3 mM $Mg(Ac)_2$, 0.1 mM EDTA, 10 mM Tris-HCL, and 0.1% Triton X-100 in Milli-Q water), 50 µL of PIC, 5 µL of 100 mM PMSF and 5 µL of 1 M DTT were added to the grinder and the grinder placed on ice until the tissue thawed. Once thawed, the tissue was dounced with pestle A 15 times and pestle B 25 times while maintaining the grinder on the ice. Homogenized tissue was filtered through a 40 µm cell strainer into a fresh tube on ice and centrifuged at 1,000 g for 10 minutes at 4 °C. The pellet was resuspended in 500 µL of NE buffer plus 5 µL of PIC, 0.5 µL of 100 mM PMSF, and 0.5 µL of 1 M DTT were added and placed on ice. Next, 750 µL of 50% (wt/vol) iodixanol (4 mL 60% iodixanol, 0.8 mL Milli-Q water containing 150 mM KCL, 30 mM $MgCl_2$, and 120 mM Tris-HCL [pH 8]), 7.5 µL of PIC, 0.75 µL of 100 mM PMSF, and 0.75 µL of 1 M DTT were added to the tube and the mixture was centrifuged at 10,000 g for 20 minutes at 4 °C. The supernatant was removed and 500 µL 2% (wt/vol) NGS/dPBS, 5 µL PIC, 0.5 µL of 100 mM PMSF, and 0.5 µL of 1 M DTT was added to the tube before incubating for 10 minutes on ice. 8 µL of nuclei suspension was set aside and diluted to 50 µL with 2% NGS/dPBS to be used as an unstained control. 4 ng of anti-NeuN Alexa 488 conjugated antibody (Millipore, MAB377X) was added to the remaining nuclei suspension and mix at 24 rpm for one hour at 4 °C in the dark. Samples were kept on ice in the dark until they could be sorted by flow cytometry into NeuN-positive (neurons) and NeuN-negative (glial).

MNase digestion of chromatin

10 µL of sorted neural nuclei suspension was combined with 0.1 µL PIC and 0.1 µL PMSF before adding 10 µL of 2x lysis buffer (4% [vol/vol] Triton X-100, 100 mM Tris-

HCL [pH 8], 100 mM NaCl, and 30 mM $MgCl_2$ in Milli-Q) and incubating at room temperature for ten minutes. We then added 1 µL of 100 mM $CaCl_2$ and 2 µL of 10 U/µL MNase (Thermo Fisher) freshly diluted in PBS before incubating for another ten minutes. MNase digestion was arrested by adding 2.2 µL of 0.5 M EDTA and the sample placed on ice for 10 minutes. After incubation, the sample was centrifuged at 16,100 g for ten minutes at 4 °C and the supernatant (~22 µL) removed to a fresh tube. 2 µL of the sample was kept as an input control and the remaining 20 µL was diluted to 50 µL with 1x lysis buffer and kept on ice before MOWChIP.

Fabrication of MOWChIP devices

PDMS devices are fabricated by multi-layer soft lithography and use a master as the mold. Masters are fabricated using photolithography. The device layout is designed using LayoutEditor (juspertor GmbH) and printed on 10k dpi transparencies (Fineline Imaging) to generate the photomasks. A photomask was generated for each of the two layers, fluidic and control layers. Next, the photoresist SU-8 2025 (MicroChem) is spun onto a 3-inch diameter silicon wafer (University Wafers). For the fluidic master, it was spun at 500 rpm for 10 seconds then at 2500 rpm for 30 seconds. For the control master, it was spun at 500 rpm for 10 seconds then at 1500 rpm for 30 seconds. The coated wafer was then baked at 95 °C for 8 minutes. The wafer was then covered with the appropriate photomask and exposed to UV light (575 mW) for 17 seconds followed by another 95 °C bake for 8 minutes. The wafer was then placed in SU-8 developer and developed for 3-5 minutes. After developing, the wafer was washed with isopropranol and dried with pressurize air. SU-8 bonding was strengthened by baking the wafer one last time at 150 °C for 15 minutes.

Once the master was prepared, the device was fabricated with polydimethylsiloxane (PDMS) polymer (Momentive, RTV 615). For the fluidic layer, 5 parts of reagent A and one part of reagent B (~36 g total) were thoroughly mixed and poured into a petri dish containing the fluidic master. For the control layer, 20 parts of reagent A and one part of reagent B (~5.25 g total) were thoroughly mixed in a weigh boat. Both PDMS mixtures were then degassed for one hour to remove air bubbles. Once degassed, the PDMS for the control layer was spun onto the control master at 500 rpm for 10 seconds followed by 1100 rpm for 30 seconds. Both PDMS covered devices were baked for ~12 minutes at 80 °C to partially cure the PDMS. Once cooled, the fluidic layer was cut and peeled. Then, it was aligned onto the control layer and baked for an additional two hours. After the bake, the PDMS device was removed from the wafer, inlet holes punched with a 2-mm hole puncher and cut into multi-unit slabs. Each slab was bonded to a cleaned glass slide and baked for an additional hour to strengthen the bond.

MOWChIP-seq

Protein A-coated Dynabeads (Life Technologies) were washed twice with IP buffer (20 mM Tris-HCl [pH 8], 140 mM NaCl, 1 mM EDTA, 0.5 mM EGTA, 0.1% (w/v) sodium doxycholate, 0.1% SDS, 1% (v/v) Triton-100X in Milli-Q water) before being resuspended in 150 µL of IP buffer and 0.5 µg of either H3K4me3 (Abcam, ab8580) or H3K27ac (Active Motif, 39133) antibody. The bead solution was then rotated at 4 °C for 2 hours. After incubation, beads were washed three times, resuspended in 5 µL of IP, and placed on ice until use.

For the operation of the MOWChIP device, the on-device valve was actuated by a solenoid valve in conjunction with a compressed air outlet. The solenoid valve was

manipulated with a data acquisition card and through the LabVIEW (National Instruments) program. First, the on chip sieve valve is filled with water (30 psi). Once all the air has been expelled, the valve is opened and IP buffer is flowed through the inlet at a flow rate of 200 µL/min by use of a syringe pump connected to PFA tubing. The flow rate was decreased to 1 µL/min, the sieve valve closed, and IP buffer flowed for an additional 2 minutes before the flow was stopped and the tubing removed. The antibody-coated beads were loaded into the inlet by pipette and guided into the main chamber with a magnet. Next, the chromatin sample was flowed through at 1.5 µL/minute and the magnet was used to form the beads into a packed bed after five minutes of flow. After the chromatin was finished, IP buffer was flowed for 5 minutes at 1.5 µL/minute. Oscillatory washing was then performed with 50 µL of Low Salt washing buffer (20 mM Tris-HCl [pH 8], 150 mM NaCl, 2 mM EDTA, 0.1% SDS, 1% (v/v) Triton-100X in Milli-Q water) for five minutes at ~0.65 psi (valve open). Another five-minute oscillatory wash was performed with High Salt washing buffer (20 mM Tris-HCl [pH 8], 500 mM NaCl, 2 mM EDTA, 0.1% SDS, 1% (v/v) Triton-100X in Milli-Q water). The sieve valve was closed and IP buffer flowed for an additional 2 minutes. Finally, the sieve valve was opened and the beads were flowed out at 200 µL/min with IP buffer.

ChIP DNA Isolation

Tubes containing IP beads were placed on a magnet and the supernatant removed. 100 µL of elution buffer (10 mM Tris-HCl [pH 8], 50 mM NaCl, 10mM EDTA, 0.03% SDS in Milli-Q water) was added to the tube, followed by 4 µL of 20 mg/mL proteinase K. For the input sample, 90 µL of elution buffer and 4 µL of proteinase K were added. Samples were then incubated at 65 °C for 8 hours. Once completed, the samples were vortexed

and briefly centrifuged. 100 µL of phenol-chloroform was added into each tube and vortexed for one minute, then centrifuged at 16,000 g for 10 minutes. The upper aqueous phase was carefully removed to a fresh tube. Next, an ethanol precipitation of the DNA was performed by adding 480 µL of 100% ethanol, 60 µL of 5 M ammonium acetate, and 6 µL of glycogen. The mixture was vortexed briefly and placed at -80 °C for two hours. Then, the samples were centrifuged at 16,100 g for 10 minutes at 4 °C and the supernatant removed. 500 µL of cold 70% ethanol was added and the samples were centrifuged for an additional five minutes. The supernatant was discarded and the DNA pellets were air dried for 10 minutes before resuspension in 12 µL of low EDTA TE buffer (Swift Biosciences).

Determining Sample Enrichment

For each sample and sample input, 2 µL of DNA was diluted to 20 µL with low EDTA TE buffer. A 20 µL qPCR reaction was assembled using 10 µL of SYBR Green Master Mix (BioRad), 1.4 µL of combined forward and reverse primers, and 8.6 µL of DNA in a 96-well plate. Each histone mark was tested with one positive and one negative primer (Table 4-1):

Table 4-1 Mouse H3K4me3 and H3K27ac Primers

Histone Mark	Name	Type	F/R	Primer
H3K4me3	Gapdh-2	Positive	F+R	Active motif cat. #71018
	Negative 1	Negative	F+R	Active motif cat. #71011
H3K27ac	Zranb3	Positive	F	GAA TGT ACC AGC GTC TCT TCT C
			R	TTT CTC TTT GGC AGC CTC TC
	N3	Negative	F	GCC CAT AAA GAA GGA GCT AGA G
			R	GCA GCT AGA GAC AAG AGT TCT G

The qPCR was then performed by first denaturing the DNA for 2 minutes at 95 °C followed by 45 cycles of 95 °C for 15 seconds, 58 °C for 20 seconds, and 72 °C for 20 seconds. Once the qPCR was completed, the enrichment was determined by the following equation:

$$Enrichment = \frac{Percent\ input\ of\ positive\ locus}{Percent\ input\ of\ negative\ locus}$$

where the positive and negative percent inputs are calculated by:

$$Percent\ Input = 2^{\left(Ct_{input} - \frac{\log(Dilution\ Factor)}{log2} - Ct_{ChIP}\right)} \times 100\%$$

The Ct values of the input and ChIP were taken from the qPCR results and the dilution factor is defined as follows:

$$Dilution\ Factor = \frac{Sample\ vol.of\ input\ DNA + Sample\ vol.of\ ChIP\ DNA}{Sample\ vol.of\ input\ DNA}$$

ChIP-seq Library Preparation

Library preparation was performed using the Accel-NGS 2S Plus DNA Library Kit protocol (Swift Biosciences) with minor modifications as described below. For each library, 8 µL of sample was used. For all steps, we used options that pertained to samples with less than 10 ng of genomic DNA. At the end of the Ligation II clean-up, beads were resuspended in 22 µL of low EDTA TE buffer. Then, 20 µL of the ChIP sample was used in the PCR-Library Amplification step, along with 2.5 µL of 20X EvaGreen dye (Biotium) to monitor the amplification. Amplification was stopped when the fluorescent intensity of a sample had increased by 3000 RFU over its baseline (typically ~13-14 cycles). After the library bead clean-up, samples were resuspended in 10 µL of low EDTA TE buffer and the library enrichment was determined.

RNA-seq Sample Preparation

RNA was extracted from nuclei with the RNeasy Mini Kit (Qiagen). It was performed as per manufacturer's instructions with the inclusion of the optional deoxyribonuclease treatment to remove DNA contamination. Complementary DNA was synthesized using ~1 ng of isolated RNA with the SMART-Seq v4 Ultra Low Input RNA Kit (Clontech), with 14 cycles of amplification. The purified cDNA was then used in the library preparation using the Nextera XT DNA Library Prep Kit (Illumina) according to manufacturer's instructions.

Data Sequencing

Libraries were quantified using a KAPA Library Quantification kit (KAPA Biosystems) and fragment sizes were verified using the High Sensitivity DNA Analysis kit on a TapeStation (Agilent). Libraries were pooled to a final concentration of 10 nM and sequenced with an Illumina HiSeq 4000 using single-end 50 bp reads.

Data Quality Control

Replicates that had fewer than 10,000 called peaks were removed from further analysis. After quality control, technical replicates were combined such that each replicate represent one histone mark of one biological sample. Any combined replicates with fewer than 10,000 called peaks were also removed. There were a total of 6 biological samples for each mark in each group, except for group A. This was due to three of the mice having poor correlation with the remaining samples. Due to the high intragroup correlation seen among all of the groups, these three mice were temporarily removed until we can raise and analyze more group A mice.

Data Processing

Unless otherwise mentioned, all data analysis was performed with Bash scripts or with R (The R Foundation) scripts in RStudio. Sequencing reads were trimmed using default settings by Trim Galore! (Babraham Institute). Trimmed reads were aligned to the mm9 genome with Bowtie[80]. Peaks were called using MACS2 ($q < 0.05$)[81]. Blacklisted regions in mm9 as defined by ENCODE were removed to improve data quality[82]. Mapped reads from ChIP and input samples were extended by 100bp on either side (250bp total) and a normalized signal was calculated.

$$Normalized\ Signal = \left(\frac{ChIP\ Signal}{No.of\ ChIP\ Reads} - \frac{Input\ Signal}{No.of\ Input\ Reads}\right) \times 10^6$$

For Pearson's correlation, the signal was calculated over the promoter region (TSS +/- 2 kb) and plotted with the corr and levelplot functions. RNA-seq data was quantified using Salmon[41] against the mm10 transcriptome using a full decoy and normalized counts were calculated with DESeq2[314]. For visualization in IGV (Broad Institute), the signal was calculated in 100 bp windows over the entire genome and output as a bigWig file.

ChIP-seq Analysis

To call enhancers, we considered H3K27ac^{high} regions that did not intersect with promoter regions to be enhancer regions. First, consensus H3K27ac peak sets were generated for each of the experimental conditions and the peak widths were set to 1000 bp long (summit +/-500 bp). Any of the H3K27ac 1kb regions that intersected with a promoter region (TSS +/- 2000 bp) was removed completely. Remaining regions were considered to be putative enhancers. Expression of the putative enhancers was correlated (Spearman) to RNA-seq gene expression values within the same topological domain with the highest correlation. Enhancer-gene linkages were only retained if the

Spearman correlation coefficient (SCC) > 0.25 and if the correlation was considered significant if both empirical and quantitative p-values were less than 0.05. The empirical p-value was calculated as the fraction of genes on the same chromosome that had a higher correlation with the enhancer than the currently linked gene. The quantitative p-value was calculated by treating the using the distribution of all SCC values calculated between the enhancer and all other genes on the same chromosome to calculate a significance. DiffBind[83,84] was used for normalization of enhancer and promoter signals, as well as to determine differentially expressed enhancers (FDR < 0.05) for the GWAS SNP analysis (see below). Motif analysis was performed to determine enriched and deficient transcription factor binding motifs among the enhancer regions with HOMER[87] (with options –size 1000 –mask –p 16 –nomotif) by alternatively setting the control set and the treatment set of enhancers as the background. Transcription factors were analyzed with Panther's[88] Overrepresentation Test (20210224 release) for biological process gene ontologies (20210201 release) against all mouse genes. Fisher's Exact test was used with False Discovery Rate.

RNA Analysis

RNA-seq data was quantified using Salmon[41] against the mm10 transcriptome using a full decoy and normalized counts were calculated with DESeq2[314]. Gene-set enrichment analysis was performed with GSEA[315,316] using the Hallmark gene set and gene-set level permutation. Gene sets were considered significant if the FDR < 0.05.

Weighted Gene Correlation Network Analysis (WGCNA)

For each of the three analyses (EFG, ADEG, and BCFG), RNA-seq data, enhancer signal, and promoter signal was clustered separately using the WGCNA package in R[452].

Unsigned networks were generated using signed topological overlap matrices, bicorrelation, and a soft-thresholding power that was calculated to be appropriate for each individual network. Each of the modules were clustered based off of group eigengene value using hierarchical clustering. Then, the genes from each cluster were separated into positive and negative correlating sets and analyzed for gene ontologies with clusterProfiler.

Association of Enhancers to SNPs

Differential enhancer locations were converted from mm10 to hg19 through UCSC's liftOver tool (minMatch=0.1). GWAS datasets were obtained from NHGRI-EBI's GWAS Catalog (https://www.ebi.ac.uk/gwas/home) and any SNPs that did not have a reference SNP ID were removed. In addition, SNPs that were not present in the 1000 Genome Project Phase 3 European population were removed. For n SNPs present in a given GWAS set, n SNPs would be randomly selected from all possible SNPs while maintaining the same SNP location distribution (e.g. 5 on chromosome 1, 2 on chromosome 2, etc.). This was performed 5,000 times, and the number of overlaps between the dummy SNP set and differential enhancers was calculated. This distribution was used to calculate the significance of the overlap between the differential enhancers and the real GWAS SNP sets.

5 Summary and Outlook

With the advancements in sequencing technology over the past two decades, we are capable of obtaining greater insights to the etiology of the diseases and illnesses that affect us. In this dissertation, I have analyzed the epigenomic and transcriptomic changes that occur due to insult or genetic mutation, and how these changes may explain the means by which disease or illness occur. This includes how mutation of the *BRCA1* gene facilitates breast cancer, how chronic low levels of lipopolysaccharide cause low-grade inflammation and how that differs from acute inflammation, and how activation of the maternal immune system during pregnancy can predispose mental illness in the offspring. More studies are still necessary, not only for other diseases, but for the ones I have examined here.

Many environmental and genetic factors can lead to breast cancer, including many genetic mutations other than BRCA1. However, BRCA1 is one of the most significant genes for breast cancer, and much is yet to be learned as to how it predisposes breast cancer. To fully map the epigenomic and transcriptomic trajectory of healthy breast tissue from BRCA1 mutant women to cancerous, would require samples taken from the same women over years. Furthermore, such studies would be most benefitted by taking into account variables such as pre/post-menopausal, parous or nulliparous, age, and resulting tumor type (if any). Yet, more timely and feasible studies are preferable. Instead, the physiology of the mutant basal cells can be inspected for similarities to non-carrier luminal progenitors, particularly in combination with transcriptomic analysis, to better understand if the subpopulation of the basal compartment is transitioning to LP cells. It is possible to

separate this subpopulation from the remainder of the basal cell compartment, which would provide more precise results.

Chronic inflammation is a widespread problem, particular for those that follow a Western lifestyle. Despite elucidating some of the mechanisms that are different between low-grade and acute inflammation, they are but one small piece of the puzzle. The immune system is vast, with many interacting cell types and competing signaling pathways. Asides from performing similar studies on other immune cell types, further study of inflammation in BMDMs is warranted. Such studies might include both time scale studies and LPS gradient studies, to determine if changes due to varied LPS dosage occur on a continuous or discrete scale. However, utilizing additional knockout or conditional knockout mice to further elucidate the mechanistic differences between low-grade and acute inflammation may lead to more rapid and substantive results. Conditional knock-out mice, in particular, are useful for understanding the *in vivo* role of a specific gene in a certain cell or tissue, while leaving the remainder of the body unaltered. This allows for deletion of otherwise critical genes, as well as genes that could cause confounding effects on the cells or tissues targeted for research.

Lastly, activation of the maternal immune system during pregnancy can happen to any woman. With the recent COVID-19 pandemic, this may have a more widespread impact in the years to come. To better understand the effect of maternal immune activation, there are multiple studies that can be performed such as time course studies in which the mice offspring are analyzed at different ages, including prenatally. Beyond traditional genomic and epigenomic analysis, as *in situ* sequencing technologies advance, analysis of how MIA affects histone modifications and gene expression across the various

regions of the brain could provide insight for potential therapies. In the study of MIA in mice, we also discovered some unexpected changes due to cross-fostering that could be further studied to better understand the post-natal effects on MIA.

If we focused a future study on the postnatal and cross-fostering aspects of MIA, several more experimental groups would be necessary. Groups A'-D' would mimic A-D, though have no co-siblings, and groups A' and D' will be reared by a different Mock and MIA mother, respectively. Groups E'-G' would undergo the same conditions as E-G, but using only MIA mice, leading to a total of 7 experimental groups. These cross-fostering experiments would have to occur 3 times, with each experiment on the prefrontal cortex occurring when the pups reach 10 weeks of age. One batch will be used for behavioral testing, utilizing tests such as, but not limited to, head twitch behavior, locomotor ability, and working memory to track schizophrenic behaviors in the experimental groups. The brains of the second group would undergo diffusion tensor imaging to measure white and gray matter volumes and neurochemical analysis to measure neurotransmitter (dopamine, serotonin, etc.) levels and their metabolites. The third batch would be utilized for epigenomic and transcriptomic profiling. While including additional epigenomic marks is ideal, particularly the gene repressors H3K27me3 and DNA methylation, it is difficult to determine if there would be enough of a return of investment to warrant the additional time and cost.

First, we hypothesize that exposure to MIA mothers leads to neural changes in the exposed offspring. If this hypothesis is fully true, we will see that groups A' and C' are distinct groups. Previously acquired experimental data from group C could also be used to determine if exposure to both an MIA mother and MIA-born pups is more substantial

than MIA mother alone. Next, we hypothesize that these effects are propagated through changes in the gut microbiota. The gut microbiome of each of the mice from Groups A'-D' should be profiled, as well as those of the mothers immediately post-weaning. We would expect changes in the microbiota of both pups and mothers in groups B' and C'. Finally, we hypothesize that cross-fostering is protective, regardless of rearing mother. By analyzing groups E' – G', we would expect to see reduced changes in both E' and F', with F' having more substantial reductions.

Altogether, current sequencing technologies provide us with vast opportunities to unravel the mysteries surrounding the diseases and illnesses that can afflict us. Despite the advancements of sequencing technologies, sometimes obtaining sufficient clinical samples necessary for study presents the greatest challenge. As such, leveraging microfluidics in conjunction with bioinformatics techniques allows us unprecedented insight into the mechanisms of disease onset, particularly in studies previously considered to be out-of-reach due to low cell numbers available for study.

References

1 Allis, C. D. & Jenuwein, T. The molecular hallmarks of epigenetic control. *Nat Rev Genet* **17**, 487-500, doi:10.1038/nrg.2016.59 (2016).

2 Feinberg, A. P. The Key Role of Epigenetics in Human Disease Prevention and Mitigation. *N Engl J Med* **378**, 1323-1334, doi:10.1056/NEJMra1402513 (2018).

3 Marchion, D. & Munster, P. Development of histone deacetylase inhibitors for cancer treatment. *Expert Rev Anticancer Ther* **7**, 583-598, doi:10.1586/14737140.7.4.583 (2007).

4 Kouzarides, T. Chromatin modifications and their function. *Cell* **128**, 693-705, doi:10.1016/j.cell.2007.02.005 (2007).

5 Over, R. S. & Michaels, S. D. Open and closed: the roles of linker histones in plants and animals. *Mol Plant* **7**, 481-491, doi:10.1093/mp/sst164 (2014).

6 Creyghton, M. P. *et al.* Histone H3K27ac separates active from poised enhancers and predicts developmental state. *Proc Natl Acad Sci U S A* **107**, 21931-21936, doi:10.1073/pnas.1016071107 (2010).

7 Rada-Iglesias, A. *et al.* A unique chromatin signature uncovers early developmental enhancers in humans. *Nature* **470**, 279-283, doi:10.1038/nature09692 (2011).

8 Gates, L. A. *et al.* Acetylation on histone H3 lysine 9 mediates a switch from transcription initiation to elongation. *J Biol Chem* **292**, 14456-14472, doi:10.1074/jbc.M117.802074 (2017).

9 Peters, A. H. F. M. *et al.* Partitioning and Plasticity of Repressive Histone Methylation States in Mammalian Chromatin. *Molecular Cell* **12**, 1577-1589, doi:10.1016/s1097-2765(03)00477-5 (2003).

10 Cao, R. *et al.* Role of histone H3 lysine 27 methylation in Polycomb-group silencing. *Science* **298**, 1039-1043, doi:10.1126/science.1076997 (2002).

11 Heintzman, N. D. *et al.* Distinct and predictive chromatin signatures of transcriptional promoters and enhancers in the human genome. *Nat Genet* **39**, 311-318, doi:10.1038/ng1966 (2007).

12 Farooq, Z., Banday, S., Pandita, T. K. & Altaf, M. The many faces of histone H3K79 methylation. *Mutat Res Rev Mutat Res* **768**, 46-52, doi:10.1016/j.mrrev.2016.03.005 (2016).

13 Collas, P. The current state of chromatin immunoprecipitation. *Mol Biotechnol* **45**, 87-100, doi:10.1007/s12033-009-9239-8 (2010).

14 Slansky, J. E. Antigen-specific T cells: analyses of the needles in the haystack. *PLoS Biol* **1**, E78, doi:10.1371/journal.pbio.0000078 (2003).

15 Cima, I. *et al.* Tumor-derived circulating endothelial cell clusters in colorectal cancer. *Sci Transl Med* **8**, 345ra389, doi:10.1126/scitranslmed.aad7369 (2016).

16 Jang, Y.-Y. & Sharkis, S. J. Stem Cell Plasticity: A Rare Cell, Not a Rare Event. *Stem Cell Reviews* **1**, 045-052, doi:10.1385/scr:1:1:045 (2005).

17 Stoler, D. L., Stewart, C. C. & Stomper, P. C. Breast epithelium procurement from stereotactic core biopsy washings: flow cytometry-sorted cell count analysis. *Clin Cancer Res* **8**, 428-432 (2002).

18 Cao, Z., Chen, C., He, B., Tan, K. & Lu, C. A microfluidic device for epigenomic profiling using 100 cells. *Nat Methods* **12**, 959-962, doi:10.1038/nmeth.3488 (2015).

19 Adli, M., Zhu, J. & Bernstein, B. E. Genome-wide chromatin maps derived from limited numbers of hematopoietic progenitors. *Nat Methods* **7**, 615-618, doi:10.1038/nmeth.1478 (2010).

20 Zhu, B. *et al.* MOWChIP-seq for low-input and multiplexed profiling of genome-wide histone modifications. *Nat Protoc* **14**, 3366-3394, doi:10.1038/s41596-019-0223-x (2019).

21 Rotem, A. *et al.* Single-cell ChIP-seq reveals cell subpopulations defined by chromatin state. *Nat Biotechnol* **33**, 1165-1172, doi:10.1038/nbt.3383 (2015).

22 Skene, P. J. & Henikoff, S. An efficient targeted nuclease strategy for high-resolution mapping of DNA binding sites. *Elife* **6**, doi:10.7554/eLife.21856 (2017).

23 Skene, P. J., Henikoff, J. G. & Henikoff, S. Targeted in situ genome-wide profiling with high efficiency for low cell numbers. *Nat Protoc* **13**, 1006-1019, doi:10.1038/nprot.2018.015 (2018).

24 Harada, A. *et al.* A chromatin integration labelling method enables epigenomic profiling with lower input. *Nat Cell Biol* **21**, 287-296, doi:10.1038/s41556-018-0248-3 (2019).

25 Sanger, F., Nicklen, S. & Coulson, A. R. DNA sequencing with chain-terminating inhibitors. *Proc Natl Acad Sci U S A* **74**, 5463-5467, doi:10.1073/pnas.74.12.5463 (1977).

26 Heather, J. M. & Chain, B. The sequence of sequencers: The history of sequencing DNA. *Genomics* **107**, 1-8, doi:10.1016/j.ygeno.2015.11.003 (2016).

27 Venter, J. C. *et al.* The sequence of the human genome. *Science* **291**, 1304-1351, doi:10.1126/science.1058040 (2001).

28 Grada, A. & Weinbrecht, K. Next-generation sequencing: methodology and application. *J Invest Dermatol* **133**, e11, doi:10.1038/jid.2013.248 (2013).

29 Park, S. T. & Kim, J. Trends in Next-Generation Sequencing and a New Era for Whole Genome Sequencing. *Int Neurourol J* **20**, S76-83, doi:10.5213/inj.1632742.371 (2016).

30 Voelkerding, K. V., Dames, S. A. & Durtschi, J. D. Next-generation sequencing: from basic research to diagnostics. *Clin Chem* **55**, 641-658, doi:10.1373/clinchem.2008.112789 (2009).

31 Ardui, S., Ameur, A., Vermeesch, J. R. & Hestand, M. S. Single molecule real-time (SMRT) sequencing comes of age: applications and utilities for medical diagnostics. *Nucleic Acids Res* **46**, 2159-2168, doi:10.1093/nar/gky066 (2018).

32 Eid, J. *et al.* Real-time DNA sequencing from single polymerase molecules. *Science* **323**, 133-138, doi:10.1126/science.1162986 (2009).

33 Clarke, J. *et al.* Continuous base identification for single-molecule nanopore DNA sequencing. *Nat Nanotechnol* **4**, 265-270, doi:10.1038/nnano.2009.12 (2009).

34 Jain, M. *et al.* Nanopore sequencing and assembly of a human genome with ultra-long reads. *Nat Biotechnol* **36**, 338-345, doi:10.1038/nbt.4060 (2018).

35 Ong, C. T. & Corces, V. G. Enhancer function: new insights into the regulation of tissue-specific gene expression. *Nat Rev Genet* **12**, 283-293, doi:10.1038/nrg2957 (2011).

36 Calo, E. & Wysocka, J. Modification of enhancer chromatin: what, how, and why? *Mol Cell* **49**, 825-837, doi:10.1016/j.molcel.2013.01.038 (2013).

37 Hnisz, D. *et al.* Super-enhancers in the control of cell identity and disease. *Cell* **155**, 934-947, doi:10.1016/j.cell.2013.09.053 (2013).

38 Bernstein, B. E. *et al.* A bivalent chromatin structure marks key developmental genes in embryonic stem cells. *Cell* **125**, 315-326, doi:10.1016/j.cell.2006.02.041 (2006).

39 Costa, V., Angelini, C., De Feis, I. & Ciccodicola, A. Uncovering the complexity of transcriptomes with RNA-Seq. *J Biomed Biotechnol* **2010**, 853916, doi:10.1155/2010/853916 (2010).

40 Stark, R., Grzelak, M. & Hadfield, J. RNA sequencing: the teenage years. *Nat Rev Genet* **20**, 631-656, doi:10.1038/s41576-019-0150-2 (2019).

41 Patro, R., Duggal, G., Love, M. I., Irizarry, R. A. & Kingsford, C. Salmon provides fast and bias-aware quantification of transcript expression. *Nat Methods* **14**, 417-419, doi:10.1038/nmeth.4197 (2017).

42 Wu, D. C., Yao, J., Ho, K. S., Lambowitz, A. M. & Wilke, C. O. Limitations of alignment-free tools in total RNA-seq quantification. *BMC Genomics* **19**, 510, doi:10.1186/s12864-018-4869-5 (2018).

43 Patel, S. Breast cancer: Lesser-known facets and hypotheses. *Biomed Pharmacother* **98**, 499-506, doi:10.1016/j.biopha.2017.12.087 (2018).

44 Harbeck, N., Salem, M., Nitz, U., Gluz, O. & Liedtke, C. Personalized treatment of early-stage breast cancer: present concepts and future directions. *Cancer Treat Rev* **36**, 584-594, doi:10.1016/j.ctrv.2010.04.007 (2010).

45 Harbeck, N. & Gnant, M. Breast cancer. *The Lancet* **389**, 1134-1150, doi:10.1016/s0140-6736(16)31891-8 (2017).

46 Miki, Y. *et al.* A strong candidate for the breast and ovarian cancer susceptibility gene BRCA1. *Science* **266**, 66-71, doi:10.1126/science.7545954 (1994).

47 Hall, J. M. *et al.* Linkage of early-onset familial breast cancer to chromosome 17q21. *Science* **250**, 1684-1689, doi:10.1126/science.2270482 (1990).

48 Ford, D. Risks of cancer in BRCA1-mutation carriers. *The Lancet* **343**, 692-695, doi:10.1016/s0140-6736(94)91578-4 (1994).

49 Chen, S. *et al.* Characterization of BRCA1 and BRCA2 mutations in a large United States sample. *J Clin Oncol* **24**, 863-871, doi:10.1200/JCO.2005.03.6772 (2006).

50 Mavaddat, N. *et al.* Cancer risks for BRCA1 and BRCA2 mutation carriers: results from prospective analysis of EMBRACE. *J Natl Cancer Inst* **105**, 812-822, doi:10.1093/jnci/djt095 (2013).

51 Romagnolo, A., Romagnolo, D. & Selmin, O. BRCA1 as Target for Breast Cancer Prevention and Therapy. *Anti-Cancer Agents in Medicinal Chemistry* **15**, 4-14, doi:10.2174/1871520614666141020153543 (2014).

52 Templeton, A. J. *et al.* Interaction between Hormonal Receptor Status, Age and Survival in Patients with BRCA1/2 Germline Mutations: A Systematic Review and Meta-Regression. *PLoS One* **11**, e0154789, doi:10.1371/journal.pone.0154789 (2016).

53 Sundquist, M., Thorstenson, S., Brudin, L., Wingren, S. & Nordenskjold, B. Incidence and prognosis in early onset breast cancer. *Breast* **11**, 30-35, doi:10.1054/brst.2001.0358 (2002).

54 Gudmundsdottir, K. & Ashworth, A. The roles of BRCA1 and BRCA2 and associated proteins in the maintenance of genomic stability. *Oncogene* **25**, 5864-5874, doi:10.1038/sj.onc.1209874 (2006).

55 Bayraktar, S. & Gluck, S. Systemic therapy options in BRCA mutation-associated breast cancer. *Breast Cancer Res Treat* **135**, 355-366, doi:10.1007/s10549-012-2158-6 (2012).

56 Suijkerbuijk, K. P. *et al.* Methylation is less abundant in BRCA1-associated compared with sporadic breast cancer. *Ann Oncol* **19**, 1870-1874, doi:10.1093/annonc/mdn409 (2008).

57 Shukla, V. *et al.* BRCA1 affects global DNA methylation through regulation of DNMT1. *Cell Res* **20**, 1201-1215, doi:10.1038/cr.2010.128 (2010).

58 Archey, W. B. *et al.* Increased CpG methylation of the estrogen receptor gene in BRCA1-linked estrogen receptor-negative breast cancers. *Oncogene* **21**, 7034-7041, doi:10.1038/sj.onc.1205844 (2002).

59 Yarden, R. I. & Brody, L. C. BRCA1 interacts with components of the histone deacetylase complex. *Proc Natl Acad Sci U S A* **96**, 4983-4988, doi:10.1073/pnas.96.9.4983 (1999).

60 Chang, S. *et al.* Tumor suppressor BRCA1 epigenetically controls oncogenic microRNA-155. *Nat Med* **17**, 1275-1282, doi:10.1038/nm.2459 (2011).

61 Zhu, Q. *et al.* BRCA1 tumour suppression occurs via heterochromatin-mediated silencing. *Nature* **477**, 179-184, doi:10.1038/nature10371 (2011).

62 Zhu, Q. *et al.* Heterochromatin-Encoded Satellite RNAs Induce Breast Cancer. *Mol Cell* **70**, 842-853 e847, doi:10.1016/j.molcel.2018.04.023 (2018).

63 Fu, N. Y., Lindeman, G. J. & Visvader, J. E. The Mammary Stem Cell Hierarchy. *Curr Top Dev Biol* **107**, 133-160, doi:10.1016/B978-0-12-416022-4.00005-6 (2014).

64 Choudhury, S. *et al.* Molecular Profiling of Human Mammary Gland Links Breast Cancer Risk to a p27(+) Cell Population with Progenitor Characteristics. *Cell Stem Cell* **13**, 117-130, doi:10.1016/j.stem.2013.05.004 (2013).

65 Pellacani, D. *et al.* Analysis of Normal Human Mammary Epigenomes Reveals Cell-Specific Active Enhancer States and Associated Transcription Factor Networks. *Cell Rep* **17**, 2060-2074, doi:10.1016/j.celrep.2016.10.058 (2016).

66 Gascard, P. *et al.* Epigenetic and transcriptional determinants of the human breast. *Nat Commun* **6**, doi:10.1038/ncomms7351 (2015).

67 dos Santos, C. O., Dolzhenko, E., Hodges, E., Smith, A. D. & Hannon, G. J. An Epigenetic Memory of Pregnancy in the Mouse Mammary Gland. *Cell Reports* **11**, 1102-1109, doi:10.1016/j.celrep.2015.04.015 (2015).

68 Molyneux, G. *et al.* BRCA1 basal-like breast cancers originate from luminal epithelial progenitors and not from basal stem cells. *Cell Stem Cell* **7**, 403-417, doi:10.1016/j.stem.2010.07.010 (2010).

69 Lim, E. *et al.* Aberrant luminal progenitors as the candidate target population for basal tumor development in BRCA1 mutation carriers. *Nat Med* **15**, 907-913, doi:10.1038/nm.2000 (2009).

70 Lim, E. *et al.* Aberrant luminal progenitors as the candidate target population for basal tumor development in BRCA1 mutation carriers. *Nat Med* **15**, 907-913, doi:10.1038/nm.2000 (2009).

71 Proia, T. A. *et al.* Genetic predisposition directs breast cancer phenotype by dictating progenitor cell fate. *Cell Stem Cell* **8**, 149-163, doi:10.1016/j.stem.2010.12.007 (2011).

72 Chiang, H. C. *et al.* BRCA1-associated R-loop affects transcription and differentiation in breast luminal epithelial cells. *Nucleic Acids Res* **47**, 5086-5099, doi:10.1093/nar/gkz262 (2019).

73 Kilpinen, H. *et al.* Coordinated effects of sequence variation on DNA binding, chromatin structure, and transcription. *Science* **342**, 744-747, doi:10.1126/science.1242463 (2013).

74 McVicker, G. *et al.* Identification of genetic variants that affect histone modifications in human cells. *Science* **342**, 747-749, doi:10.1126/science.1242429 (2013).

75 Kasowski, M. *et al.* Extensive variation in chromatin states across humans. *Science* **342**, 750-752, doi:10.1126/science.1242510 (2013).

76 Zhang, X. *et al.* BRCA1 mutations attenuate super-enhancer function and chromatin looping in haploinsufficient human breast epithelial cells. *Breast Cancer Res* **21**, 51, doi:10.1186/s13058-019-1132-1 (2019).

77 Toland, A. E. *et al.* Clinical testing of BRCA1 and BRCA2: a worldwide snapshot of technological practices. *NPJ Genom Med* **3**, 7, doi:10.1038/s41525-018-0046-7 (2018).

78 Kharchenko, P. V., Tolstorukov, M. Y. & Park, P. J. Design and analysis of ChIP-seq experiments for DNA-binding proteins. *Nat Biotechnol* **26**, 1351-1359, doi:10.1038/nbt.1508 (2008).

79 Landt, S. G. *et al.* ChIP-seq guidelines and practices of the ENCODE and modENCODE consortia. *Genome Res* **22**, 1813-1831, doi:10.1101/gr.136184.111 (2012).

80 Langmead, B., Trapnell, C., Pop, M. & Salzberg, S. L. Ultrafast and memory-efficient alignment of short DNA sequences to the human genome. *Genome Biol* **10**, R25, doi:10.1186/gb-2009-10-3-r25 (2009).

81 Zhang, Y. *et al.* Model-based analysis of ChIP-Seq (MACS). *Genome Biol* **9**, R137, doi:10.1186/gb-2008-9-9-r137 (2008).

82 Amemiya, H. M., Kundaje, A. & Boyle, A. P. The ENCODE Blacklist: Identification of Problematic Regions of the Genome. *Sci Rep* **9**, 9354, doi:10.1038/s41598-019-45839-z (2019).

83 Stark, R. & Brown, G. D. DiffBind: differential binding analysis of ChIP-seq peak data. *Bioconductor*.

84 Ross-Innes, C. S. *et al.* Differential oestrogen receptor binding is associated with clinical outcome in breast cancer. *Nature* **481**, 389-393, doi:10.1038/nature10730 (2012).

85 Wickham, H. *ggplot2: Elegant Graphics for Data Analysis*. (Springer-Verlag New York, 2016).

86 McLean, C. Y. *et al.* GREAT improves functional interpretation of cis-regulatory regions. *Nat Biotechnol* **28**, 495-501, doi:10.1038/nbt.1630 (2010).

87 Heinz, S. *et al.* Simple combinations of lineage-determining transcription factors prime cis-regulatory elements required for macrophage and B cell identities. *Mol Cell* **38**, 576-589, doi:10.1016/j.molcel.2010.05.004 (2010).

88 Mi, H., Muruganujan, A., Ebert, D., Huang, X. & Thomas, P. D. PANTHER version 14: more genomes, a new PANTHER GO-slim and improvements in enrichment analysis tools. *Nucleic Acids Res* **47**, D419-D426, doi:10.1093/nar/gky1038 (2019).

89 Yu, G., Wang, L. G. & He, Q. Y. ChIPseeker: an R/Bioconductor package for ChIP peak annotation, comparison and visualization. *Bioinformatics* **31**, 2382-2383, doi:10.1093/bioinformatics/btv145 (2015).

90 Buniello, A. *et al.* The NHGRI-EBI GWAS Catalog of published genome-wide association studies, targeted arrays and summary statistics 2019. *Nucleic Acids Res* **47**, D1005-D1012, doi:10.1093/nar/gky1120 (2019).

91 Chiang, H. C. *et al.* Association of radiotherapy with preferential depletion of luminal epithelial cells in a BRCA1 mutation carrier. *Exp Hematol Oncol* **1**, 31, doi:10.1186/2162-3619-1-31 (2012).

92 Barski, A. *et al.* High-resolution profiling of histone methylations in the human genome. *Cell* **129**, 823-837, doi:10.1016/j.cell.2007.05.009 (2007).

93 Lauberth, S. M. *et al.* H3K4me3 interactions with TAF3 regulate preinitiation complex assembly and selective gene activation. *Cell* **152**, 1021-1036, doi:10.1016/j.cell.2013.01.052 (2013).

94 Katiyar, P. *et al.* Regulation of progesterone receptor signaling by BRCA1 in mammary cancer. *Nucl Recept Signal* **4**, e006, doi:10.1621/nrs.04006 (2006).

95 Calvo, V. & Beato, M. BRCA1 counteracts progesterone action by ubiquitination leading to progesterone receptor degradation and epigenetic silencing of target promoters. *Cancer Res* **71**, 3422-3431, doi:10.1158/0008-5472.CAN-10-3670 (2011).

96 Davaadelger, B. *et al.* BRCA1 mutation influences progesterone response in human benign mammary organoids. *Breast Cancer Res* **21**, 124, doi:10.1186/s13058-019-1214-0 (2019).

97 Ma, Y. *et al.* The breast cancer susceptibility gene BRCA1 regulates progesterone receptor signaling in mammary epithelial cells. *Mol Endocrinol* **20**, 14-34, doi:10.1210/me.2004-0488 (2006).

98 Scully, R. *et al.* BRCA1 is a component of the RNA polymerase II holoenzyme. *Proc Natl Acad Sci U S A* **94**, 5605-5610, doi:10.1073/pnas.94.11.5605 (1997).

99 Krum, S. A., Miranda, G. A., Lin, C. & Lane, T. F. BRCA1 associates with processive RNA polymerase II. *J Biol Chem* **278**, 52012-52020, doi:10.1074/jbc.M308418200 (2003).

100 Nair, S. J. *et al.* Genetic suppression reveals DNA repair-independent antagonism between BRCA1 and COBRA1 in mammary gland development. *Nat Commun* **7**, 10913, doi:10.1038/ncomms10913 (2016).

101 Yeung, B. H. *et al.* Glucose-regulated protein 78 as a novel effector of BRCA1 for inhibiting stress-induced apoptosis. *Oncogene* **27**, 6782-6789, doi:10.1038/onc.2008.290 (2008).

102 Andrews, H. N. *et al.* BRCA1 regulates the interferon gamma-mediated apoptotic response. *J Biol Chem* **277**, 26225-26232, doi:10.1074/jbc.M201316200 (2002).

103 Thangaraju, M., Kaufmann, S. H. & Couch, F. J. BRCA1 facilitates stress-induced apoptosis in breast and ovarian cancer cell lines. *J Biol Chem* **275**, 33487-33496, doi:10.1074/jbc.M005824200 (2000).

104 Strickland, K. C. *et al.* Association and prognostic significance of BRCA1/2-mutation status with neoantigen load, number of tumor-infiltrating lymphocytes and expression of PD-1/PD-L1 in high grade serous ovarian cancer. *Oncotarget* **7**, 13587-13598, doi:10.18632/oncotarget.7277 (2016).

105 Green, A. R. *et al.* Clinical Impact of Tumor DNA Repair Expression and T-cell Infiltration in Breast Cancers. *Cancer Immunol Res* **5**, 292-299, doi:10.1158/2326-6066.CIR-16-0195 (2017).

106 Lu, L. *et al.* BRCA1 mRNA expression modifies the effect of T cell activation score on patient survival in breast cancer. *BMC Cancer* **19**, 387, doi:10.1186/s12885-019-5595-3 (2019).

107 Yoshida, K. & Miki, Y. Role of BRCA1 and BRCA2 as regulators of DNA repair, transcription, and cell cycle in response to DNA damage. *Cancer Sci* **95**, 866-871, doi:10.1111/j.1349-7006.2004.tb02195.x (2004).

108 Wu, J., Lu, L. Y. & Yu, X. The role of BRCA1 in DNA damage response. *Protein Cell* **1**, 117-123, doi:10.1007/s13238-010-0010-5 (2010).

109 Hedgepeth, S. C. *et al.* The BRCA1 tumor suppressor binds to inositol 1,4,5-trisphosphate receptors to stimulate apoptotic calcium release. *J Biol Chem* **290**, 7304-7313, doi:10.1074/jbc.M114.611186 (2015).

110 Ahmad, K. & Henikoff, S. The Histone Variant H3.3 Marks Active Chromatin by Replication-Independent Nucleosome Assembly. *Molecular Cell* **9**, 1191-1200, doi:10.1016/s1097-2765(02)00542-7 (2002).

111 Frey, A., Listovsky, T., Guilbaud, G., Sarkies, P. & Sale, J. E. Histone H3.3 is required to maintain replication fork progression after UV damage. *Curr Biol* **24**, 2195-2201, doi:10.1016/j.cub.2014.07.077 (2014).

112 Dhar, S., Gursoy-Yuzugullu, O., Parasuram, R. & Price, B. D. The tale of a tail: histone H4 acetylation and the repair of DNA breaks. *Philos Trans R Soc Lond B Biol Sci* **372**, doi:10.1098/rstb.2016.0284 (2017).

113 Yasmeen, A. *et al.* BRCA1 mutations contribute to cell motility and invasion by affecting its main regulators. *Cell Cycle* **7**, 3781-3783, doi:10.4161/cc.7.23.6993 (2008).

114 Coene, E. D. *et al.* A novel role for BRCA1 in regulating breast cancer cell spreading and motility. *J Cell Biol* **192**, 497-512, doi:10.1083/jcb.201004136 (2011).

115 Gau, D. M. *et al.* BRCA1 deficiency in ovarian cancer is associated with alteration in expression of several key regulators of cell motility - A proteomics study. *Cell Cycle* **14**, 1884-1892, doi:10.1080/15384101.2015.1036203 (2015).

116 Holliday, H., Baker, L. A., Junankar, S. R., Clark, S. J. & Swarbrick, A. Epigenomics of mammary gland development. *Breast Cancer Res* **20**, 100, doi:10.1186/s13058-018-1031-x (2018).

117 Branham, M. T. *et al.* Epigenetic regulation of ID4 in the determination of the BRCAness phenotype in breast cancer. *Breast Cancer Res Treat* **155**, 13-23, doi:10.1007/s10549-015-3648-0 (2016).

118 Lamber, E. P., Horwitz, A. A. & Parvin, J. D. BRCA1 Represses Amphiregulin Gene Expression. *Cancer Research* **70**, 996-1005, doi:10.1158/0008-5472.Can-09-2842 (2010).

119 Shin, S. Y., Kim, C. G. & Lee, Y. H. Egr-1 regulates the transcription of the BRCA1 gene by etoposide. *BMB Rep* **46**, 92-96, doi:10.5483/bmbrep.2013.46.2.202 (2013).

120 Ibrahim, N. *et al.* BRCA1-Associated Epigenetic Regulation of p73 Mediates an Effector Pathway for Chemosensitivity in Ovarian Carcinoma. *Cancer Research* **70**, 7155-7165, doi:10.1158/0008-5472.Can-10-0668 (2010).

121 Li, W. X. *et al.* Comprehensive tissue-specific gene set enrichment analysis and transcription factor analysis of breast cancer by integrating 14 gene expression datasets. *Oncotarget* **8**, 6775-6786, doi:10.18632/oncotarget.14286 (2017).

122 Gregory, K. J., Morin, S. M. & Schneider, S. S. Regulation of early growth response 2 expression by secreted frizzled related protein 1. *BMC Cancer* **17**, 473, doi:10.1186/s12885-017-3426-y (2017).

123 Hur, H., Lee, J. Y., Yun, H. J., Park, B. W. & Kim, M. H. Analysis of HOX gene expression patterns in human breast cancer. *Mol Biotechnol* **56**, 64-71, doi:10.1007/s12033-013-9682-4 (2014).

124 Hur, H. *et al.* HOXC9 Induces Phenotypic Switching between Proliferation and Invasion in Breast Cancer Cells. *J Cancer* **7**, 768-773, doi:10.7150/jca.13894 (2016).

125 Gokmen-Polar, Y. & Badve, S. Upregulation of HSF1 in estrogen receptor positive breast cancer. *Oncotarget* **7**, 84239-84245, doi:10.18632/oncotarget.12438 (2016).

126 Carpenter, R. L. *et al.* Combined inhibition of AKT and HSF1 suppresses breast cancer stem cells and tumor growth. *Oncotarget* **8**, 73947-73963, doi:10.18632/oncotarget.18166 (2017).

127 Fujimoto, M. *et al.* The HSF1-PARP13-PARP1 complex facilitates DNA repair and promotes mammary tumorigenesis. *Nat Commun* **8**, 1638, doi:10.1038/s41467-017-01807-7 (2017).

128 Lesicka, M. *et al.* Altered circadian genes expression in breast cancer tissue according to the clinical characteristics. *PLoS One* **13**, e0199622, doi:10.1371/journal.pone.0199622 (2018).

129 Ramos, A. *et al.* Phosphorylation of E-box binding USF-1 by PI3K/AKT enhances its transcriptional activation of the WBP2 oncogene in breast cancer cells. *FASEB J*, fj201801167RR, doi:10.1096/fj.201801167RR (2018).

130 Li, H., Sekine, M., Tung, N. & Avraham, H. K. Wild-type BRCA1, but not mutated BRCA1, regulates the expression of the nuclear form of beta-catenin. *Mol Cancer Res* **8**, 407-420, doi:10.1158/1541-7786.MCR-09-0403 (2010).

131 Wu, Z. Q. *et al.* Canonical Wnt signaling regulates Slug activity and links epithelial-mesenchymal transition with epigenetic Breast Cancer 1, Early Onset (BRCA1) repression. *Proc Natl Acad Sci U S A* **109**, 16654-16659, doi:10.1073/pnas.1205822109 (2012).

132 De Luca, P. *et al.* BRCA1 and p53 regulate critical prostate cancer pathways. *Prostate Cancer Prostatic Dis* **16**, 233-238, doi:10.1038/pcan.2013.12 (2013).

133 Zhang, W. *et al.* BRCA1 regulates PIG3-mediated apoptosis in a p53-dependent manner. *Oncotarget* **6**, 7608-7618, doi:10.18632/oncotarget.3263 (2015).

134 Dong, C. *et al.* p53 suppresses hyper-recombination by modulating BRCA1 function. *DNA Repair (Amst)* **33**, 60-69, doi:10.1016/j.dnarep.2015.06.005 (2015).

135 Peng, L., Xu, T., Long, T. & Zuo, H. Association Between BRCA Status and P53 Status in Breast Cancer: A Meta-Analysis. *Med Sci Monit* **22**, 1939-1945, doi:10.12659/msm.896260 (2016).

136 Huerta-Reyes, M. *et al.* Treatment of Breast Cancer With Gonadotropin-Releasing Hormone Analogs. *Front Oncol* **9**, 943, doi:10.3389/fonc.2019.00943 (2019).

137 Ma, S., Hsieh, Y. P., Ma, J. & Lu, C. Low-input and multiplexed microfluidic assay reveals epigenomic variation across cerebellum and prefrontal cortex. *Sci Adv* **4**, eaar8187, doi:10.1126/sciadv.aar8187 (2018).

138 Rakha, E. A., Reis-Filho, J. S. & Ellis, I. O. Basal-like breast cancer: a critical review. *J Clin Oncol* **26**, 2568-2581, doi:10.1200/JCO.2007.13.1748 (2008).

139 Foulkes, W. D., Smith, I. E. & Reis-Filho, J. S. Triple-negative breast cancer. *N Engl J Med* **363**, 1938-1948, doi:10.1056/NEJMra1001389 (2010).

140 Mavaddat, N. *et al.* Pathology of breast and ovarian cancers among BRCA1 and BRCA2 mutation carriers: results from the Consortium of Investigators of Modifiers of BRCA1/2 (CIMBA). *Cancer Epidemiol Biomarkers Prev* **21**, 134-147, doi:10.1158/1055-9965.EPI-11-0775 (2012).

141 Roadmap Epigenomics, C. *et al.* Integrative analysis of 111 reference human epigenomes. *Nature* **518**, 317-330, doi:10.1038/nature14248 (2015).

142 Raouf, A. *et al.* Transcriptome analysis of the normal human mammary cell commitment and differentiation process. *Cell Stem Cell* **3**, 109-118, doi:10.1016/j.stem.2008.05.018 (2008).

143 Chakrabarti, R. *et al.* Elf5 inhibits the epithelial-mesenchymal transition in mammary gland development and breast cancer metastasis by transcriptionally repressing Snail2. *Nat Cell Biol* **14**, 1212-1222, doi:10.1038/ncb2607 (2012).

144 Theodorou, V., Stark, R., Menon, S. & Carroll, J. S. GATA3 acts upstream of FOXA1 in mediating ESR1 binding by shaping enhancer accessibility. *Genome Res* **23**, 12-22, doi:10.1101/gr.139469.112 (2013).

145 Kouros-Mehr, H., Slorach, E. M., Sternlicht, M. D. & Werb, Z. GATA-3 maintains the differentiation of the luminal cell fate in the mammary gland. *Cell* **127**, 1041-1055, doi:10.1016/j.cell.2006.09.048 (2006).

146 Asselin-Labat, M. L. *et al.* Gata-3 is an essential regulator of mammary-gland morphogenesis and luminal-cell differentiation. *Nature Cell Biology* **9**, 201-U103, doi:10.1038/ncb1530 (2007).

147 McDaniell, R. *et al.* Heritable individual-specific and allele-specific chromatin signatures in humans. *Science* **328**, 235-239, doi:10.1126/science.1184655 (2010).

148 Garg, P., Joshi, R. S., Watson, C. & Sharp, A. J. A survey of inter-individual variation in DNA methylation identifies environmentally responsive co-regulated networks of epigenetic variation in the human genome. *PLoS Genet* **14**, e1007707, doi:10.1371/journal.pgen.1007707 (2018).

149 Pal, B. *et al.* Construction of developmental lineage relationships in the mouse mammary gland by single-cell RNA profiling. *Nat Commun* **8**, 1627, doi:10.1038/s41467-017-01560-x (2017).

150 Tao, Q. *et al.* Association of Chronic Low-grade Inflammation With Risk of Alzheimer Disease in ApoE4 Carriers. *JAMA Netw Open* **1**, e183597, doi:10.1001/jamanetworkopen.2018.3597 (2018).

151 Slavich, G. M. & Irwin, M. R. From stress to inflammation and major depressive disorder: a social signal transduction theory of depression. *Psychol Bull* **140**, 774-815, doi:10.1037/a0035302 (2014).

152 Burhans, M. S., Hagman, D. K., Kuzma, J. N., Schmidt, K. A. & Kratz, M. Contribution of Adipose Tissue Inflammation to the Development of Type 2 Diabetes Mellitus. *Compr Physiol* **9**, 1-58, doi:10.1002/cphy.c170040 (2018).

153 Wang, D. & DuBois, R. N. Immunosuppression associated with chronic inflammation in the tumor microenvironment. *Carcinogenesis* **36**, 1085-1093, doi:10.1093/carcin/bgv123 (2015).

154 Ferrucci, L. & Fabbri, E. Inflammageing: chronic inflammation in ageing, cardiovascular disease, and frailty. *Nat Rev Cardiol* **15**, 505-522, doi:10.1038/s41569-018-0064-2 (2018).

155 Furman, D. *et al.* Chronic inflammation in the etiology of disease across the life span. *Nat Med* **25**, 1822-1832, doi:10.1038/s41591-019-0675-0 (2019).

156 Morrisette-Thomas, V. *et al.* Inflamm-aging does not simply reflect increases in pro-inflammatory markers. *Mech Ageing Dev* **139**, 49-57, doi:10.1016/j.mad.2014.06.005 (2014).

157 Alpert, A. *et al.* A clinically meaningful metric of immune age derived from high-dimensional longitudinal monitoring. *Nat Med* **25**, 487-495, doi:10.1038/s41591-019-0381-y (2019).

158 Zitvogel, L., Pietrocola, F. & Kroemer, G. Nutrition, inflammation and cancer. *Nat Immunol* **18**, 843-850, doi:10.1038/ni.3754 (2017).

159 Raichlen, D. A. *et al.* Physical activity patterns and biomarkers of cardiovascular disease risk in hunter-gatherers. *Am J Hum Biol* **29**, doi:10.1002/ajhb.22919 (2017).

160 Burini, R. C., Anderson, E., Durstine, J. L. & Carson, J. A. Inflammation, physical activity, and chronic disease: An evolutionary perspective. *Sports Medicine and Health Science* **2**, 1-6, doi:10.1016/j.smhs.2020.03.004 (2020).

161 Carroll, J. E. *et al.* Partial sleep deprivation activates the DNA damage response (DDR) and the senescence-associated secretory phenotype (SASP) in aged adult humans. *Brain Behav Immun* **51**, 223-229, doi:10.1016/j.bbi.2015.08.024 (2016).

162 Razzoli, M. *et al.* Social stress shortens lifespan in mice. *Aging Cell* **17**, e12778, doi:10.1111/acel.12778 (2018).

163 Miller, G. E., Chen, E. & Parker, K. J. Psychological stress in childhood and susceptibility to the chronic diseases of aging: moving toward a model of behavioral and biological mechanisms. *Psychol Bull* **137**, 959-997, doi:10.1037/a0024768 (2011).

164 Brodin, P. *et al.* Variation in the human immune system is largely driven by non-heritable influences. *Cell* **160**, 37-47, doi:10.1016/j.cell.2014.12.020 (2015).

165 Bianchi, M. E. DAMPs, PAMPs and alarmins: all we need to know about danger. *J Leukoc Biol* **81**, 1-5, doi:10.1189/jlb.0306164 (2007).

166 Chen, L. *et al.* Inflammatory responses and inflammation-associated diseases in organs. *Oncotarget* **9**, 7204-7218, doi:10.18632/oncotarget.23208 (2018).

167 Mai, J., Virtue, A., Shen, J., Wang, H. & Yang, X. F. An evolving new paradigm: endothelial cells--conditional innate immune cells. *J Hematol Oncol* **6**, 61, doi:10.1186/1756-8722-6-61 (2013).

168 Medzhitov, R. Origin and physiological roles of inflammation. *Nature* **454**, 428-435, doi:10.1038/nature07201 (2008).

169 Iwasaki, A. & Medzhitov, R. Toll-like receptor control of the adaptive immune responses. *Nat Immunol* **5**, 987-995, doi:10.1038/ni1112 (2004).

170 Takeuchi, O. & Akira, S. Pattern recognition receptors and inflammation. *Cell* **140**, 805-820, doi:10.1016/j.cell.2010.01.022 (2010).

171 Gasteiger, G. *et al.* Cellular Innate Immunity: An Old Game with New Players. *J Innate Immun* **9**, 111-125, doi:10.1159/000453397 (2017).

172 Netea, M. G. *et al.* A guiding map for inflammation. *Nat Immunol* **18**, 826-831, doi:10.1038/ni.3790 (2017).

173 Zhang, L. & Wang, C.-C. Inflammatory response of macrophages in infection. *Hepatobiliary & Pancreatic Diseases International* **13**, 138-152, doi:10.1016/s1499-3872(14)60024-2 (2014).

174 Fenyo, I. M. & Gafencu, A. V. The involvement of the monocytes/macrophages in chronic inflammation associated with atherosclerosis. *Immunobiology* **218**, 1376-1384, doi:10.1016/j.imbio.2013.06.005 (2013).

175 Finsterbusch, M. *et al.* Patrolling monocytes promote intravascular neutrophil activation and glomerular injury in the acutely inflamed glomerulus. *Proc Natl Acad Sci U S A* **113**, E5172-5181, doi:10.1073/pnas.1606253113 (2016).

176 Thiesen, S. *et al.* CD14(hi)HLA-DR(dim) macrophages, with a resemblance to classical blood monocytes, dominate inflamed mucosa in Crohn's disease. *J Leukoc Biol* **95**, 531-541, doi:10.1189/jlb.0113021 (2014).

177 Sindrilaru, A. *et al.* An unrestrained proinflammatory M1 macrophage population induced by iron impairs wound healing in humans and mice. *J Clin Invest* **121**, 985-997, doi:10.1172/JCI44490 (2011).

178 Ma, W. T., Gao, F., Gu, K. & Chen, D. K. The Role of Monocytes and Macrophages in Autoimmune Diseases: A Comprehensive Review. *Front Immunol* **10**, 1140, doi:10.3389/fimmu.2019.01140 (2019).

179 Erridge, C., Attina, T., Spickett, C. M. & Webb, D. J. A high-fat meal induces low-grade endotoxemia: evidence of a novel mechanism of postprandial inflammation. *Am J Clin Nutr* **86**, 1286-1292, doi:10.1093/ajcn/86.5.1286 (2007).

180 Morris, M. C., Gilliam, E. A. & Li, L. Innate immune programing by endotoxin and its pathological consequences. *Front Immunol* **5**, 680, doi:10.3389/fimmu.2014.00680 (2014).

181 Rahtes, A. & Li, L. Polarization of Low-Grade Inflammatory Monocytes Through TRAM-Mediated Up-Regulation of Keap1 by Super-Low Dose Endotoxin. *Front Immunol* **11**, 1478, doi:10.3389/fimmu.2020.01478 (2020).

182 Deng, H., Maitra, U., Morris, M. & Li, L. Molecular mechanism responsible for the priming of macrophage activation. *J Biol Chem* **288**, 3897-3906, doi:10.1074/jbc.M112.424390 (2013).

183 Maitra, U. *et al.* Molecular mechanisms responsible for the selective and low-grade induction of proinflammatory mediators in murine macrophages by lipopolysaccharide. *J Immunol* **189**, 1014-1023, doi:10.4049/jimmunol.1200857 (2012).

184 Ullah, M. O., Sweet, M. J., Mansell, A., Kellie, S. & Kobe, B. TRIF-dependent TLR signaling, its functions in host defense and inflammation, and its potential as a therapeutic target. *J Leukoc Biol* **100**, 27-45, doi:10.1189/jlb.2RI1115-531R (2016).

185 Ciesielska, A., Matyjek, M. & Kwiatkowska, K. TLR4 and CD14 trafficking and its influence on LPS-induced pro-inflammatory signaling. *Cell Mol Life Sci*, doi:10.1007/s00018-020-03656-y (2020).

186 Sakai, J. *et al.* Lipopolysaccharide-induced NF-kappaB nuclear translocation is primarily dependent on MyD88, but TNFalpha expression requires TRIF and MyD88. *Sci Rep* **7**, 1428, doi:10.1038/s41598-017-01600-y (2017).

187 Ito, T., Connett, J. M., Kunkel, S. L. & Matsukawa, A. The linkage of innate and adaptive immune response during granulomatous development. *Front Immunol* **4**, 10, doi:10.3389/fimmu.2013.00010 (2013).

188 Lavin, Y. *et al.* Tissue-resident macrophage enhancer landscapes are shaped by the local microenvironment. *Cell* **159**, 1312-1326, doi:10.1016/j.cell.2014.11.018 (2014).

189 Lantz, C., Radmanesh, B., Liu, E., Thorp, E. B. & Lin, J. Single-cell RNA sequencing uncovers heterogenous transcriptional signatures in macrophages during efferocytosis. *Sci Rep* **10**, 14333, doi:10.1038/s41598-020-70353-y (2020).

190 Chiariotti, L., Coretti, L., Pero, R. & Lembo, F. Epigenetic Alterations Induced by Bacterial Lipopolysaccharides. *Adv Exp Med Biol* **879**, 91-105, doi:10.1007/978-3-319-24738-0_5 (2016).

191 Foster, S. L., Hargreaves, D. C. & Medzhitov, R. Gene-specific control of inflammation by TLR-induced chromatin modifications. *Nature* **447**, 972-978, doi:10.1038/nature05836 (2007).

192 Patel, U. *et al.* Macrophage polarization in response to epigenetic modifiers during infection and inflammation. *Drug Discov Today* **22**, 186-193, doi:10.1016/j.drudis.2016.08.006 (2017).

193 Herrera-Uribe, J. *et al.* Changes in H3K27ac at Gene Regulatory Regions in Porcine Alveolar Macrophages Following LPS or PolyIC Exposure. *Front Genet* **11**, 817, doi:10.3389/fgene.2020.00817 (2020).

194 Chen, S., Yang, J., Wei, Y. & Wei, X. Epigenetic regulation of macrophages: from homeostasis maintenance to host defense. *Cell Mol Immunol* **17**, 36-49, doi:10.1038/s41423-019-0315-0 (2020).

195 Ruenjaiman, V. *et al.* Profile of Histone H3 Lysine 4 Trimethylation and the Effect of Lipopolysaccharide/Immune Complex-Activated Macrophages on Endotoxemia. *Front Immunol* **10**, 2956, doi:10.3389/fimmu.2019.02956 (2019).

196 Novakovic, B. *et al.* beta-Glucan Reverses the Epigenetic State of LPS-Induced Immunological Tolerance. *Cell* **167**, 1354-1368 e1314, doi:10.1016/j.cell.2016.09.034 (2016).

197 Orecchioni, M., Ghosheh, Y., Pramod, A. B. & Ley, K. Macrophage Polarization: Different Gene Signatures in M1(LPS+) vs. Classically and M2(LPS-) vs. Alternatively Activated Macrophages. *Front Immunol* **10**, 1084, doi:10.3389/fimmu.2019.01084 (2019).

198 Das, A. *et al.* High-Resolution Mapping and Dynamics of the Transcriptome, Transcription Factors, and Transcription Co-Factor Networks in Classically and Alternatively Activated Macrophages. *Front Immunol* **9**, 22, doi:10.3389/fimmu.2018.00022 (2018).

199 Baillie, J. K. *et al.* Analysis of the human monocyte-derived macrophage transcriptome and response to lipopolysaccharide provides new insights into genetic aetiology of inflammatory bowel disease. *PLoS Genet* **13**, e1006641, doi:10.1371/journal.pgen.1006641 (2017).

200 Das, A. *et al.* Dual transcriptome sequencing reveals resistance of TLR4 ligand-activated bone marrow-derived macrophages to inflammation mediated by the BET inhibitor JQ1. *Sci Rep* **5**, 16932, doi:10.1038/srep16932 (2015).

201 Cao, Z. N., Chen, C. Y., He, B., Tan, K. & Lu, C. A microfluidic device for epigenomic profiling using 100 cells. *Nature Methods* **12**, 959-962, doi:10.1038/Nmeth.3488 (2015).

202 Picelli, S. *et al.* Smart-seq2 for sensitive full-length transcriptome profiling in single cells. *Nat Methods* **10**, 1096-1098, doi:10.1038/nmeth.2639 (2013).

203 Picelli, S. *et al.* Full-length RNA-seq from single cells using Smart-seq2. *Nat Protoc* **9**, 171-181, doi:10.1038/nprot.2014.006 (2014).

204 Lyroni, K. *et al.* Epigenetic and Transcriptional Regulation of IRAK-M Expression in Macrophages. *J Immunol* **198**, 1297-1307, doi:10.4049/jimmunol.1600009 (2017).

205 Gates, L. A., Foulds, C. E. & O'Malley, B. W. Histone Marks in the 'Driver's Seat': Functional Roles in Steering the Transcription Cycle. *Trends Biochem Sci* **42**, 977-989, doi:10.1016/j.tibs.2017.10.004 (2017).

206 Muller, W. A. Getting leukocytes to the site of inflammation. *Vet Pathol* **50**, 7-22, doi:10.1177/0300985812469883 (2013).

207 Leick, M., Azcutia, V., Newton, G. & Luscinskas, F. W. Leukocyte recruitment in inflammation: basic concepts and new mechanistic insights based on new models and microscopic imaging technologies. *Cell Tissue Res* **355**, 647-656, doi:10.1007/s00441-014-1809-9 (2014).

208 Waltz, P. *et al.* Lipopolysaccaride induces autophagic signaling in macrophages via a TLR4, heme oxygenase-1 dependent pathway. *Autophagy* **7**, 315-320, doi:10.4161/auto.7.3.14044 (2011).

209 Vural, A. & Kehrl, J. H. Autophagy in macrophages: impacting inflammation and bacterial infection. *Scientifica (Cairo)* **2014**, 825463, doi:10.1155/2014/825463 (2014).

210 Liu, K. *et al.* Impaired macrophage autophagy increases the immune response in obese mice by promoting proinflammatory macrophage polarization. *Autophagy* **11**, 271-284, doi:10.1080/15548627.2015.1009787 (2015).

211 Zhong, Z. *et al.* NF-kappaB Restricts Inflammasome Activation via Elimination of Damaged Mitochondria. *Cell* **164**, 896-910, doi:10.1016/j.cell.2015.12.057 (2016).

212 Liu, W. *et al.* Trem2 promotes anti-inflammatory responses in microglia and is suppressed under pro-inflammatory conditions. *Hum Mol Genet* **29**, 3224-3248, doi:10.1093/hmg/ddaa209 (2020).

213 Keping, Y. *et al.* Sestrin1 inhibits oxidized low-density lipoprotein-induced activation of NLRP3 inflammasome in macrophages in a murine atherosclerosis model. *Eur J Immunol* **50**, 1154-1166, doi:10.1002/eji.201948427 (2020).

214 Wu, M. Y. *et al.* PI3KC3 complex subunit NRBF2 is required for apoptotic cell clearance to restrict intestinal inflammation. *Autophagy*, 1-16, doi:10.1080/15548627.2020.1741332 (2020).

215 Tanaka, T., Narazaki, M. & Kishimoto, T. IL-6 in inflammation, immunity, and disease. *Cold Spring Harb Perspect Biol* **6**, a016295, doi:10.1101/cshperspect.a016295 (2014).

216 Cotton, J. A. *et al.* Interleukin-8 in gastrointestinal inflammation and malignancy: induction and clinical consequences. *International Journal of Interferon, Cytokine and Mediator Research*, doi:10.2147/IJICMR.S63682 (2016).

217 Rattigan, K. M. *et al.* Metabolomic profiling of macrophages determines the discrete metabolomic signature and metabolomic interactome triggered by polarising immune stimuli. *PLoS One* **13**, e0194126, doi:10.1371/journal.pone.0194126 (2018).

218 Nagy, C. & Haschemi, A. Time and Demand are Two Critical Dimensions of Immunometabolism: The Process of Macrophage Activation and the Pentose Phosphate Pathway. *Front Immunol* **6**, 164, doi:10.3389/fimmu.2015.00164 (2015).

219 Lauterbach, M. A. *et al.* Toll-like Receptor Signaling Rewires Macrophage Metabolism and Promotes Histone Acetylation via ATP-Citrate Lyase. *Immunity* **51**, 997-1011 e1017, doi:10.1016/j.immuni.2019.11.009 (2019).

220 Lee, H. T., Oh, S., Ro, D. H., Yoo, H. & Kwon, Y. W. The Key Role of DNA Methylation and Histone Acetylation in Epigenetics of Atherosclerosis. *J Lipid Atheroscler* **9**, 419-434, doi:10.12997/jla.2020.9.3.419 (2020).

221 Karami, J. *et al.* Epigenetics in rheumatoid arthritis; fibroblast-like synoviocytes as an emerging paradigm in the pathogenesis of the disease. *Immunol Cell Biol* **98**, 171-186, doi:10.1111/imcb.12311 (2020).

222 Angiolilli, C. *et al.* Inflammatory cytokines epigenetically regulate rheumatoid arthritis fibroblast-like synoviocyte activation by suppressing HDAC5 expression. *Ann Rheum Dis* **75**, 430-438, doi:10.1136/annrheumdis-2014-205635 (2016).

223 Adukpo, S. *et al.* Triggering receptor expressed on myeloid cells 1 (TREM-1) and cytokine gene variants in complicated and uncomplicated malaria. *Trop Med Int Health* **21**, 1592-1601, doi:10.1111/tmi.12787 (2016).

224 Krausgruber, T. *et al.* IRF5 promotes inflammatory macrophage polarization and TH1-TH17 responses. *Nat Immunol* **12**, 231-238, doi:10.1038/ni.1990 (2011).

225 Lin, W. *et al.* Function of CSF1 and IL34 in Macrophage Homeostasis, Inflammation, and Cancer. *Front Immunol* **10**, 2019, doi:10.3389/fimmu.2019.02019 (2019).

226 Fontana, M. F. *et al.* JUNB is a key transcriptional modulator of macrophage activation. *J Immunol* **194**, 177-186, doi:10.4049/jimmunol.1401595 (2015).

227 Liu, X. *et al.* LPSinduced proinflammatory cytokine expression in human airway epithelial cells and macrophages via NFkappaB, STAT3 or AP1 activation. *Mol Med Rep* **17**, 5484-5491, doi:10.3892/mmr.2018.8542 (2018).

228 Liu, W. *et al.* AP-1 activated by toll-like receptors regulates expression of IL-23 p19. *J Biol Chem* **284**, 24006-24016, doi:10.1074/jbc.M109.025528 (2009).

229 Zhang, C. *et al.* ATF4 is directly recruited by TLR4 signaling and positively regulates TLR4-trigged cytokine production in human monocytes. *Cell Mol Immunol* **10**, 84-94, doi:10.1038/cmi.2012.57 (2013).

230 Bush, S. J. *et al.* Species-Specificity of Transcriptional Regulation and the Response to Lipopolysaccharide in Mammalian Macrophages. *Front Cell Dev Biol* **8**, 661, doi:10.3389/fcell.2020.00661 (2020).

231 Kobayashi, T. *et al.* NFIL3 is a regulator of IL-12 p40 in macrophages and mucosal immunity. *J Immunol* **186**, 4649-4655, doi:10.4049/jimmunol.1003888 (2011).

232 Morgan, R. & Whiting, K. Differential expression of HOX genes upon activation of leukocyte sub-populations. *Int J Hematol* **87**, 246-249, doi:10.1007/s12185-008-0057-8 (2008).

233 Yin, S. & Cao, W. Toll-Like Receptor Signaling Induces Nrf2 Pathway Activation through p62-Triggered Keap1 Degradation. *Mol Cell Biol* **35**, 2673-2683, doi:10.1128/MCB.00105-15 (2015).

234 Hong, S., Skaist, A. M., Wheelan, S. J. & Friedman, A. D. AP-1 protein induction during monopoiesis favors C/EBP: AP-1 heterodimers over C/EBP homodimerization and stimulates FosB transcription. *J Leukoc Biol* **90**, 643-651, doi:10.1189/jlb.0111043 (2011).

235 Wang, D., Paz-Priel, I. & Friedman, A. D. NF-kappa B p50 regulates C/EBP alpha expression and inflammatory cytokine-induced neutrophil production. *J Immunol* **182**, 5757-5762, doi:10.4049/jimmunol.0803861 (2009).

236 Lu, S. C. *et al.* A novel role for Oct-2 in the lipopolysaccharide-mediated induction of resistin gene expression in RAW264.7 cells. *Biochem J* **402**, 387-395, doi:10.1042/BJ20061096 (2007).

237 Lu, S. C., Wu, H. W., Lin, Y. J. & Chang, S. F. The essential role of Oct-2 in LPS-induced expression of iNOS in RAW 264.7 macrophages and its regulation by trichostatin A. *Am J Physiol Cell Physiol* **296**, C1133-1139, doi:10.1152/ajpcell.00031.2009 (2009).

238 Cui, H., Banerjee, S., Guo, S., Xie, N. & Liu, G. IFN Regulatory Factor 2 Inhibits Expression of Glycolytic Genes and Lipopolysaccharide-Induced Proinflammatory Responses in Macrophages. *J Immunol* **200**, 3218-3230, doi:10.4049/jimmunol.1701571 (2018).

239 Nhu, Q. M., Cuesta, N. & Vogel, S. N. Transcriptional regulation of lipopolysaccharide (LPS)-induced Toll-like receptor (TLR) expression in murine macrophages: role of interferon regulatory factors 1 (IRF-1) and 2 (IRF-2). *J Endotoxin Res* **12**, 285-295, doi:10.1179/096805106X118834 (2006).

240 Das, H. *et al.* Kruppel-like factor 2 (KLF2) regulates proinflammatory activation of monocytes. *Proc Natl Acad Sci U S A* **103**, 6653-6658, doi:10.1073/pnas.0508235103 (2006).

241 Blaszczyk, K. *et al.* The unique role of STAT2 in constitutive and IFN-induced transcription and antiviral responses. *Cytokine Growth Factor Rev* **29**, 71-81, doi:10.1016/j.cytogfr.2016.02.010 (2016).

242 Thygesen, S. J. & Stacey, K. J. IRF1 and IRF2 regulate the non-canonical inflammasome. *EMBO Rep* **20**, e48891, doi:10.15252/embr.201948891 (2019).

243 Liu, T., Zhang, L., Joo, D. & Sun, S. C. NF-kappaB signaling in inflammation. *Signal Transduct Target Ther* **2**, doi:10.1038/sigtrans.2017.23 (2017).

244 Hajishengallis, G. & Genco, R. J. Downregulation of the DNA-binding activity of nuclear factor-kappaB p65 subunit in Porphyromonas gingivalis fimbria-induced tolerance. *Infect Immun* **72**, 1188-1191, doi:10.1128/iai.72.2.1188-1191.2004 (2004).

245 Kang, X. *et al.* Macrophage TCF-4 co-activates p65 to potentiate chronic inflammation and insulin resistance in mice. *Clin Sci (Lond)* **130**, 1257-1268, doi:10.1042/CS20160192 (2016).

246 Riedlinger, T. *et al.* NF-kappaB p65 dimerization and DNA-binding is important for inflammatory gene expression. *FASEB J* **33**, 4188-4202, doi:10.1096/fj.201801638R (2019).

247 Olejnik, J., Hume, A. J. & Muhlberger, E. Toll-like receptor 4 in acute viral infection: Too much of a good thing. *PLoS Pathog* **14**, e1007390, doi:10.1371/journal.ppat.1007390 (2018).

248 Otero, Y. F. *et al.* Enhanced Glucose Transport, but not Phosphorylation Capacity, Ameliorates Lipopolysaccharide-Induced Impairments in Insulin-Stimulated Muscle Glucose Uptake. *Shock* **45**, 677-685, doi:10.1097/SHK.0000000000000550 (2016).

249 Feingold, K. R. *et al.* Endotoxin rapidly induces changes in lipid metabolism that produce hypertriglyceridemia: low doses stimulate hepatic triglyceride production while high doses inhibit clearance. *Journal of Lipid Research* **33**, 1765-1776 (1992).

250 Roberts, C. A., Dickinson, A. K. & Taams, L. S. The Interplay Between Monocytes/Macrophages and CD4(+) T Cell Subsets in Rheumatoid Arthritis. *Front Immunol* **6**, 571, doi:10.3389/fimmu.2015.00571 (2015).

251 Imam, T., Park, S., Kaplan, M. H. & Olson, M. R. Effector T Helper Cell Subsets in Inflammatory Bowel Diseases. *Front Immunol* **9**, 1212, doi:10.3389/fimmu.2018.01212 (2018).

252 Tan, C. *et al.* Decreased Histone Deacetylase 2 (HDAC2) in Peripheral Blood Monocytes (PBMCs) of COPD Patients. *PLoS One* **11**, e0147380, doi:10.1371/journal.pone.0147380 (2016).

253 Fang, W. F. *et al.* Histone deacetylase 2 (HDAC2) attenuates lipopolysaccharide (LPS)-induced inflammation by regulating PAI-1 expression. *J Inflamm (Lond)* **15**, 3, doi:10.1186/s12950-018-0179-6 (2018).

254 Wu, C., Li, A., Hu, J. & Kang, J. Histone deacetylase 2 is essential for LPS-induced inflammatory responses in macrophages. *Immunol Cell Biol* **97**, 72-84, doi:10.1111/imcb.12203 (2019).

255 Wang, B. *et al.* Glycolysis-dependent histone deacetylase 4 degradation regulates inflammatory cytokine production. *Mol Biol Cell* **25**, 3300-3307, doi:10.1091/mbc.E13-12-0757 (2014).

256 Park, E. J., Kim, Y. M., Kim, H. J. & Chang, K. C. Degradation of histone deacetylase 4 via the TLR4/JAK/STAT1 signaling pathway promotes the acetylation of high mobility group box 1 (HMGB1) in lipopolysaccharide-activated macrophages. *FEBS Open Bio* **8**, 1119-1126, doi:10.1002/2211-5463.12456 (2018).

257 Scarl, R. T., Lawrence, C. M., Gordon, H. M. & Nunemaker, C. S. STEAP4: its emerging role in metabolism and homeostasis of cellular iron and copper. *J Endocrinol* **234**, R123-R134, doi:10.1530/JOE-16-0594 (2017).

258 Metais, J. Y. *et al.* BCL2A1a over-expression in murine hematopoietic stem and progenitor cells decreases apoptosis and results in hematopoietic transformation. *PLoS One* **7**, e48267, doi:10.1371/journal.pone.0048267 (2012).

259 Chait, A. *et al.* Presence of serum amyloid A3 in mouse plasma is dependent on the nature and extent of the inflammatory stimulus. *Sci Rep* **10**, 10397, doi:10.1038/s41598-020-66898-7 (2020).

260 van der Laan, L. J. *et al.* Regulation and functional involvement of macrophage scavenger receptor MARCO in clearance of bacteria in vivo. *J Immunol* **162**, 939-947 (1999).

261 Luo, C., Chen, M., Madden, A. & Xu, H. Expression of complement components and regulators by different subtypes of bone marrow-derived macrophages. *Inflammation* **35**, 1448-1461, doi:10.1007/s10753-012-9458-1 (2012).

262 Fensterl, V. & Sen, G. C. The ISG56/IFIT1 gene family. *J Interferon Cytokine Res* **31**, 71-78, doi:10.1089/jir.2010.0101 (2011).

263 Wu, C. *et al.* LRRC14 attenuates Toll-like receptor-mediated NF-kappaB signaling through disruption of IKK complex. *Exp Cell Res* **347**, 65-73, doi:10.1016/j.yexcr.2016.07.011 (2016).

264 Wammers, M. *et al.* Reprogramming of pro-inflammatory human macrophages to an anti-inflammatory phenotype by bile acids. *Sci Rep* **8**, 255, doi:10.1038/s41598-017-18305-x (2018).

265 Marietta, E. V., Weis, J. J. & Weis, J. H. CD28 expression by mouse mast cells is modulated by lipopolysaccharide and outer surface protein A lipoprotein from Borrelia burgdorferi. *J Immunol* **159**, 2840-2848 (1997).

266 Introna, M., Hamilton, T. A., Kaufman, R. E., Adams, D. O. & Bast, R. C., Jr. Treatment of murine peritoneal macrophages with bacterial lipopolysaccharide alters expression of c-fos and c-myc oncogenes. *J Immunol* **137**, 2711-2715 (1986).

267 Nie, Z. *et al.* c-Myc is a universal amplifier of expressed genes in lymphocytes and embryonic stem cells. *Cell* **151**, 68-79, doi:10.1016/j.cell.2012.08.033 (2012).

268 Blouin, C. C., Page, E. L., Soucy, G. M. & Richard, D. E. Hypoxic gene activation by lipopolysaccharide in macrophages: implication of hypoxia-inducible factor 1alpha. *Blood* **103**, 1124-1130, doi:10.1182/blood-2003-07-2427 (2004).

269 Vijayan, V. *et al.* Human and murine macrophages exhibit differential metabolic responses to lipopolysaccharide - A divergent role for glycolysis. *Redox Biol* **22**, 101147, doi:10.1016/j.redox.2019.101147 (2019).

270 Soto-Pantoja, D. R. *et al.* Unfolded protein response signaling impacts macrophage polarity to modulate breast cancer cell clearance and melanoma immune checkpoint therapy responsiveness. *Oncotarget* **8**, 80545-80559, doi:10.18632/oncotarget.19849 (2017).

271 Zuo, H. & Wan, Y. Metabolic Reprogramming in Mitochondria of Myeloid Cells. *Cells* **9**, doi:10.3390/cells9010005 (2019).

272 O'Neill, L. A., Kishton, R. J. & Rathmell, J. A guide to immunometabolism for immunologists. *Nat Rev Immunol* **16**, 553-565, doi:10.1038/nri.2016.70 (2016).

273 Raulien, N. *et al.* Fatty Acid Oxidation Compensates for Lipopolysaccharide-Induced Warburg Effect in Glucose-Deprived Monocytes. *Front Immunol* **8**, 609, doi:10.3389/fimmu.2017.00609 (2017).

274 Zhang, R., Wang, L., Pan, J. H. & Han, J. A critical role of E2F transcription factor 2 in proinflammatory cytokines-dependent proliferation and invasiveness of fibroblast-like synoviocytes in rheumatoid Arthritis. *Sci Rep* **8**, 2623, doi:10.1038/s41598-018-20782-7 (2018).

275 Ribeiro, M. C. *et al.* LPS Induces mTORC1 and mTORC2 Activation During Monocyte Adhesion. *Front Mol Biosci* **5**, 67, doi:10.3389/fmolb.2018.00067 (2018).

276 Greenhill, C. J. *et al.* IL-6 trans-signaling modulates TLR4-dependent inflammatory responses via STAT3. *J Immunol* **186**, 1199-1208, doi:10.4049/jimmunol.1002971 (2011).

277 Cronin, J. G., Kanamarlapudi, V., Thornton, C. A. & Sheldon, I. M. Signal transducer and activator of transcription-3 licenses Toll-like receptor 4-dependent interleukin (IL)-6 and IL-8 production via IL-6 receptor-positive feedback in endometrial cells. *Mucosal Immunol* **9**, 1125-1136, doi:10.1038/mi.2015.131 (2016).

278 Hoareau, L. *et al.* Signaling pathways involved in LPS induced TNFalpha production in human adipocytes. *J Inflamm (Lond)* **7**, 1, doi:10.1186/1476-9255-7-1 (2010).

279 van der Bruggen, T., Nijenhuis, S., van Raaij, E., Verhoef, J. & van Asbeck, B. S. Lipopolysaccharide-induced tumor necrosis factor alpha production by human monocytes involves the raf-1/MEK1-MEK2/ERK1-ERK2 pathway. *Infect Immun* **67**, 3824-3829, doi:10.1128/IAI.67.8.3824-3829.1999 (1999).

280 Lee, J. Y. & Sullivan, K. E. Gamma interferon and lipopolysaccharide interact at the level of transcription to induce tumor necrosis factor alpha expression. *Infect Immun* **69**, 2847-2852, doi:10.1128/IAI.69.5.2847-2852.2001 (2001).

281 Dallagi, A. *et al.* The activating effect of IFN-gamma on monocytes/macrophages is regulated by the LIF-trophoblast-IL-10 axis via Stat1 inhibition and Stat3 activation. *Cell Mol Immunol* **12**, 326-341, doi:10.1038/cmi.2014.50 (2015).

282 Akbar, A. N., Lord, J. M. & Salmon, M. IFN-α and IFN-β: a link between immune memory and chronic inflammation. *Immunology Today* **21**, 337-342, doi:10.1016/s0167-5699(00)01652-2 (2000).

283 Kirou, K. A. *et al.* Coordinate overexpression of interferon-alpha-induced genes in systemic lupus erythematosus. *Arthritis Rheum* **50**, 3958-3967, doi:10.1002/art.20798 (2004).

284 Catalina, M. D., Bachali, P., Geraci, N. S., Grammer, A. C. & Lipsky, P. E. Gene expression analysis delineates the potential roles of multiple interferons in systemic lupus erythematosus. *Commun Biol* **2**, 140, doi:10.1038/s42003-019-0382-x (2019).

285 Molina, J. R. & Adjei, A. A. The Ras/Raf/MAPK Pathway. *Journal of Thoracic Oncology* **1**, 7-9, doi:10.1016/s1556-0864(15)31506-9 (2006).

286 Lin, J. *et al.* Transcriptome-Wide Analysis Reveals Modulation of Human Macrophage Inflammatory Phenotype Through Alternative Splicing. *Arterioscler Thromb Vasc Biol* **36**, 1434-1447, doi:10.1161/ATVBAHA.116.307573 (2016).

287 Chunfa, L. *et al.* The Central Role of IFI204 in IFN-beta Release and Autophagy Activation during Mycobacterium bovis Infection. *Front Cell Infect Microbiol* **7**, 169, doi:10.3389/fcimb.2017.00169 (2017).

288 Robbins, C. S. *et al.* Local proliferation dominates lesional macrophage accumulation in atherosclerosis. *Nat Med* **19**, 1166-1172, doi:10.1038/nm.3258 (2013).

289 Griffin, C. *et al.* TLR4, TRIF, and MyD88 are essential for myelopoiesis and CD11c(+) adipose tissue macrophage production in obese mice. *J Biol Chem* **293**, 8775-8786, doi:10.1074/jbc.RA117.001526 (2018).

290 Kawasaki, T. & Kawai, T. Toll-like receptor signaling pathways. *Front Immunol* **5**, 461, doi:10.3389/fimmu.2014.00461 (2014).

291 An, H. *et al.* Up-regulation of TLR9 gene expression by LPS in mouse macrophages via activation of NF-κB, ERK and p38 MAPK signal pathways. *Immunology Letters* **81**, 165-169, doi:10.1016/s0165-2478(02)00010-x (2002).

292 Plitas, G., Burt, B. M., Nguyen, H. M., Bamboat, Z. M. & DeMatteo, R. P. Toll-like receptor 9 inhibition reduces mortality in polymicrobial sepsis. *J Exp Med* **205**, 1277-1283, doi:10.1084/jem.20080162 (2008).

293 Tsuji, N. *et al.* Role of Mitochondrial DNA in Septic AKI via Toll-Like Receptor 9. *J Am Soc Nephrol* **27**, 2009-2020, doi:10.1681/ASN.2015040376 (2016).

294 Hu, D. *et al.* Inhibition of Toll-like receptor 9 attenuates sepsis-induced mortality through suppressing excessive inflammatory response. *Cell Immunol* **295**, 92-98, doi:10.1016/j.cellimm.2015.03.009 (2015).

295 Celhar, T. *et al.* TLR7 and TLR9 ligands regulate antigen presentation by macrophages. *Int Immunol* **28**, 223-232, doi:10.1093/intimm/dxv066 (2016).

296 Hoshino, K. *et al.* IkappaB kinase-alpha is critical for interferon-alpha production induced by Toll-like receptors 7 and 9. *Nature* **440**, 949-953, doi:10.1038/nature04641 (2006).

297 De Nardo, D., De Nardo, C. M., Nguyen, T., Hamilton, J. A. & Scholz, G. M. Signaling crosstalk during sequential TLR4 and TLR9 activation amplifies the inflammatory response of mouse macrophages. *J Immunol* **183**, 8110-8118, doi:10.4049/jimmunol.0901031 (2009).

298 Jefferies, C. A. Regulating IRFs in IFN Driven Disease. *Front Immunol* **10**, 325, doi:10.3389/fimmu.2019.00325 (2019).

299 Marie, I., Durbin, J. E. & Levy, D. E. Differential viral induction of distinct interferon-alpha genes by positive feedback through interferon regulatory factor-7. *EMBO J* **17**, 6660-6669, doi:10.1093/emboj/17.22.6660 (1998).

300 Sin, W. X. *et al.* IRF-7 Mediates Type I IFN Responses in Endotoxin-Challenged Mice. *Front Immunol* **11**, 640, doi:10.3389/fimmu.2020.00640 (2020).

301 Krischuns, T. *et al.* Phosphorylation of TRIM28 Enhances the Expression of IFN-beta and Proinflammatory Cytokines During HPAIV Infection of Human Lung Epithelial Cells. *Front Immunol* **9**, 2229, doi:10.3389/fimmu.2018.02229 (2018).

302 Gong, P. *et al.* Phosphorylation of mitogen- and stress-activated protein kinase-1 in astrocytic inflammation: a possible role in inhibiting production of inflammatory cytokines. *PLoS One* **8**, e81747, doi:10.1371/journal.pone.0081747 (2013).

303 Litvak, V. *et al.* A FOXO3-IRF7 gene regulatory circuit limits inflammatory sequelae of antiviral responses. *Nature* **490**, 421-425, doi:10.1038/nature11428 (2012).

304 Gates-Tanzer, L. T. & Shisler, J. L. Cellular FLIP long isoform (cFLIPL)-IKKalpha interactions inhibit IRF7 activation, representing a new cellular strategy to inhibit IFNalpha expression. *J Biol Chem* **293**, 1745-1755, doi:10.1074/jbc.RA117.000541 (2018).

305 Li, L., McCall, C. & Hu, X. Editorial: Innate Immunity Programming and Memory in Resolving and Non-Resolving Inflammation. *Front Immunol* **11**, 177, doi:10.3389/fimmu.2020.00177 (2020).

306 Saravia, J., Raynor, J. L., Chapman, N. M., Lim, S. A. & Chi, H. Signaling networks in immunometabolism. *Cell Res* **30**, 328-342, doi:10.1038/s41422-020-0301-1 (2020).

307 Bhattacharyya, N. D. & Feng, C. G. Regulation of T Helper Cell Fate by TCR Signal Strength. *Front Immunol* **11**, 624, doi:10.3389/fimmu.2020.00624 (2020).

308 Glaros, T. G. *et al.* Causes and consequences of low grade endotoxemia and inflammatory diseases. *Front Biosci (Schol Ed)* **5**, 754-765, doi:10.2741/s405 (2013).

309 Rimmele, T. *et al.* Immune Cell Phenotype and Function in Sepsis. *Shock* **45**, 282-291, doi:10.1097/SHK.0000000000000495 (2016).

310 Boomer, J. S., Green, J. M. & Hotchkiss, R. S. The changing immune system in sepsis: is individualized immuno-modulatory therapy the answer? *Virulence* **5**, 45-56, doi:10.4161/viru.26516 (2014).

311 Chen, H. J., Tas, S. W. & de Winther, M. P. J. Type-I interferons in atherosclerosis. *J Exp Med* **217**, doi:10.1084/jem.20190459 (2020).

312 Voloshyna, I., Littlefield, M. J. & Reiss, A. B. Atherosclerosis and interferon-gamma: new insights and therapeutic targets. *Trends Cardiovasc Med* **24**, 45-51, doi:10.1016/j.tcm.2013.06.003 (2014).

313 Yuan, R. *et al.* Low-grade inflammatory polarization of monocytes impairs wound healing. *J Pathol* **238**, 571-583, doi:10.1002/path.4680 (2016).

314 Love, M. I., Huber, W. & Anders, S. Moderated estimation of fold change and dispersion for RNA-seq data with DESeq2. *Genome Biol* **15**, 550, doi:10.1186/s13059-014-0550-8 (2014).

315 Subramanian, A. *et al.* Gene set enrichment analysis: a knowledge-based approach for interpreting genome-wide expression profiles. *Proc Natl Acad Sci U S A* **102**, 15545-15550, doi:10.1073/pnas.0506580102 (2005).

316 Mootha, V. K. *et al.* PGC-1alpha-responsive genes involved in oxidative phosphorylation are coordinately downregulated in human diabetes. *Nat Genet* **34**, 267-273, doi:10.1038/ng1180 (2003).

317 Vitting-Seerup, K. & Sandelin, A. The Landscape of Isoform Switches in Human Cancers. *Mol Cancer Res* **15**, 1206-1220, doi:10.1158/1541-7786.MCR-16-0459 (2017).

318 Vitting-Seerup, K. & Sandelin, A. IsoformSwitchAnalyzeR: analysis of changes in genome-wide patterns of alternative splicing and its functional consequences. *Bioinformatics* **35**, 4469-4471, doi:10.1093/bioinformatics/btz247 (2019).

319 Anders, S., Reyes, A. & Huber, W. Detecting differential usage of exons from RNA-seq data. *Genome Res* **22**, 2008-2017, doi:10.1101/gr.133744.111 (2012).

320 Wang, L. *et al.* CPAT: Coding-Potential Assessment Tool using an alignment-free logistic regression model. *Nucleic Acids Res* **41**, e74, doi:10.1093/nar/gkt006 (2013).

321 Punta, M. *et al.* The Pfam protein families database. *Nucleic Acids Res* **40**, D290-301, doi:10.1093/nar/gkr1065 (2012).

322 Almagro Armenteros, J. J. *et al.* SignalP 5.0 improves signal peptide predictions using deep neural networks. *Nat Biotechnol* **37**, 420-423, doi:10.1038/s41587-019-0036-z (2019).

323 Klausen, M. S. *et al.* NetSurfP-2.0: Improved prediction of protein structural features by integrated deep learning. *Proteins* **87**, 520-527, doi:10.1002/prot.25674 (2019).

324 Brown, A. S. *et al.* Maternal exposure to respiratory infections and adult schizophrenia spectrum disorders: a prospective birth cohort study. *Schizophr Bull* **26**, 287-295, doi:10.1093/oxfordjournals.schbul.a033453 (2000).

325 Buka, S. L. Maternal Infections and Subsequent Psychosis Among Offspring. *Archives of General Psychiatry* **58**, 1032-1037, doi:10.1001/archpsyc.58.11.1032 (2001).

326 Brown, A. S. *et al.* Elevated maternal interleukin-8 levels and risk of schizophrenia in adult offspring. *Am J Psychiatry* **161**, 889-895, doi:10.1176/appi.ajp.161.5.889 (2004).

327 Brown, A. S. *et al.* Serologic evidence of prenatal influenza in the etiology of schizophrenia. *Arch Gen Psychiatry* **61**, 774-780, doi:10.1001/archpsyc.61.8.774 (2004).

328 Brown, A. S. *et al.* Maternal exposure to toxoplasmosis and risk of schizophrenia in adult offspring. *Am J Psychiatry* **162**, 767-773, doi:10.1176/appi.ajp.162.4.767 (2005).

329 Babulas, V., Factor-Litvak, P., Goetz, R., Schaefer, C. A. & Brown, A. S. Prenatal exposure to maternal genital and reproductive infections and adult schizophrenia. *Am J Psychiatry* **163**, 927-929, doi:10.1176/ajp.2006.163.5.927 (2006).

330 Mortensen, P. B. *et al.* Toxoplasma gondii as a risk factor for early-onset schizophrenia: analysis of filter paper blood samples obtained at birth. *Biol Psychiatry* **61**, 688-693, doi:10.1016/j.biopsych.2006.05.024 (2007).

331 Buka, S. L., Cannon, T. D., Torrey, E. F., Yolken, R. H. & Collaborative Study Group on the Perinatal Origins of Severe Psychiatric, D. Maternal exposure to herpes simplex virus and risk of psychosis among adult offspring. *Biol Psychiatry* **63**, 809-815, doi:10.1016/j.biopsych.2007.09.022 (2008).

332 Brown, A. S. *et al.* Prenatal infection and cavum septum pellucidum in adult schizophrenia. *Schizophr Res* **108**, 285-287, doi:10.1016/j.schres.2008.11.018 (2009).

333 Brown, A. S. *et al.* Prenatal exposure to maternal infection and executive dysfunction in adult schizophrenia. *Am J Psychiatry* **166**, 683-690, doi:10.1176/appi.ajp.2008.08010089 (2009).

334 Sorensen, H. J., Mortensen, E. L., Reinisch, J. M. & Mednick, S. A. Association between prenatal exposure to bacterial infection and risk of schizophrenia. *Schizophr Bull* **35**, 631-637, doi:10.1093/schbul/sbn121 (2009).

335 Clarke, M. C., Tanskanen, A., Huttunen, M., Whittaker, J. C. & Cannon, M. Evidence for an interaction between familial liability and prenatal exposure to infection in the causation of schizophrenia. *Am J Psychiatry* **166**, 1025-1030, doi:10.1176/appi.ajp.2009.08010031 (2009).

336 Mortensen, P. B. *et al.* A Danish National Birth Cohort study of maternal HSV-2 antibodies as a risk factor for schizophrenia in their offspring. *Schizophr Res* **122**, 257-263, doi:10.1016/j.schres.2010.06.010 (2010).

337 Brown, A. S. *et al.* Association of maternal genital and reproductive infections with verbal memory and motor deficits in adult schizophrenia. *Psychiatry Res* **188**, 179-186, doi:10.1016/j.psychres.2011.04.020 (2011).

338 Atladottir, H. O. *et al.* Maternal infection requiring hospitalization during pregnancy and autism spectrum disorders. *J Autism Dev Disord* **40**, 1423-1430, doi:10.1007/s10803-010-1006-y (2010).

339 Grether, J. K., Croen, L. A., Anderson, M. C., Nelson, K. B. & Yolken, R. H. Neonatally measured immunoglobulins and risk of autism. *Autism Res* **3**, 323-332, doi:10.1002/aur.160 (2010).

340 Goines, P. E. *et al.* Increased midgestational IFN-gamma, IL-4 and IL-5 in women bearing a child with autism: A case-control study. *Mol Autism* **2**, 13, doi:10.1186/2040-2392-2-13 (2011).

341 Abdallah, M. W. *et al.* Neonatal levels of cytokines and risk of autism spectrum disorders: an exploratory register-based historic birth cohort study utilizing the Danish Newborn Screening Biobank. *J Neuroimmunol* **252**, 75-82, doi:10.1016/j.jneuroim.2012.07.013 (2012).

342 Saha, S., Chant, D., Welham, J. & McGrath, J. A systematic review of the prevalence of schizophrenia. *PLoS Med* **2**, e141, doi:10.1371/journal.pmed.0020141 (2005).

343 Owen, M. J., Sawa, A. & Mortensen, P. B. Schizophrenia. *The Lancet* **388**, 86-97, doi:10.1016/s0140-6736(15)01121-6 (2016).

344 Joyce, E. M. & Roiser, J. P. Cognitive heterogeneity in schizophrenia. *Curr Opin Psychiatry* **20**, 268-272, doi:10.1097/YCO.0b013e3280ba4975 (2007).

345 Chan, V. Schizophrenia and Psychosis: Diagnosis, Current Research Trends, and Model Treatment Approaches with Implications for Transitional Age Youth. *Child Adolesc Psychiatr Clin N Am* **26**, 341-366, doi:10.1016/j.chc.2016.12.014 (2017).

346 Gejman, P. V., Sanders, A. R. & Duan, J. The role of genetics in the etiology of schizophrenia. *Psychiatr Clin North Am* **33**, 35-66, doi:10.1016/j.psc.2009.12.003 (2010).

347 Cariaga-Martinez, A., Saiz-Ruiz, J. & Alelu-Paz, R. From Linkage Studies to Epigenetics: What We Know and What We Need to Know in the Neurobiology of Schizophrenia. *Front Neurosci* **10**, 202, doi:10.3389/fnins.2016.00202 (2016).

348 Szatkiewicz, J. *et al.* The genomics of major psychiatric disorders in a large pedigree from Northern Sweden. *Transl Psychiatry* **9**, 60, doi:10.1038/s41398-019-0414-9 (2019).

349 Gottesman, II & Shields, J. A polygenic theory of schizophrenia. *Proc Natl Acad Sci U S A* **58**, 199-205, doi:10.1073/pnas.58.1.199 (1967).

350 International Schizophrenia, C. *et al.* Common polygenic variation contributes to risk of schizophrenia and bipolar disorder. *Nature* **460**, 748-752, doi:10.1038/nature08185 (2009).

351 Purcell, S. M. *et al.* A polygenic burden of rare disruptive mutations in schizophrenia. *Nature* **506**, 185-190, doi:10.1038/nature12975 (2014).

352 Walsh, T. *et al.* Rare structural variants disrupt multiple genes in neurodevelopmental pathways in schizophrenia. *Science* **320**, 539-543, doi:10.1126/science.1155174 (2008).

353 Stefansson, H. *et al.* Common variants conferring risk of schizophrenia. *Nature* **460**, 744-747, doi:10.1038/nature08186 (2009).

354 Pouget, J. G. The Emerging Immunogenetic Architecture of Schizophrenia. *Schizophr Bull* **44**, 993-1004, doi:10.1093/schbul/sby038 (2018).

355 Schizophrenia Working Group of the Psychiatric Genomics, C. Biological insights from 108 schizophrenia-associated genetic loci. *Nature* **511**, 421-427, doi:10.1038/nature13595 (2014).

356 Fromer, M. *et al.* De novo mutations in schizophrenia implicate synaptic networks. *Nature* **506**, 179-184, doi:10.1038/nature12929 (2014).

357 Tsuang, M. T., Stone, W. S. & Faraone, S. V. Genes, environment and schizophrenia. *British Journal of Psychiatry* **178**, s18-s24, doi:10.1192/bjp.178.40.s18 (2018).

358 Stabenau, J. R. Heredity and Environment in Schizophrenia. *Archives of General Psychiatry* **18**, doi:10.1001/archpsyc.1968.01740040074009 (1968).

359 Dong, E., Nelson, M., Grayson, D. R., Costa, E. & Guidotti, A. Clozapine and sulpiride but not haloperidol or olanzapine activate brain DNA demethylation. *Proc Natl Acad Sci U S A* **105**, 13614-13619, doi:10.1073/pnas.0805493105 (2008).

360 Abdolmaleky, H. M. *et al.* Epigenetic dysregulation of HTR2A in the brain of patients with schizophrenia and bipolar disorder. *Schizophr Res* **129**, 183-190, doi:10.1016/j.schres.2011.04.007 (2011).

361 Carrard, A., Salzmann, A., Malafosse, A. & Karege, F. Increased DNA methylation status of the serotonin receptor 5HTR1A gene promoter in schizophrenia and bipolar disorder. *J Affect Disord* **132**, 450-453, doi:10.1016/j.jad.2011.03.018 (2011).

362 Ghadirivasfi, M. *et al.* Hypomethylation of the serotonin receptor type-2A Gene (HTR2A) at T102C polymorphic site in DNA derived from the saliva of patients with schizophrenia and bipolar disorder. *Am J Med Genet B Neuropsychiatr Genet* **156B**, 536-545, doi:10.1002/ajmg.b.31192 (2011).

363 Abdolmaleky, H. M. *et al.* DNA hypermethylation of serotonin transporter gene promoter in drug naive patients with schizophrenia. *Schizophr Res* **152**, 373-380, doi:10.1016/j.schres.2013.12.007 (2014).

364 Abdolmaleky, H. M. *et al.* Hypomethylation of MB-COMT promoter is a major risk factor for schizophrenia and bipolar disorder. *Hum Mol Genet* **15**, 3132-3145, doi:10.1093/hmg/ddl253 (2006).

365 Mill, J. *et al.* Epigenomic Profiling Reveals DNA-Methylation Changes Associated with Major Psychosis. *The American Journal of Human Genetics* **82**, 696-711, doi:10.1016/j.ajhg.2008.01.008 (2008).

366 Abdolmaleky, H. M. *et al.* Hypermethylation of the reelin (RELN) promoter in the brain of schizophrenic patients: a preliminary report. *Am J Med Genet B Neuropsychiatr Genet* **134B**, 60-66, doi:10.1002/ajmg.b.30140 (2005).

367 Grayson, D. R. *et al.* Reelin promoter hypermethylation in schizophrenia. *Proc Natl Acad Sci U S A* **102**, 9341-9346, doi:10.1073/pnas.0503736102 (2005).

368 Dempster, E. L. *et al.* Disease-associated epigenetic changes in monozygotic twins discordant for schizophrenia and bipolar disorder. *Hum Mol Genet* **20**, 4786-4796, doi:10.1093/hmg/ddr416 (2011).

369 Pidsley, R. *et al.* Methylomic profiling of human brain tissue supports a neurodevelopmental origin for schizophrenia. *Genome Biol* **15**, 483, doi:10.1186/s13059-014-0483-2 (2014).

370 Chen, C. *et al.* Correlation between DNA methylation and gene expression in the brains of patients with bipolar disorder and schizophrenia. *Bipolar Disord* **16**, 790-799, doi:10.1111/bdi.12255 (2014).

371 Wockner, L. F. *et al.* Genome-wide DNA methylation analysis of human brain tissue from schizophrenia patients. *Transl Psychiatry* **4**, e339, doi:10.1038/tp.2013.111 (2014).

372 Castellani, C. A., Melka, M. G., Gui, J. L., O'Reilly, R. L. & Singh, S. M. Integration of DNA sequence and DNA methylation changes in monozygotic twin pairs discordant for schizophrenia. *Schizophr Res* **169**, 433-440, doi:10.1016/j.schres.2015.09.021 (2015).

373 Akbarian, S. The molecular pathology of schizophrenia--focus on histone and DNA modifications. *Brain Res Bull* **83**, 103-107, doi:10.1016/j.brainresbull.2009.08.018 (2010).

374 Huang, H. S. *et al.* Prefrontal dysfunction in schizophrenia involves mixed-lineage leukemia 1-regulated histone methylation at GABAergic gene promoters. *J Neurosci* **27**, 11254-11262, doi:10.1523/JNEUROSCI.3272-07.2007 (2007).

375 Lewis, D. A., Hashimoto, T. & Volk, D. W. Cortical inhibitory neurons and schizophrenia. *Nat Rev Neurosci* **6**, 312-324, doi:10.1038/nrn1648 (2005).

376 Gavin, D. P. *et al.* Dimethylated lysine 9 of histone 3 is elevated in schizophrenia and exhibits a divergent response to histone deacetylase inhibitors in lymphocyte cultures. *J Psychiatr Neurosci* **34**, 232-237 (2009).

377 Chase, K. A., Gavin, D. P., Guidotti, A. & Sharma, R. P. Histone methylation at H3K9: evidence for a restrictive epigenome in schizophrenia. *Schizophr Res* **149**, 15-20, doi:10.1016/j.schres.2013.06.021 (2013).

378 Patterson, P. H. Immune involvement in schizophrenia and autism: etiology, pathology and animal models. *Behav Brain Res* **204**, 313-321, doi:10.1016/j.bbr.2008.12.016 (2009).

379 Estes, M. L. & McAllister, A. K. Maternal immune activation: Implications for neuropsychiatric disorders. *Science* **353**, 772-777, doi:10.1126/science.aag3194 (2016).

380 Shi, L. *et al.* Activation of the maternal immune system alters cerebellar development in the offspring. *Brain Behav Immun* **23**, 116-123, doi:10.1016/j.bbi.2008.07.012 (2009).

381 Fatemi, S. H. *et al.* Human influenza viral infection in utero alters glial fibrillary acidic protein immunoreactivity in the developing brains of neonatal mice. *Mol Psychiatry* **7**, 633-640, doi:10.1038/sj.mp.4001046 (2002).

382 Fatemi, S. H. *et al.* Maternal infection leads to abnormal gene regulation and brain atrophy in mouse offspring: implications for genesis of neurodevelopmental disorders. *Schizophr Res* **99**, 56-70, doi:10.1016/j.schres.2007.11.018 (2008).

383 Winter, C. *et al.* Dopamine and serotonin levels following prenatal viral infection in mouse--implications for psychiatric disorders such as schizophrenia and autism. *Eur Neuropsychopharmacol* **18**, 712-716, doi:10.1016/j.euroneuro.2008.06.001 (2008).

384 Meyer, U. Prenatal poly(i:C) exposure and other developmental immune activation models in rodent systems. *Biol Psychiatry* **75**, 307-315, doi:10.1016/j.biopsych.2013.07.011 (2014).

385 Cai, Z., Pan, Z.-L., Pang, Y., Evans, O. B. & Rhodes, P. G. Cytokine Induction in Fetal Rat Brains and Brain Injury in Neonatal Rats after Maternal Lipopolysaccharide Administration. *Pediatric Research* **47**, 64-64, doi:10.1203/00006450-200001000-00013 (2000).

386 Urakubo, A., Jarskog, L. F., Lieberman, J. A. & Gilmore, J. H. Prenatal exposure to maternal infection alters cytokine expression in the placenta, amniotic fluid, and fetal brain. *Schizophrenia Research* **47**, 27-36, doi:10.1016/s0920-9964(00)00032-3 (2001).

387 Paintlia, M. K., Paintlia, A. S., Barbosa, E., Singh, I. & Singh, A. K. N-acetylcysteine prevents endotoxin-induced degeneration of oligodendrocyte progenitors and hypomyelination in developing rat brain. *J Neurosci Res* **78**, 347-361, doi:10.1002/jnr.20261 (2004).

388 Golan, H. M., Lev, V., Hallak, M., Sorokin, Y. & Huleihel, M. Specific neurodevelopmental damage in mice offspring following maternal inflammation during pregnancy. *Neuropharmacology* **48**, 903-917, doi:10.1016/j.neuropharm.2004.12.023 (2005).

389 Gilmore, J. H., Jarskog, L. F. & Vadlamudi, S. Maternal poly I:C exposure during pregnancy regulates TNF alpha, BDNF, and NGF expression in neonatal brain and the maternal-fetal unit of the rat. *J Neuroimmunol* **159**, 106-112, doi:10.1016/j.jneuroim.2004.10.008 (2005).

390 Elovitz, M. A., Mrinalini, C. & Sammel, M. D. Elucidating the early signal transduction pathways leading to fetal brain injury in preterm birth. *Pediatr Res* **59**, 50-55, doi:10.1203/01.pdr.0000191141.21932.b6 (2006).

391 Ashdown, H. *et al.* The role of cytokines in mediating effects of prenatal infection on the fetus: implications for schizophrenia. *Mol Psychiatry* **11**, 47-55, doi:10.1038/sj.mp.4001748 (2006).

392 Meyer, U. *et al.* The time of prenatal immune challenge determines the specificity of inflammation-mediated brain and behavioral pathology. *J Neurosci* **26**, 4752-4762, doi:10.1523/JNEUROSCI.0099-06.2006 (2006).

393 Liverman, C. S. *et al.* Altered expression of pro-inflammatory and developmental genes in the fetal brain in a mouse model of maternal infection. *Neurosci Lett* **399**, 220-225, doi:10.1016/j.neulet.2006.01.064 (2006).

394 Meyer, U. *et al.* Adult behavioral and pharmacological dysfunctions following disruption of the fetal brain balance between pro-inflammatory and IL-10-mediated anti-inflammatory signaling. *Mol Psychiatry* **13**, 208-221, doi:10.1038/sj.mp.4002042 (2008).

395 Samuelsson, A. M., Jennische, E., Hansson, H. A. & Holmang, A. Prenatal exposure to interleukin-6 results in inflammatory neurodegeneration in hippocampus with NMDA/GABA(A) dysregulation and impaired spatial learning. *Am J Physiol Regul Integr Comp Physiol* **290**, R1345-1356, doi:10.1152/ajpregu.00268.2005 (2006).

396 Smith, S. E., Li, J., Garbett, K., Mirnics, K. & Patterson, P. H. Maternal immune activation alters fetal brain development through interleukin-6. *J Neurosci* **27**, 10695-10702, doi:10.1523/JNEUROSCI.2178-07.2007 (2007).

397 Richetto, J., Calabrese, F., Meyer, U. & Riva, M. A. Prenatal versus postnatal maternal factors in the development of infection-induced working memory impairments in mice. *Brain Behav Immun* **33**, 190-200, doi:10.1016/j.bbi.2013.07.006 (2013).

398 McCarty, R. Cross-fostering: Elucidating the effects of genexenvironment interactions on phenotypic development. *Neurosci Biobehav Rev* **73**, 219-254, doi:10.1016/j.neubiorev.2016.12.025 (2017).

399 Ozaki, K. *et al.* Maternal immune activation induces sustained changes in fetal microglia motility. *Sci Rep* **10**, 21378, doi:10.1038/s41598-020-78294-2 (2020).

400 Holloway, T. *et al.* Prenatal stress induces schizophrenia-like alterations of serotonin 2A and metabotropic glutamate 2 receptors in the adult offspring: role of maternal immune system. *J Neurosci* **33**, 1088-1098, doi:10.1523/JNEUROSCI.2331-12.2013 (2013).

401 Champagne, F. A., Francis, D. D., Mar, A. & Meaney, M. J. Variations in maternal care in the rat as a mediating influence for the effects of environment on development. *Physiology & Behavior* **79**, 359-371, doi:10.1016/s0031-9384(03)00149-5 (2003).

402 van der Veen, R., Abrous, D. N., de Kloet, E. R., Piazza, P. V. & Koehl, M. Impact of intra- and interstrain cross-fostering on mouse maternal care. *Genes Brain Behav* **7**, 184-192, doi:10.1111/j.1601-183X.2007.00337.x (2008).

403 Ronovsky, M. *et al.* Maternal immune activation transgenerationally modulates maternal care and offspring depression-like behavior. *Brain Behav Immun* **63**, 127-136, doi:10.1016/j.bbi.2016.10.016 (2017).

404 Jensen Pena, C. & Champagne, F. A. Implications of temporal variation in maternal care for the prediction of neurobiological and behavioral outcomes in offspring. *Behav Neurosci* **127**, 33-46, doi:10.1037/a0031219 (2013).

405 Ma, S. *et al.* Cell-type-specific brain methylomes profiled via ultralow-input microfluidics. *Nature Biomedical Engineering* **2**, 183-194, doi:10.1038/s41551-018-0204-3 (2018).

406 Watts, M. E., Pocock, R. & Claudianos, C. Brain Energy and Oxygen Metabolism: Emerging Role in Normal Function and Disease. *Front Mol Neurosci* **11**, 216, doi:10.3389/fnmol.2018.00216 (2018).

407 Jin, E. J., Kiral, F. R. & Hiesinger, P. R. The where, what, and when of membrane protein degradation in neurons. *Dev Neurobiol* **78**, 283-297, doi:10.1002/dneu.22534 (2018).

408 Dulka, B. N., Pullins, S. E., Cullen, P. K., Moyer, J. R., Jr. & Helmstetter, F. J. Age-related memory deficits are associated with changes in protein degradation in brain regions critical for trace fear conditioning. *Neurobiol Aging* **91**, 160-166, doi:10.1016/j.neurobiolaging.2020.03.001 (2020).

409 Bousman, C. A. *et al.* Elevated ubiquitinated proteins in brain and blood of individuals with schizophrenia. *Sci Rep* **9**, 2307, doi:10.1038/s41598-019-38490-1 (2019).

410 Zhang, J. & Jiao, J. Molecular Biomarkers for Embryonic and Adult Neural Stem Cell and Neurogenesis. *Biomed Res Int* **2015**, 727542, doi:10.1155/2015/727542 (2015).

411 Rosso, S. B. & Inestrosa, N. C. WNT signaling in neuronal maturation and synaptogenesis. *Front Cell Neurosci* **7**, 103, doi:10.3389/fncel.2013.00103 (2013).

412 Runge, K., Cardoso, C. & de Chevigny, A. Dendritic Spine Plasticity: Function and Mechanisms. *Front Synaptic Neurosci* **12**, 36, doi:10.3389/fnsyn.2020.00036 (2020).

413 Kapur, M., Monaghan, C. E. & Ackerman, S. L. Regulation of mRNA Translation in Neurons-A Matter of Life and Death. *Neuron* **96**, 616-637, doi:10.1016/j.neuron.2017.09.057 (2017).

414 Zhang, P., Dilley, C. & Mattson, M. P. DNA damage responses in neural cells: Focus on the telomere. *Neuroscience* **145**, 1439-1448, doi:10.1016/j.neuroscience.2006.11.052 (2007).

415 Murase, S., Kim, E., Lin, L., Hoffman, D. A. & McKay, R. D. Loss of signal transducer and activator of transcription 3 (STAT3) signaling during elevated activity causes vulnerability in hippocampal neurons. *J Neurosci* **32**, 15511-15520, doi:10.1523/JNEUROSCI.2940-12.2012 (2012).

416 Genaro-Mattos, T. C., Anderson, A., Allen, L. B., Korade, Z. & Mirnics, K. Cholesterol Biosynthesis and Uptake in Developing Neurons. *ACS Chem Neurosci* **10**, 3671-3681, doi:10.1021/acschemneuro.9b00248 (2019).

417 Zhang, J. & Liu, Q. Cholesterol metabolism and homeostasis in the brain. *Protein Cell* **6**, 254-264, doi:10.1007/s13238-014-0131-3 (2015).

418 Jin, U., Park, S. J. & Park, S. M. Cholesterol Metabolism in the Brain and Its Association with Parkinson's Disease. *Exp Neurobiol* **28**, 554-567, doi:10.5607/en.2019.28.5.554 (2019).

419 Tracey, T. J., Steyn, F. J., Wolvetang, E. J. & Ngo, S. T. Neuronal Lipid Metabolism: Multiple Pathways Driving Functional Outcomes in Health and Disease. *Front Mol Neurosci* **11**, 10, doi:10.3389/fnmol.2018.00010 (2018).

420 Liu, L., MacKenzie, K. R., Putluri, N., Maletic-Savatic, M. & Bellen, H. J. The Glia-Neuron Lactate Shuttle and Elevated ROS Promote Lipid Synthesis in Neurons and Lipid Droplet Accumulation in Glia via APOE/D. *Cell Metab* **26**, 719-737 e716, doi:10.1016/j.cmet.2017.08.024 (2017).

421 Schwarz, E. *et al.* High throughput lipidomic profiling of schizophrenia and bipolar disorder brain tissue reveals alterations of free fatty acids, phosphatidylcholines, and ceramides. *J Proteome Res* **7**, 4266-4277, doi:10.1021/pr800188y (2008).

422 Maas, D. A. *et al.* Key role for lipids in cognitive symptoms of schizophrenia. *Transl Psychiatry* **10**, 399, doi:10.1038/s41398-020-01084-x (2020).

423 Sarandol, A. *et al.* First-episode psychosis is associated with oxidative stress: Effects of short-term antipsychotic treatment. *Psychiatry Clin Neurosci* **69**, 699-707, doi:10.1111/pcn.12333 (2015).

424 Patel, S., Sharma, D., Kalia, K. & Tiwari, V. Crosstalk between endoplasmic reticulum stress and oxidative stress in schizophrenia: The dawn of new therapeutic approaches. *Neurosci Biobehav Rev* **83**, 589-603, doi:10.1016/j.neubiorev.2017.08.025 (2017).

425 Tucker, G. C., Duband, J.-L., Dufour, S. & Thiery, J. P. Cell-adhesion and substrate-adhesion molecules: their instructive roles in neural crest cell migration. *Development* **103**, 81-94 (1988).

426 Kaneko, N., Sawada, M. & Sawamoto, K. Mechanisms of neuronal migration in the adult brain. *J Neurochem* **141**, 835-847, doi:10.1111/jnc.14002 (2017).

427 Kim, J. Y. *et al.* Wnt signal activation induces midbrain specification through direct binding of the beta-catenin/TCF4 complex to the EN1 promoter in human pluripotent stem cells. *Exp Mol Med* **50**, 1-13, doi:10.1038/s12276-018-0044-y (2018).

428 Fusar-Poli, P. *et al.* Abnormal prefrontal activation directly related to pre-synaptic striatal dopamine dysfunction in people at clinical high risk for psychosis. *Mol Psychiatry* **16**, 67-75, doi:10.1038/mp.2009.108 (2011).

429 Kesby, J. P., Eyles, D. W., McGrath, J. J. & Scott, J. G. Dopamine, psychosis and schizophrenia: the widening gap between basic and clinical neuroscience. *Transl Psychiatry* **8**, 30, doi:10.1038/s41398-017-0071-9 (2018).

430 Ortega-Martinez, S. A new perspective on the role of the CREB family of transcription factors in memory consolidation via adult hippocampal neurogenesis. *Front Mol Neurosci* **8**, 46, doi:10.3389/fnmol.2015.00046 (2015).

431 Barco, A. & Marie, H. Genetic approaches to investigate the role of CREB in neuronal plasticity and memory. *Mol Neurobiol* **44**, 330-349, doi:10.1007/s12035-011-8209-x (2011).

432 Wang, H., Xu, J., Lazarovici, P., Quirion, R. & Zheng, W. cAMP Response Element-Binding Protein (CREB): A Possible Signaling Molecule Link in the Pathophysiology of Schizophrenia. *Front Mol Neurosci* **11**, 255, doi:10.3389/fnmol.2018.00255 (2018).

433 Ryskalin, L., Limanaqi, F., Frati, A., Busceti, C. L. & Fornai, F. mTOR-Related Brain Dysfunctions in Neuropsychiatric Disorders. *Int J Mol Sci* **19**, doi:10.3390/ijms19082226 (2018).

434 Frantseva, M. V. *et al.* Evidence for impaired long-term potentiation in schizophrenia and its relationship to motor skill learning. *Cereb Cortex* **18**, 990-996, doi:10.1093/cercor/bhm151 (2008).

435 Hirayama-Kurogi, M. *et al.* Downregulation of GNA13-ERK network in prefrontal cortex of schizophrenia brain identified by combined focused and targeted quantitative proteomics. *J Proteomics* **158**, 31-42, doi:10.1016/j.jprot.2017.02.009 (2017).

436 Pereira, A. *et al.* Clozapine induction of ERK1/2 cell signalling via the EGF receptor in mouse prefrontal cortex and striatum is distinct from other antipsychotic drugs. *Int J Neuropsychopharmacol* **15**, 1149-1160, doi:10.1017/S1461145711001404 (2012).

437 Cheng, A. *et al.* Telomere protection mechanisms change during neurogenesis and neuronal maturation: newly generated neurons are hypersensitive to telomere and DNA damage. *J Neurosci* **27**, 3722-3733, doi:10.1523/JNEUROSCI.0590-07.2007 (2007).

438 Coffey, E. T. Nuclear and cytosolic JNK signalling in neurons. *Nat Rev Neurosci* **15**, 285-299, doi:10.1038/nrn3729 (2014).

439 Frade, J. M. & Ovejero-Benito, M. C. Neuronal cell cycle: the neuron itself and its circumstances. *Cell Cycle* **14**, 712-720, doi:10.1080/15384101.2015.1004937 (2015).

440 Liu, X. J. *et al.* TLR signaling adaptor protein MyD88 in primary sensory neurons contributes to persistent inflammatory and neuropathic pain and neuroinflammation. *Sci Rep* **6**, 28188, doi:10.1038/srep28188 (2016).

441 Comer, A. L., Carrier, M., Tremblay, M. E. & Cruz-Martin, A. The Inflamed Brain in Schizophrenia: The Convergence of Genetic and Environmental Risk Factors That Lead to Uncontrolled Neuroinflammation. *Front Cell Neurosci* **14**, 274, doi:10.3389/fncel.2020.00274 (2020).

442 de Jonge, J. C., Vinkers, C. H., Hulshoff Pol, H. E. & Marsman, A. GABAergic Mechanisms in Schizophrenia: Linking Postmortem and In Vivo Studies. *Front Psychiatry* **8**, 118, doi:10.3389/fpsyt.2017.00118 (2017).

443 Konefal, S. C. & Stellwagen, D. Tumour necrosis factor-mediated homeostatic synaptic plasticity in behavioural models: testing a role in maternal immune activation. *Philos Trans R Soc Lond B Biol Sci* **372**, doi:10.1098/rstb.2016.0160 (2017).

444 O'Connell, K. S., McGregor, N. W., Lochner, C., Emsley, R. & Warnich, L. The genetic architecture of schizophrenia, bipolar disorder, obsessive-compulsive disorder and autism spectrum disorder. *Mol Cell Neurosci* **88**, 300-307, doi:10.1016/j.mcn.2018.02.010 (2018).

445 Horiuchi, Y. *et al.* Molecular signatures associated with cognitive deficits in schizophrenia: a study of biopsied olfactory neural epithelium. *Transl Psychiatry* **6**, e915, doi:10.1038/tp.2016.154 (2016).

446 Maletic, V., Eramo, A., Gwin, K., Offord, S. J. & Duffy, R. A. The Role of Norepinephrine and Its alpha-Adrenergic Receptors in the Pathophysiology and Treatment of Major Depressive Disorder and Schizophrenia: A Systematic Review. *Front Psychiatry* **8**, 42, doi:10.3389/fpsyt.2017.00042 (2017).

447 Crayton, J. W. & Meltzer, H. Y. Degeneration and regeneration of motor neurons in psychotic patients. *Biol Psychiatry* **14**, 803-819 (1979).

448 Kubicki, M., McCarley, R. W. & Shenton, M. E. Evidence for white matter abnormalities in schizophrenia. *Curr Opin Psychiatry* **18**, 121-134, doi:10.1097/00001504-200503000-00004 (2005).

449 Bhandari, A., Voineskos, D., Daskalakis, Z. J., Rajji, T. K. & Blumberger, D. M. A Review of Impaired Neuroplasticity in Schizophrenia Investigated with Non-invasive Brain Stimulation. *Front Psychiatry* **7**, 45, doi:10.3389/fpsyt.2016.00045 (2016).

450 Njoroge, M. M., Irungu Mwangi, V., Owalla, T. J., Ozwara, H. & Egwang, T. G. Mice Pups Breastfed by Foster Mothers Whose Breast Milk Contains Plasmodium falciparum Recombinant SE36 Antigen Develop Specific Antibodies. *Am J Trop Med Hyg*, doi:10.4269/ajtmh.20-0206 (2020).

451 Curley, J. P. & Champagne, F. A. Influence of maternal care on the developing brain: Mechanisms, temporal dynamics and sensitive periods. *Front Neuroendocrinol* **40**, 52-66, doi:10.1016/j.yfrne.2015.11.001 (2016).

452 Langfelder, P. & Horvath, S. WGCNA: an R package for weighted correlation network analysis. *BMC Bioinformatics* **9**, 559, doi:10.1186/1471-2105-9-559 (2008).

Publications

Journal Articles (denotes equal contribution)*

1. Liu, Z., **Naler, L. B.**, Zhu, Y., Deng, C., Zhang, Q., Zhu, B., Zhou, Z., Sarma, M., Murray, A., Xie, H., & Lu, C. Native MOWChIP-seq as a general technology for low-input profiling of genome-wide protein binding. *In preparation.*
2. **Naler, L. B.***, Hsieh, Y.*, Geng, S., Zhou, Z., Li, L., & Lu, C. Epigenomic and transcriptomic differences between low-grade and acute inflammation in LPS-induced murine immune cells. *bioRxiv* **2021.03.28.437377** (2021). *Submitted.*
3. De la Fuente Revenga, M., Zhu, B.*, Guevara, C. A.*, **Naler, L. B.**, Saunders, J. M., Zhou, Z., Toneatti, R., Sierra, S., Wolstenholme J. T., Beardsley, P. M., Huntley, G. W., Lu, C., & Gonzalez-Maeso, J. Prolonged epigenetic and synaptic plasticity alterations following single exposure to a psychedelic in mice. *bioRxiv* **2021.02.24.432725** (2021). *Submitted.*
4. Hsieh, Y.*, **Naler, L. B.***, Ma, S., & Lu, C. Cell-type-specific epigenomic variations associated with BRCA1 mutation in pre-cancer human breast tissues. *bioRxiv* **2020.08.24.265199** (2020). *Submitted.*
5. Deng, C., Murphy, T., Zhang, Q., **Naler, L.**, Xu, A., & Lu, C. Multiplexed and ultralow-input ChIP-seq enabled by tagmentation-based indexing and facile microfluidics. *Analytical Chemistry* **92**, 13661 – 13666 (2020).
6. Murphy, T., Hsieh, Y., Zhu, B., **Naler, L. B.**, & Lu, C. Microfluidic platform for next-generation sequencing library preparation with low-input samples. *Analytical Chemistry* **92**, 2519-2526 (2020).
7. Zhu, B.*****, Hsieh, Y.*****, Murphy, T. W., Zhang, Q., **Naler, L. B.**, & Lu, C. MOWChIP-seq for low-input and multiplexed profiling of genome-wide histone modifications. *Nature Protocols* **14**, 3366-3394 (2019).
8. Deng, C.*****, **Naler, L. B.***, & Lu, C. Microfluidic epigenomic mapping technologies for precision medicine. *Lab on a Chip* **19**, 2630-2650 (2019).
9. Zhu, W., **Naler, L.**, Maul, R., Sallin, M., & Sen, J. M. Immune system development and age-dependent maintenance in Klotho-hypomorphic mice. *Aging* **11** (14), 5246-5257 (2019).

10. Murphy, T. W.*****, Sheng, J.*****, **Naler, L. B.**, Feng, X., & Lu, C. On-chip manufacturing of synthetic proteins for point-of-care therapeutics. *Microsystems & Nanoengineering* **5**, 13 (2019).
11. Cox, M.*****, Deng, C.*****, **Naler, L. B.**, Lu, C., & Verbridge, S. Effects of culture condition on epigenomic profiles of brain tumor cells. *ACS Biomaterials Science & Engineering* **5**, 1544 – 1552 (2019).
12. Murphy, T. W., Zhang, Q., **Naler, L. B.**, Ma, S., Lu, C. Recent advances in the use of microfluidic technologies for single cell analysis. *Analyst* **143**, 60 – 80 (2018).

Seminars

1. Mid-Atlantic Micro/Nano Alliance Virtual Seminar Series**.** Profiling Cell-Type-Specific Epigenomic Variations in Pre-Cancer Human Breast Tissue via Low-Input Microfluidics. April 30, 2020. Link: https://youtu.be/MvkHi0NVBaI

Book Chapters

1. Heller, N. M., Berga-Bolanos, R., **Naler, L**., & Sen, J. Natural Killer T (NKT) Cells in Mice and Men. In *Signaling Mechanisms Regulating T Cell Diversity and Function*; Soboloff, J., Kappes, D. J., Eds.; Methods in Signal Transduction Series; CRC Press: Boca Raton, 2017.